Lappeenranta-Lahti University of Technology LUT
School of Engineering Science
Degree programme in Chemical and Process Engineering

Janne Holappa

SCALE-UP OF ULTRASOUND-ASSISTED EXTRACTION FROM LABORATORY SCALE BATCH PROCESS TO PILOT SCALE CONTINUOUS PROCESS

Examiners: Professor Tuomas Koiranen
D.Sc. (Tech.) Dmitry Gradov

ABSTRACT

Lappeenranta-Lahti University of Technology LUT
School of Engineering Science
Degree programme in Chemical and Process Engineering

Janne Holappa

Scale-up of ultrasound-assisted extraction from laboratory scale batch process to pilot scale continuous process

Master's Thesis
2020
112 pages, 67 figures, 12 tables, and 1 appendix

Examiners: Professor Tuomas Koiranen and D.Sc. (Tech.) Dmitry Gradov
Supervisor: M.Sc. (Tech.) Jussi Tamminen

Keywords: ultrasound, ultrasound-assisted extraction, solid-liquid extraction, natural product extraction, scale-up, sonochemistry

Ultrasound-assisted extraction (UAE) is a novel extraction method in which a conventional extraction process is intensified by the introduction of ultrasonic waves to the extraction system. In recent years, UAE has been widely studied in laboratory scale due to its numerous beneficial effects on extraction processes. However, scale-up of UAE has proven to be complicated, and there are few examples of large-scale UAE processes or equipment in literature.

The aim of this master's thesis was to develop a functional and workable pilot process for the UAE of natural products from plant organic matter. An UAE process was upscaled from laboratory to pilot scale and converted from batch to continuous operation mode.

Principles and significance of extraction as a separation method, followed by fundamentals and phenomena of UAE, are discussed in the literature part. In addition, existing UAE technologies are reviewed, and the issues and considerations in the scale-up of UAE systems are discussed. In the experimental part, UAE experiments for the extraction of chlorophylls *a* and *b* as well as carotenoids from spinach leaves were performed. Experiments were conducted first at laboratory scale in a batch reactor with an immersed ultrasonic horn, and later at pilot scale in tubular flow cells of different dimensional parameters.

The experimental results showed that successful extraction of spinach extractives was achieved at both scales. Even though effective sonication intensity in the pilot scale modules was significantly reduced due to constructive features of the flow cell geometry, ultrasonication was shown to improve the extraction in every investigated set of operational conditions.

TIIVISTELMÄ

Lappeenrannan-Lahden teknillinen yliopisto LUT
School of Engineering Science
Kemiantekniikan koulutusohjelma

Janne Holappa

Ultraääniuuttoprosessin skaalaus laboratoriomittakaavan panosprosessista jatkuvatoimiseksi pilot-prosessiksi

Diplomityö
2020
112 sivua, 67 kuvaa, 12 taulukkoa, ja 1 liite

Tarkastajat: Professori Tuomas Koiranen and TkT Dmitry Gradov
Ohjaaja: DI Jussi Tamminen

Avainsanat: ultraääni, ultraääniuutto, kiintoaine-nesteuutto, luonnonaineiden uutto, skaalaus, sonokemia

Ultraääniuutto on uudenlainen uuttoprosessi, jossa tavallista uuttoprosessia tehostetaan ultraääniaaltojen avulla. Ultraääniuutolla voidaan saavuttaa useita hyötyjä perinteisiin uuttoprosesseihin verrattuna, ja sitä onkin viime vuosien aikana tutkittu laajalti laboratoriomittakaavan kokeissa. Ultraääniuuton skaalaus on kuitenkin osoittautunut mutkikkaaksi, eikä suuremman mittakaavan prosesseista juurikaan ole kirjallisuustietoa saatavilla.

Tämän diplomityön tavoitteena oli luoda toimiva ja muokattava pilot-mittakaavan ultraääniuuttoprosessi kasvipohjaisten luonnonaineiden uuttoa varten. Ultraääniuuttoprosessi skaalattiin laboratoriomittakaavan panosprosessista jatkuvatoimiseksi pilot-mittakaavan prosessiksi.

Työn kirjallisuusosassa käsitellään ensin kiintoaine-nesteuuttoprosesseja yleisellä tasolla, minkä jälkeen siirrytään ultraääniuuton perusteisiin ja ilmiöihin. Lisäksi käydään läpi olemassa olevia ultraääniuuttolaitteistoja sekä ultraääniuuton skaalaukseen liittyviä haasteita. Soveltavassa osassa tehtiin uuttokokeita lehtivihreä a:n ja b:n sekä karotenoidien erottamiseksi pinaatista ensin laboratoriomittakaavan ultraäänisarvella ja myöhemmin kahdella eri pilot-mittakaavan ultraääniputkireaktorilla.

Kokeellisten tulosten perusteella uuteaineita saatiin irti pinaatista kummassakin mittakaavassa. Vaikka vaikuttava ultraääniteho oli pilot-mittakaavassa pieni reaktorien geometrian aiheuttaman ääniaaltojen heijastumisen vuoksi, ultraäänen käyttö tehosti uuttoa kaikissa työssä käsitellyissä koeolosuhteissa.

ACKNOWLEDGEMENTS

This thesis work was carried out at LUT University in Lappeenranta during the spring and early summer of 2020 as a part of a project aiming to commercialize UAE technology. Even though the times were shadowed by the highly irregular global situation, the work was successfully brought to completion.

I would like to express my gratitude to professor Tuomas Koiranen and D.Sc. (Tech.) Dmitry Gradov for providing me with the opportunity to participate in this project and for sharing their professional expertise and insight with me throughout the work. I also wish to thank M.Sc. (Tech.) Jussi Tamminen for his extensive and valuable guidance in both theoretical and practical matters. In addition, I would like to thank Jussi for his contributions to the experimental work, and these thanks are extended to M.Sc. (Tech.) Dmitry Safonov as well.

Last, but definitely not least, I wish to express my thanks and appreciation to my amazing, loving partner at home for continuously brightening my life with her sincerity and companionship.

Contents

Symbols

A	Area of ultrasound-emitting surface of probe, m^2
A_p	Area of particle, m^2
A_{470}	Sample absorbance at 470 nm, -
A_{647}	Sample absorbance at 647 nm, -
A_{647}	Sample absorbance at 649 nm, -
A_{663}	Sample absorbance at 663 nm, -
A_{663}	Sample absorbance at 664 nm, -
AED	Acoustic energy density (=P/V), W/m^3
AED_{el}	Acoustic energy density based on electric power input, W/m^3
AED_{nom}	Nominal acoustic energy density, W/m^3
c	Speed of sound in medium, m/s
$C(t)$	Outlet tracer concentration, mol/m^3
C_0	Initial tracer concentration in feed solution, mol/m^3
C_a	Chlorophyll *a* concentration, g/m^3
C_b	Chlorophyll *b* concentration, g/m^3
C_{car}	Total carotenoid concentration, g/m^3
C_{max}	Concentration of tracer solution, mol/m^3
C_p	Specific heat capacity of material, J/(kg·K)
d	Diameter, m
d_{CE}	Diameter of a circle with an area equal to that of particle, m
d_i	Inner diameter, m
d_o	Outer diameter, m
d_s	Distance from sound source, m
d_V	Mean volume diameter of particle, m
E	Fraction extracted, %
f	Frequency, Hz
$F(t)$	Cumulative residence time distribution, -
$f_{A,i}$	Fraction of particle area in size class *i*, -
$f_{n,i}$	Fraction of particle number in size class *i*, -
$f_{V,i}$	Fraction of particle volume in size class *i*, -
I	Ultrasonic intensity, W/m^2

I_0	Intensity of ultrasound emitted by sound source, W/m^2
l_p	Particle thickness, m
m	Sample mass, kg
$\dot{m}$	Mass flow rate, kg/s
m_0	Initial mass of extracted compound in raw material, kg
m_e	Mass of extracted compound, kg
m_d	Mass of dried sample, kg
m_w	Mass of fresh sample, kg
n_p	Number of particles, -
P	Ultrasonic power, W
P_{cal}	Calorimetric ultrasonic power, W
P_{nom}	Nominal ultrasonic power, W
p_j	Pressure generated by thermostat pump, Pa
Q	Volumetric flow rate, m^3/s
Q_c	Heat in reaction vessel, J
R	Reflection coefficient, -
Re	Reynolds number, -
r_I	Ramp rate, s^{-1}
t	Time, s
T	Temperature, °C
t_d	Dead time, s
V	Volume, m^3
v	Flow velocity, m/s
V_p	Particle volume, m^3
V_R	Reactor volume, m^3
$W(t)$	Washout function, -
Z	Acoustic impedance, kg/(m^2·s)
Z_1	Acoustic impedance of phase 1, kg/(m^2·s)
Z_2	Acoustic impedance of phase 2, kg/(m^2·s)
α	Attenuation coefficient, m^{-1}
ΔT	Temperature change of material, K
ε_{US}	Electrical efficiency of ultrasonication, -

μ	Dynamic viscosity, Pa·s
ρ	Fluid density, kg/m^3
ρ_G	Density of aqueous glycerol, kg/m^3
τ	Residence time, s
τ_m	Mean residence time, s
τ_P	Process time constant, s

Abbreviations

Car	Carotenoids
Chl *a*	Chlorophyll *a*
Chl *b*	Chlorophyll *b*
CMC	Carboxymethyl cellulose
DC	Direct current
DOE	Design of experiments
EAE	Enzyme-assisted extraction
EOD	Electro-osmotic dewatering
GRAS	Generally recognized as safe
HD	Hydro distillation
MAE	Microwave-assisted extraction
PEF	Pulsed electric field extraction
PIV	Particle image velocimetry
PLE	Pressurized liquid extraction
PLS	Partial least squares
PSD	Particle size distribution
RTD	Residence time distribution
R/S	Raw material to solvent ratio
SD	Steam distillation
SEM	Scanning electron microscopy
SFE	Supercritical fluid extraction
UAE	Ultrasound-assisted extraction
US	Ultrasound
vol%	Volume percentage
wt%	Weight percentage

1 INTRODUCTION

The nature is an incredibly diverse source of chemical compounds refined by evolution over hundreds of millions of years. Natural products – chemical compounds produced by living organisms – have been utilized by humans for millennia. Ancient Egyptians, for example, are known to have used natural products such as herbal oils, honey, and beeswax in medicine and cosmetics (Aboelsoud, 2009; Khaiat, 2002). However, it was not before the 19th century, when the field of organic chemistry began to develop, that it was understood why such products had their observed beneficial effects (Beutler, 2009). Since then, plant-based natural products and their derivatives have been a major source of novel drugs, notable examples of which include the painkiller morphine, malaria drug quinine, antibiotic penicillin, and anti-cancer drug paclitaxel (Beutler, 2009; Krause & Tobin, 2013).

Today, natural products separated from plant and animal matter have a large market, with a rapidly growing global share of over 300 billion USD (Uhlenbrock et al., 2018). This growth is driven by a desire to replace synthetic and fossil-based chemicals used in cosmetics, pharmaceuticals, agrochemicals, flavorings, and nutrients, with natural and sustainable alternatives. As the demand for these chemicals and extracts grows, it is becoming increasingly relevant for industrial manufacturers to investigate the design and optimization of suitable production processes.

During the design of any process producing natural products, it is important to consider the selection of suitable production steps to meet the standards of natural products, which are defined by food related legislation. In the case of flavorings, for example, European Flavouring Regulation (EC) No 1334/2008 (2008) defines natural flavorings so that their source material is of vegetable, animal, or microbiological origin either in the raw state or processed by an approved method, such as distillation or extraction. In addition, the compounds must be previously identified in nature. Otherwise, the flavoring cannot be labelled and sold as natural.

In the chemical and food industries, valuable compounds in natural products are often separated from solid organic gangue via solid-liquid extraction. However, traditional extraction methods, such as maceration and percolation, tend to inherently possess

unfavorable qualities, such as high solvent consumptions, long processing times, and the need to use toxic organic solvents (Zhang et al., 2018). Furthermore, high operating temperatures are often needed, potentially resulting in thermal decomposition of desired products. These shortcomings have generated a need for novel and intensified extraction processes.

Ultrasound-assisted extraction (UAE) is a promising novel extraction method in which conventional extraction is intensified by the application of ultrasonic waves. The use of ultrasound in extraction processes offers the potentials to improve process efficiency by increasing product yield and decreasing extraction time, to significantly improve extraction of thermolabile compounds, and also to reduce the consumption of toxic solvents or to completely replace them with safe and green alternatives (Tiwari, 2015).

In recent decades, UAE has seen wide use in laboratory scale experiments to test the intensification of existing natural product extraction processes. Examples include the extraction of carotenoids, flavonoids, antioxidants, polyphenols, and colorants from fruits and fruit peels, anthocyanins from berries, capsaicinoids from peppers, and oils from oleaginous seeds (Pingret et al., 2013; Shirsath et al., 2012). In spite of the promising results, there is a lack of large-scale UAE processes presented in literature. Therefore, it is necessary to investigate the scale-up process of UAE systems with the goal of creating commercially feasible technological solutions for the extraction.

1.1 Aim of the work

The aim of this work was to create a functional and workable pilot process for the UAE of natural products from solid plant matter by upscaling a laboratory scale batch UAE process to a continuous process at pilot scale. In the literature part, principles and phenomena related to UAE are introduced, and existing technologies related to UAE applications are reviewed. In the experimental part, extraction of chlorophylls *a* and *b* as well as carotenoids from spinach leaves is investigated at laboratory scale using a batch reactor equipped with an ultrasonic horn, and at pilot scale using tubular flow cell modules equipped with ultrasound

sources. To limit the scope of the work, techno-economic analysis concerning capital and operating costs as well as economic feasibility of the process was not included.

LITERATURE PART

2 PRINCIPLES AND METHODS OF NATURAL PRODUCT EXTRACTION

As human use of plant extracts has a long history, many methods have been developed and used for the separation of extracts from solid plant matter. Most of the methods are based on solid-liquid extraction, in which solutes are transported from solid matter to a solvent via dissolution (Berk, 2009). The solutes can then be separated from the solvent by, for example, evaporation of the solvent. The resulting extracts are complex mixtures of organic compounds, and if isolation of specific pure compounds is desired, a subsequent separation method such as chromatography, membrane filtration, and molecular distillation can be used (Zhang et al., 2018).

2.1 Main parameters of extraction

In any solid-liquid extraction process, the selection of a suitable solvent is of high importance. As listed by Takeuchi et al. (2009), a solvent for the natural product extraction should show high selectivity towards the target solutes to avoid the extraction of impurities, be non-toxic and safe to humans and environment, be chemically and thermally stable at the extraction conditions, have a low viscosity to improve mass transfer, be inflammable, have a low boiling point if there is a desire to evaporate the solvent after the extraction, and have low costs to increase economic feasibility of the process. In addition, the solvent should not participate in chemical reactions with the target solutes.

Pre-processing of the solid raw material is also crucial. Generally, smaller particle sizes favor the extraction due to promoted mass transfer with the solvent via increased solid-liquid contact area. However, excessively fine particles may impair the extraction by the formation of compressed solid beds, and by causing complications in the solid-liquid separation step

following the extraction (Palma et al., 2013; Zhang et al., 2018). Another matter is the moisture content of the sample. When extracting hydrosoluble compounds, moisture can quicken the transfer of solutes from a solid particle to the solvent medium. However, if the solutes are liposoluble and an organic solvent is used, it is beneficial to dry the raw material before the extraction in order to avoid the formation of a separate aqueous phase that contains part of the solutes (Palma et al., 2013).

Other important parameters contributing to a successful solid-liquid extraction include raw material to solvent ratio (R/S), extraction temperature, and extraction time. These parameters are closely related to each other: A decrease in R/S or an increase in temperature or time will improve extraction yield, but at the same time, economic feasibility of the process will decrease due to the increased solvent usage, energy consumption, or decreased production volume. Therefore, these parameters should be optimized to maximize the profitability of the process.

2.2 Conventional extraction methods

Maceration is a traditional, very simple extraction method, in which the solid plant matter is placed in a container filled with suitable solvent. The mixture is then left untouched for a long time, usually at least several days, with the possible exception of periodic agitation (Vinatoru et al., 1999). After sufficient time has passed, the solids are pressed and removed by filtration (Singh, 2008). Percolation is a similar method, but it is performed in a specialized vessel called percolator. The solids are placed on a filter and subjected to a continuous flow of solvent, which extracts solutes as it passes through the solids. The solvent and extracted solutes then separate from the solids by passing through the filter (Singh, 2008). Another extraction method, decoction, involves simply boiling the sample in water (Belwal et al., 2018). Basic principles of these methods are illustrated in Figure 1.

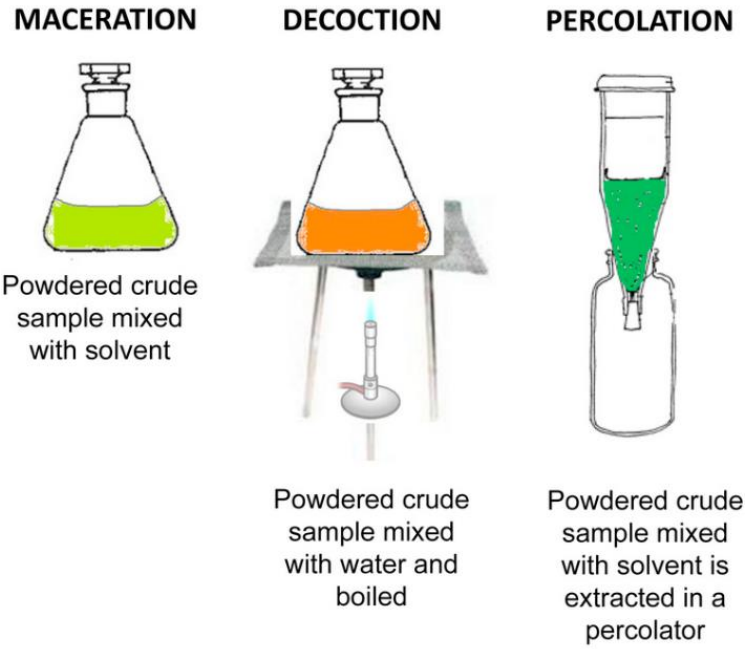

Figure 1 Basic principles of maceration, decoction, and percolation. Modified from Belwal et al. (2018).

Slightly more sophisticated extraction methods include hydro distillation (HD), steam distillation (SD), reflux extraction and Soxhlet extraction. In HD, the sample is boiled in water, which then evaporates into steam and carries the extracted volatile oils to a condenser, while in SD, the extraction is achieved with separately pre-generated steam flowing through the sample (Nasardin et al., 2018). In reflux extraction, the solvent is continuously boiled by external heating and returned to the reaction vessel by a reflux condenser (Chua et al., 2016). In Soxhlet extraction, the solids are contained in a small, separate pocket above the solvent flask (Tandon & Rane, 2008). The solvent is heated, boiled, and condensed so that it drips on the solids. The container with solids will eventually overflow and the liquid level will rise higher than the siphon arm, after which the solvent and dissolved solutes are physically pulled back to the solvent flask by the siphon. Fresh solvent is continuously brought in contact with the solids, and the cycle repeats. Schematic of a Soxhlet extractor is shown in Figure 2.

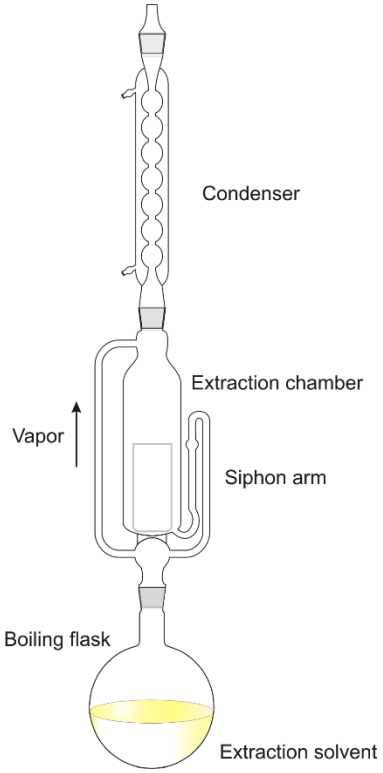

Figure 2 Schematic of a Soxhlet extractor (Generalic, 2018).

2.3 Novel extraction methods

While conventional extraction methods are applicable in many natural product extraction processes, they have several disadvantages, such as high consumption of organic solvents and non-selectivity of the extraction (Marathe et al., 2017). Extraction of thermolabile compounds may also prove infeasible, as heating the process to improve extraction effectiveness could instead lead to decomposition of the products. In order to tackle these shortcomings and to speed up extraction processes, several novel extraction methods have been developed.

Ultrasound-assisted extraction (UAE) and microwave-assisted extraction (MAE) intensify the extraction process by rupturing plant cells via ultrasound waves or microwaves, respectively, which releases the solutes within into the solvent (Pangarkar, 2008). Pulsed electric field extraction (PEF) and enzyme-assisted extraction (EAE), on the other hand, increase cell membrane permeability by electric fields or enzymatic activity, respectively, which leads to improved mass transport through the cells (Belwal et al., 2018).

In pressurized liquid extraction (PLE), high pressures, typically 10-15 MPa, are used to keep solvents in liquid phase as they are heated past their normal boiling point, which results in faster extraction kinetics (Tandon & Rane, 2008). In supercritical fluid extraction (SFE), the solvent, usually CO_2, is brought to temperature and pressure conditions above its critical point, which alters the solvent's properties to enable selective extraction. The advantages of SFE include the opportunity to completely exclude the usage of organic solvents in the process and simple separation of solutes, achieved by bringing the solvent to non-supercritical conditions (Bertucco & Franceschin, 2008).

Of course, novel extraction methods also have their own limitations and disadvantages. UAE can produce highly reactive free radicals, which may be undesirable in some extraction systems, while MAE mostly affects particle surfaces and struggles with uniform treatment of large particles (Pangarkar, 2008). In addition, MAE applies heat to the system, making it unsuitable for thermolabile compounds (Belwal et al., 2018). PEF, on the other hand, is highly dependent on the conductivity of the medium (Martínez et al., 2020), while EAE is limited by high cost and low efficiency of commercially available enzymes (Marathi et al., 2017). Finally, PLE typically requires temperatures of 50-200 °C, which makes it unsuitable for thermolabile compounds (Tandon & Rane, 2008), while SFE is hindered by high equipment cost and the fact that used solvents are nonpolar and ill-suited for the extraction of polar compounds (Belwal et al., 2018).

2.4 Applicability of extraction methods

Extraction methods and factors affecting their applicability and feasibility for natural product extraction processes are summarized in Table 1.

Table 1 Extraction methods and factors affecting their applicability and feasibility for natural product extraction. (Azwanida, 2015; Barba et al., 2015; Bendicho et al., 2012; Tandon & Rane, 2008; Zhang et al., 2018)

Method	**Suitable target compounds**	**Suitable for thermolabile compounds**	**Pressurization needed**	**Typical processing time**	**Costs (Notable contributors)**
Maceration	Hydrophilic, lipophilic	Yes	No	Several hours to days	Low (Solvent consumption)
Percolation	Hydrophilic, lipophilic	Yes	No	Several hours to days	Low (Solvent consumption)
Decoction	Hydrophilic	No	No	20-120 min	Low (Energy for heating)
Reflux extraction	Hydrophilic, lipophilic	No	No	20-120 min	Low to moderate (Solvent consumption, energy for heating)
Soxhlet extraction	Lipophilic	No	No	6-24 h	Low to moderate (Solvent consumption, energy for heating)
Hydro distillation and steam distillation	Essential oils	No	No	Several hours	Low (Energy for heating)
Pressurized liquid extraction	Hydrophilic, lipophilic	No	Yes (10-15 MPa)	10-20 min	High (Expensive equipment, energy for heating and pressurization)
Supercritical fluid extraction	Mostly lipophilic	Yes	Yes, depending on solvent and target solutes	10-60 min	High (Expensive equipment, energy for pressurization)
Ultrasound-assisted extraction	Hydrophilic, lipophilic	Yes	No	5-60 min	Low (Ultrasound equipment, energy for ultrasonication)
Microwave-assisted extraction	Hydrophilic, lipophilic	No	No	1-40 min	Low (Microwave equipment, energy for microwave heating)
Pulsed electric field extraction	Hydrophilic, lipophilic	Yes	No	Few seconds to 1 h	Moderate (Expensive equipment)
Enzyme-assisted extraction	Hydrophilic, lipophilic	Yes	No	1-12 h	High (Expensive and inefficient enzymes)

3 ULTRASOUND-ASSISTED EXTRACTION

The potential of ultrasound usage in chemistry was first discovered by Robert W. Wood and Alfred L. Loomis (1927), but it was not until the 1980s that inexpensive and reliable laboratory ultrasonicators were developed (Suslick, 1994). Since then, the utilization of ultrasound in chemical engineering applications, also known as sonochemistry, has gained significant scientific and industrial interest for its efficiency, cost-effectiveness, and environmental-friendly nature.

As an example of the benefits of ultrasound, in an experiment conducted by Pingret et al. (2013), UAE was used for the extraction of β-carotene from carrots into sunflower oil. It was found that UAE allowed for the complete removal of conventional organic solvent and therefore filtration and evaporation process steps were discarded (Figure 3). In addition, the process time was lowered from 2 h to 20 min, and the product yield increased by 4 %.

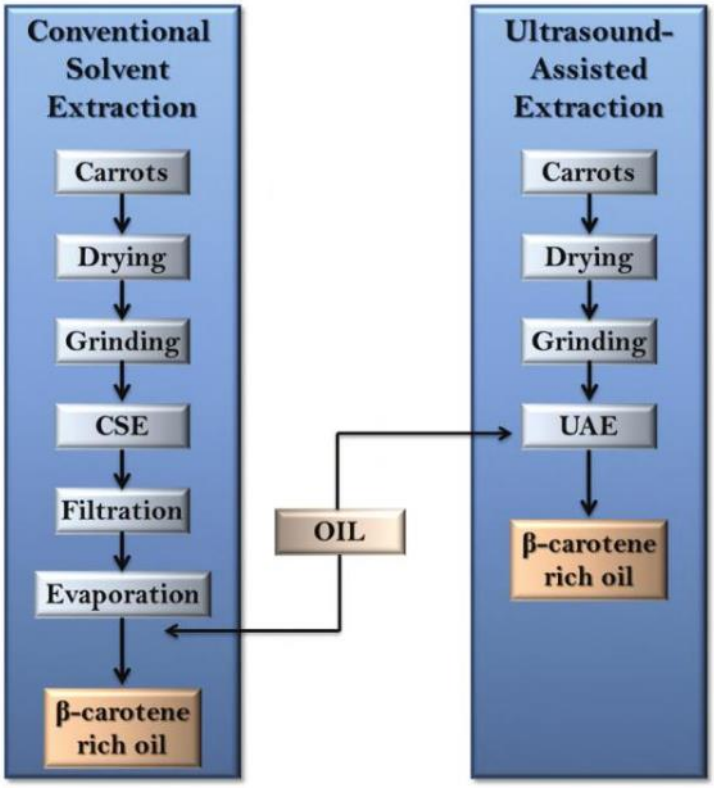

Figure 3 Comparison of the process steps in conventional solvent extraction (CSE) to the process steps in ultrasound-assisted extraction (UAE) for the extraction of β-carotene from carrots into sunflower oil. (Pingret et al., 2013)

3.1 Effects of ultrasonication

The mechanisms behind the beneficial effects of ultrasonication for extraction processes are known as acoustic cavitation and acoustic streaming (Tiwari, 2015). In extraction applications, acoustic cavitation is the more important of the two, as it applies intense physical forces into the medium.

3.1.1 Acoustic cavitation

In UAE, the sample is treated with ultrasound mainly to introduce acoustic cavitation into the extraction process. As ultrasonic waves propagate through a liquid medium, they move molecules back and forth with alternating phases of compression and rarefaction, leading into the formation of small, expanding bubbles of dissolved vapors. When a bubble reaches its critical size, it collapses, releasing high amounts of energy and rapidly pulling surrounding matter to fill the void (Tiwari, 2015). As a result, a local hot spot with extreme conditions and high shear forces is briefly created. The hot spots have been estimated to have temperatures higher than 5000 K, pressures of 500-5000 bar, and form liquid jets with velocities of up to 280 m/s (Hielscher Ultrasonics, 2020; Pingret et al., 2013). In various experimental measurements performed by Suslick et al. (2018), bubble collapse temperatures of up to 9500 K and pressures higher than 300 bar were detected for multi-bubble systems, and even more intense conditions at 15000 K and 3700 bar for single-bubble systems. However, it is important to emphasize on the extremely brief and local nature of these conditions – bubble radii and implosion times are in the magnitude of micrometers and picoseconds, respectively (Suslick et al., 2018). The principle of acoustic cavitation is shown in Figure 4.

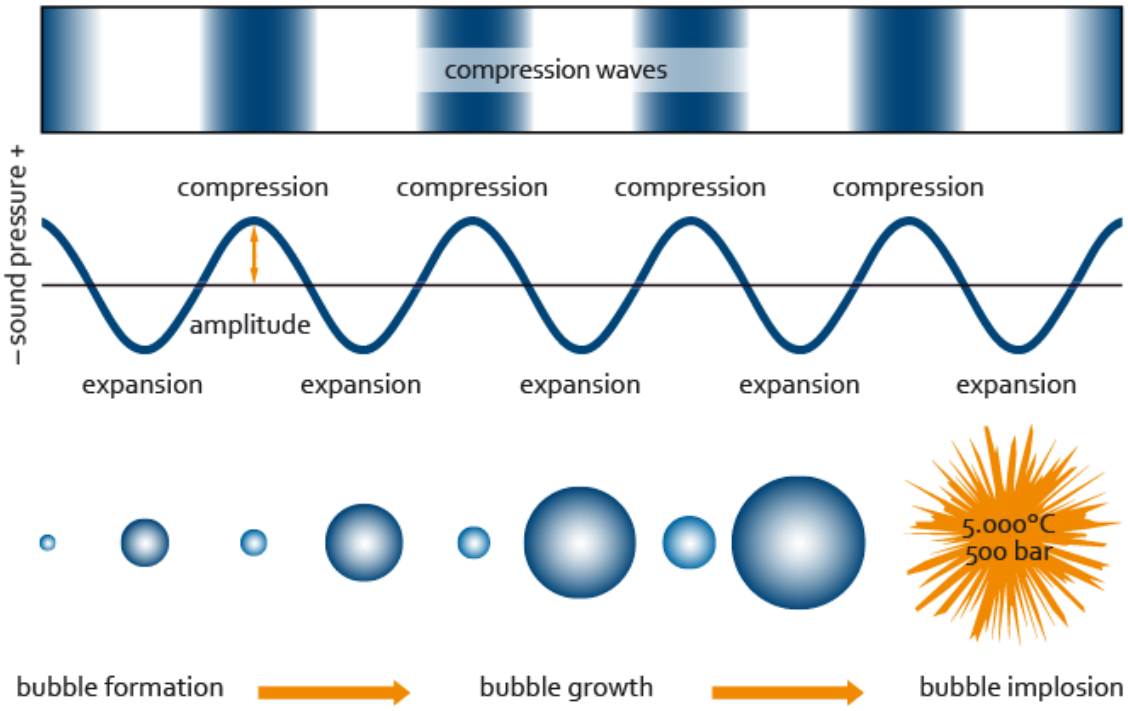

Figure 4 Principle of acoustic cavitation (ULTRAWAVES GmbH, 2018). Cycle of compression and rarefaction caused by ultrasonic waves results in the formation of cavitation bubbles. The bubbles eventually collapse, creating brief hot spots with extreme conditions.

In a liquid sample, acoustic cavitation increases micromixing and reactivity of components present. If the sample also contains solid particles, they will be subjected to the violent conditions created by collapsing bubbles. In addition, they will repeatedly collide with each other at high velocities (Suslick & Price, 1999). As a result, the particles will be damaged in different ways, such as fragmentation to smaller particles, erosion of particle surfaces, and formation of intra-particle cavities (Chemat et al., 2017). Soft materials, such as yeasts and leaves are more easily damaged than sturdier materials, such as seeds and bracket fungi. The effect of ultrasonication on a yeast sample is shown in Figure 5.

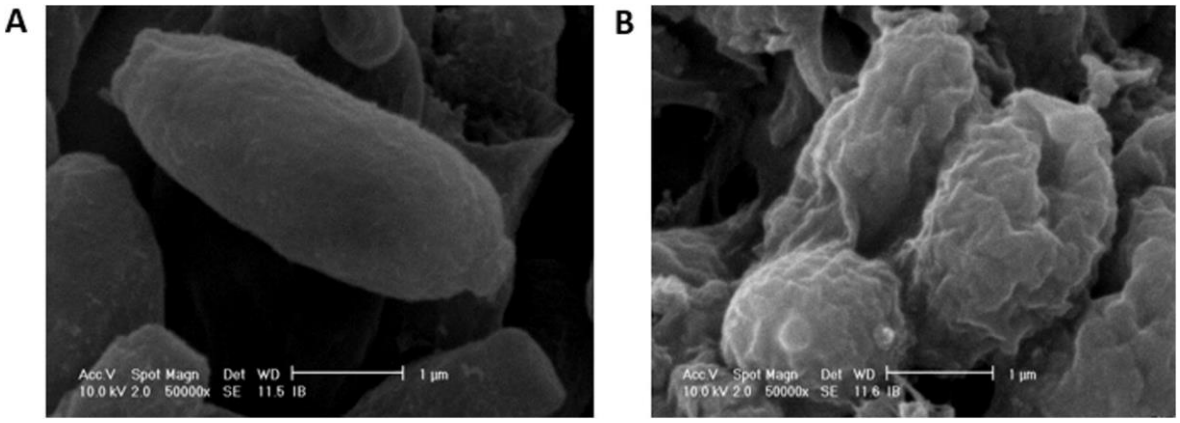

Figure 5 Effects of ultrasonication on yeast (*Yarrowia Lipolityca*) seen through scanning electron microscopy (SEM). A: Untreated sample; B: Sample after ultrasonication. (Chemat et al., 2017)

The changes caused by ultrasonication leads to accelerated and more effective extraction, as contact area between the solid particles and the solvent medium is increased. However, if the solids contain organic cell matter, cavitation bubbles that collapse close to cell walls will additionally damage the cell structure and rupture the walls, releasing extractives into the solvent medium and allowing the solvent to enter the cell (Pingret et al., 2013). Release of extractives from plant cells is illustrated in Figure 6.

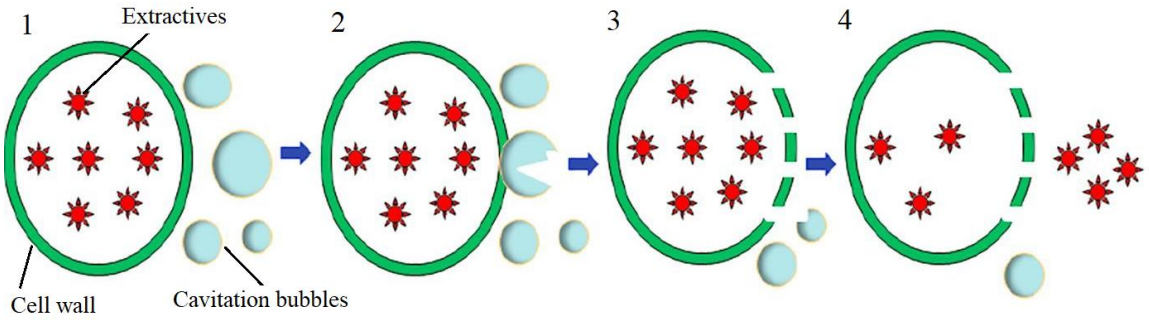

Figure 6 Release of extractives from plant cells via acoustic cavitation. 1: Cavitation bubbles are formed; 2: Cavitation bubbles collapse near the cell wall; 3: The cell wall is ruptured; 4: Extractives are released from the cell. Modified from Wen et al. (2018).

3.1.2 Acoustic streaming and promoted micromixing

As sound waves propagate through a liquid medium, the resulting pressure gradient generates liquid flow codirectional to the waves' travel direction (Rudenko et al., 1996). This phenomenon, known as acoustic streaming, therefore provides additional macromixing to any liquid system where ultrasound is used. Since efficient mixing is highly important in processes that require continuous mass transfer, such as solid-liquid extraction, acoustic streaming contributes to the beneficial effects of ultrasonication.

With utilization of acoustic streaming, it is also possible to design chemical reactors without the need for mechanical agitators. The advantages of such designs include increased simplicity, as fewer moving parts are needed inside the system, and improved safety with hazardous processes. On the other hand, careful positioning of transducers is then required to ensure high mixing efficiency. (Suri et al., 2002)

In addition to the macromixing generated by acoustic streaming, ultrasound has been reported to generate significant micromixing as well (Monnier et al., 1999; Parvizian et al., 2012; Rahimi et al., 2014). Three different mechanisms have been proposed for the generation of micromixing (Jordens et al., 2016): micro-jets and shockwaves caused by imploding acoustic cavitation bubbles, vibration caused by stable cavitation bubbles, and small vortices caused by acoustic streaming.

3.2 Main parameters of ultrasound

As UAE is an extraction process, it is of course important to consider conventional extraction-defining parameters, such as selection of solvent, solid-to-solvent ratio, temperature, and time. However, the application of ultrasound also introduces several new parameters into the extraction system. These parameters must be considered to ensure efficient ultrasonication.

3.2.1 Frequency and amplitude

Sound waves are mechanical waves that can be characterized by their amplitude, frequency, and wavelength. By definition, ultrasound refers to sound waves with frequencies higher than those audible to humans. Ultrasounds can be divided into two categories based on their frequency: power ultrasound from 20 kHz to 100 kHz and diagnostic ultrasound from 2000 kHz to 10000 kHz. Diagnostic ultrasound is generally used in non-destructive applications, such as medical sonography and quality control of materials, while power ultrasound is often used to apply force, such as in ultrasonic cutting, ultrasonic welding, and sonochemistry (Pingret et al., 2013).

For sonochemical applications, an extended frequency range for power ultrasound is used, also including frequencies between 100 kHz and 2 MHz (Pingret et al., 2013). This is because even though the high-impact physical effects of acoustic cavitation disappear as the frequency is increased beyond that of conventional power ultrasound, it has been demonstrated that higher frequency ultrasound has potential for use in many chemical applications, such as oxidative processes and degradation of organic pollutants (Pétrier et al., 1992; Francony & Pétrier, 1996; Toma et al., 2011). The frequencies used in UAE processes, however, typically correspond to those of the conventional power ultrasound range, as the physical effects of acoustic cavitation are desirable in extraction applications (Shirsath et al., 2012).

Ultrasound amplitude is also an important parameter to consider in UAE processes, because it is proportional to ultrasound power, which is then proportional to ultrasound intensity as shown in Equation (1). High intensity, in turn, is required for physically destructive cavitation. Ultrasound energy entering the system can also be given as acoustic energy density, which takes into account the system volume as shown in Equation (2). (Tiwari et al., 2015)

$$I = \frac{P}{A} \quad (1)$$

$$AED = \frac{P}{V_R} \quad (2)$$

Where	P	Ultrasonic power, W
	I	Ultrasonic intensity, W/m^2
	A	Area of the ultrasound-emitting surface on the probe, m^2
	AED	Acoustic energy density, W/m^3
	V_R	Reactor volume, m^3

However, some of the ultrasonic energy generated by an ultrasonic transducer will be lost due to attenuation of the sound waves in the medium, and as such it can be difficult to estimate the actual sonication power that contributes to acoustic cavitation (Fay & Rinker, 1996). In addition, the generation of ultrasound using electricity has its own losses. In the context of ultrasonic power, such as in Equations (1-2), it is therefore vital to distinguish between nominal and effective power. There are several available methods for the estimation of effective applied ultrasound power, such as calorimetry and chemical dosimetry (Koda et al., 2003).

3.2.2 Determination of effective ultrasonic power

The calorimetric method involves irradiating a material with ultrasound and measuring the resulting change in temperature. Water is a typical choice for the material due to its safety, availability, and well-known properties. To ensure accuracy of the results, the experiment should be designed so that thermal loss of the material is minimized and that all of the sound waves are absorbed by the material (Kikuchi & Uchida, 2011). Calorimetric ultrasonic power can then be calculated with Equation (3) (Tiwari et al., 2015).

$$P_{cal} = mC_p\left(\frac{dT}{dt}\right) \quad (3)$$

Where	P_{cal}	Calorimetric ultrasonic power, W
	m	Sample mass, kg
	C_p	Specific heat capacity of material, J/(kg·K)
	T	Temperature, K
	t	Time, s

Chemical dosimetry, on the other hand, involves the determination of radiation dose by irradiating a dosimeter, which is a chemical solution of a specific composition, and measuring the resulting chemical changes. Unlike calorimetry, chemical dosimetry is not a primary method for radiation dose measurement, but it is still widely considered a highly accurate and reliable method for many applications such as calibration of gamma irradiation chambers (Malathi et al., 2013).

The most established chemical dosimeter is the Fricke dosimeter, which contains $FeSO_4$ and NaCl in an aqueous H_2SO_4 solution (Izewska & Rajan, 2005). As the solution is irradiated, ferrous iron (Fe^{2+}) is oxidized into ferric iron (Fe^{3+}). Since there is no ferric iron present before irradiation, concentration of produced ferric ions can then be determined via spectrophotometry at 304 nm, where they absorb light but ferrous ions do not. This concentration corresponds to the amount of energy introduced by the radiation, or in the case of ultrasonic waves, effective ultrasonic power. Other chemical dosimeters include, for example, aqueous solutions of potassium iodide, saturated or dual-phase chloroform, and organic acids (Koda et al., 2003; Malathi et al., 2013).

A simple method for estimating the effectiveness of ultrasonication equipment is to treat a water sample with ultrasound (Feng et al., 2002). Water typically contains small amounts of dissolved nitrogen and oxygen, which do not normally react with each other. As a result of acoustic cavitation, however, they will form NO, which is then oxidized to NO_2, which further reacts with water to form HNO_2 and HNO_3. As a result, conductivity of the sample increases, and sonication effectiveness can be estimated by comparing conductivities of water samples before and after ultrasonication tests.

3.2.3 Acoustic attenuation

Attenuation refers to the gradual reduction in amplitude and intensity of a wave as it travels through a medium. Sound waves propagating forward in a gas or liquid phase can be attenuated through diffraction, refraction, scattering, reflection, or most importantly, absorption, where kinetic energy of the wave is converted into heat. Decreased ultrasound intensity can be calculated with Equation (4). (Mason & Lorimer, 1988)

$$I = I_0 e^{-2\alpha d_s} \qquad (4)$$

Where I_0 Intensity of ultrasound emitted by sound source, W/m^2

α Attenuation coefficient, m^{-1}

d_s Distance from sound source, m

While attenuation coefficient α derives from physical properties of the medium, it is also a function of frequency *f*: an increase in frequency also increases attenuation, and as a result higher frequency sound waves are less effective at penetrating media (Mason & Lorimer, 1988). For some media, such as pure water, the value of attenuation coefficient divided by square of frequency (α/f^2) has been shown to be constant at a given temperature, which allows for simple calculation of attenuation coefficients with different frequencies. These values are shown for selected media in Table 2.

Table 2 Attenuation coefficients divided by square of frequency for selected media. (Saito, 2015)

Medium	**α/f^2, 10^{-15} s^2/m**	**Temperature, °C**
Water	25	20
Methanol	34	20
Ethanol	52	20
Glycerol	493	22
Toluene	93	20
Acetone	104	24
Olive oil	1350	21.7

Mechanisms of attenuation in heterogeneous slurry-like mixtures containing small solid particles suspended in a liquid are not well known. Amarillo et al. (2019) experimented with the application of high-frequency ultrasound in an olive oil extraction system, which consisted of water, olive oil, and up to 2.4 wt% of solid olive paste. It was shown that increasing the solids content rapidly increased attenuation as well, indicating that scattering and reflection of sound waves due to contact with solids was the main source of attenuation in the system (Figure 7).

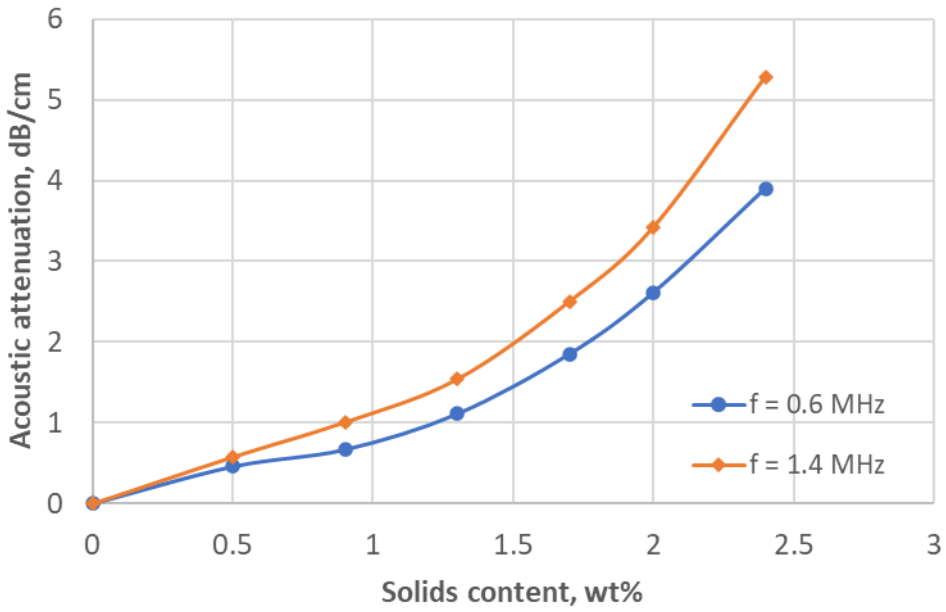

Figure 7 Attenuation of ultrasound measured in decibels per propagated centimeter in olive oils systems containing up to 2.4 wt% of solid olive paste. Data from Amarillo et al. (2019).

3.2.4 Acoustic impedance

Acoustic impedance of a medium is a measure of the mechanical resistance sound waves continuously meet as they propagate through it. It is defined as the product of density of the medium and speed of sound in the medium as shown in Equation (5) (Selfridge, 1985). Acoustic impedance is a highly important property when dealing with systems that contain phase boundaries. When sound waves reach a boundary, the impedance difference between

the two phases determine the fraction of energy reflected shown as in Equation (6) (NDT Resource Center, 2006).

$$Z = \rho c \tag{5}$$

Where Z Acoustic impedance, kg/(m^2·s)

ρ Density of the medium, kg/m^3

c Speed of sound in the medium, m/s

$$R = \left(\frac{Z_2 - Z_1}{Z_2 + Z_1}\right)^2 \tag{6}$$

Where R Reflection coefficient, -

Z_2 Acoustic impedance of phase 2, kg/(m^2·s)

Z_1 Acoustic impedance of phase 1, kg/(m^2·s)

An example of acoustic impedance in a water-steel system is shown in Figure 8.

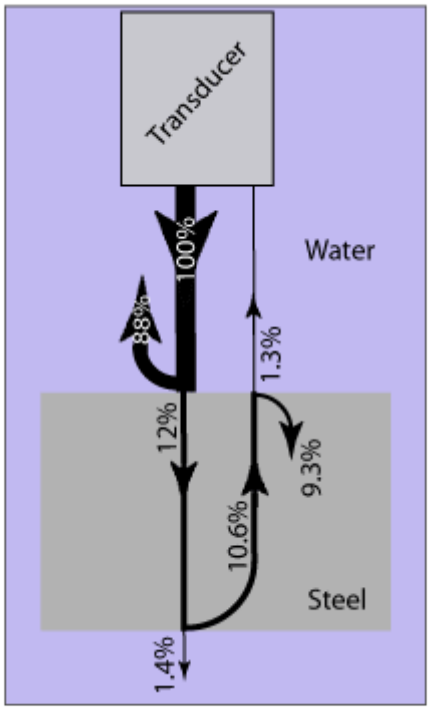

Figure 8 The effect of acoustic impedance when ultrasound passes through AISI 4340 steel submerged in water. System temperature is 20 °C. Acoustic attenuation is not taken into account. (NDT Resource Center, 2006)

In the example shown in Figure 8, an ultrasonic transducer submerged in water generates sound waves of a specific intensity. Acoustic impedances of water ($1.48 \cdot 10^6$ kg/(m^2·s)) and AISI 4340 steel ($46.2 \cdot 10^6$ kg/(m^2·s)) are fed into Equation (6), which gives a reflection coefficient of 0.88. Therefore, at the water-steel phase boundary, 88 % of the energy is reflected back due to the much higher acoustic impedance of steel. Of the remaining 12 % that is transmitted into the steel, 88 % is once again reflected at the steel-water boundary. As a result, even with no attenuation taken into account, only 1.4 % of the initially generated sound waves completely penetrate the steel.

Acoustic impedances of various media based on their respective densities and speeds of sound are shown in Table 3.

Table 3 Acoustic properties of various media (Saito, 2015; Selfridge, 1985).

Medium	**State**	**Density, g/cm^3**	**Speed of sound, m/s**	**Acoustic impedance, 10^6 kg/m^{2}s**
Air	Gas	0.0013	330	0.00043
Acetone	Liquid	0.79	1174	1.07
Aluminum	Solid	2.70	6420	17.33
Ethanol	Liquid	0.79	1180	0.93
Glass, Pyrex	Solid	2.24	5640	13.10
Glass, silica	Solid	2.20	5900	12.98
Glycerol	Liquid	1.26	1920	2.42
Methanol	Liquid	0.79	1120	0.88
Olive oil	Liquid	0.90	1380	1.24
Polyethylene (PE)	Solid	0.90	1950	1.76
Polypropylene (PP)	Solid	0.89	2660	2.36
Steel, SS 347	Solid	7.89	5790	45.68
Teflon (PTFE)	Solid	2.14	1390	2.97
Titanium	Solid	4.48	6100	27.33
Water, 20 °C	Liquid	1.00	1480	1.48

By recalculating the example shown in Figure 8 using a better compatible pair of materials, such as Pyrex glass (Z = $13.10 \cdot 10^6$ kg/(m^2·s)) and glycerol (Z = $2.42 \cdot 10^6$ kg/(m^2·s)), reflection due to impedance changes greatly. Reflection is then 47.4 % at each phase boundary, and without attenuation, 24.9 % of the acoustic energy passes through the solid glass.

3.3 Optimization of cavitation phenomena

To produce acoustic cavitation bubbles, ultrasonic irradiation must have enough energy to pass a so-called cavitation threshold which is determined by the physical properties of a multiphase system (Gogate & Pandit, 2004). Furthermore, cavitation bubbles can be categorized into violently imploding transient bubbles and non-collapsing stable bubbles, but only transient bubbles and their high-energy implosions are typically desirable for the UAE applications. Like the cavitation threshold, whether bubbles are formed as stable or transient is also determined the properties of the system, and usually high intensities and low frequencies are required to produce transient bubbles (Gogate & Pandit, 2004). Effects of various properties on cavitation phenomena are shown in Table 4.

Table 4 Effects of various properties on cavitation phenomena (Gogate & Pandit, 2004; Pingret et al., 2013)

Property	Affected phenomena	Preferable value
Ultrasound intensity	Intensity of bubble collapse, number of bubbles	High enough to produce intense cavitation, low enough to not damage equipment or products
Ultrasound frequency	Attenuation, collapse time of bubbles, intensity of bubble collapse	Optimum varies by medium, usually low
Temperature	Physical properties, reaction rates, intensity of bubble collapse, cavitation threshold	As low as possible, but high enough to reach desired product yield
Viscosity	Cavitation threshold	Low
Surface tension	Cavitation threshold	Low
Vapor pressure	Reaction rates, cavitation threshold, intensity of bubble collapse	Low
Dissolved gas solubility	Gas content in medium, cavitation threshold	Low
Dissolved gas properties	Intensity of bubble collapse	Low thermal conductivity and high polytropic constant (monoatomic gases)

Out of the properties shown in Table 4, ultrasound intensity and frequency are limited by ultrasonication equipment, and as such they are not always the most convenient properties to adjust – it may not be desirable to purchase and install different equipment for every new extraction application. Process temperature, on the other hand, is easy to adjust and has a major impact on extraction, but when dealing with natural products, it is often limited by thermolabile compounds. The remaining properties in the table are all directly related to the

solvent used, which underlines the importance of solvent selection. However, even if a potential solvent has physical properties favorable to UAE, solvent applicability for a given system is still limited by various factors, such as safety, selectivity, and extractive solubility. Therefore, extraction optimization in practical applications should be started by screening potential solvent options.

4 ASPECTS OF TECHNOLOGICAL SOLUTIONS FOR UAE

Extraction processes for plant-based raw materials can typically be simplified to consist of three distinct steps: Material pre-treatment prior to extraction, followed by the actual extraction step, which then leads to a solid-liquid separation step where extracts are separated from the solid matrix of the raw materials. UAE mainly differs from other extraction methods at the extraction step, which is naturally characterized by the usage of ultrasound, but it is not always technologically straightforward to introduce ultrasonication to a reaction system.

4.1 Pre-treatment of raw materials

In any solvent extraction process, it would be desirable to have the raw material consisting solely of particles of uniform size and composition in order to maximize extractive acquisition from each particle, leading to extracts of high and stable quality. In practice this is, of course, impossible to achieve, and the purpose of raw material pre-treatment is to find a balance between this goal and practical feasibility.

Conventional pre-treatment methods include disintegration and drying. In disintegration, the goal is to break down raw materials into small particles with a consistent and preferably narrow particle size distribution (PSD). The particles are simultaneously mixed, which homogenizes the material further. For small scale applications, disintegration can be done in batches by simple kitchenware, such as mortar and pestle, knives, and blenders, while larger scales of production require automated processing equipment, such as knife mills, ball mills, or hammer mills. It is also important to consider raw material hardness – hard materials,

such as some seeds and bracket fungi, may require crushing while softer materials, such as plant leaves and berries, may need to be cut and shredded instead.

In drying, moisture is removed from the raw materials with the goal of producing feed with a constant composition. There may also be additional goals, such as reducing the total feed mass or minimizing the amount of water in the reaction matrix. Drying is conventionally done by thermal or mechanical methods, using equipment such as industrial ovens and screw presses.

It is also possible to pre-treat raw materials with methods similar to those used in novel, intensified extraction procedures. Namely ultrasound, pulsed electric field, or enzymes, which can be used to rupture plant cells or increase cell permeability during the extraction step, can also be applied to a similar effect during the pre-treatment stage (Zhao et al., 2014). Other cell disruption methods during pre-treatment include blanching, where the material is rapidly heated and then cooled, rapid depressurization of CO_2, where cells are saturated with pressurized gas which is then rapidly depressurized, and freeze-thawing, where cells are damaged by formation and melting of ice crystals (Aggarwal & Jain, 2019; Zhao et al., 2014).

4.2 Generation of ultrasound

In addition to extraction, ultrasound has found use in a variety of chemical engineering applications, such as degassing, crystallization, filtration, and dispersion of solids (Mason & Lorimer, 1988). Naturally, it follows that numerous different process configurations for the application of ultrasound have been devised. With few exceptions, they rely on the same principle for ultrasound generation, which involves the use of an electrical generator, a transducer, and an emitter (Bermúdez-Aguirre et al., 2011).

An electrical generator serves as the power source for ultrasound generation. It produces a set and constant amount of electrical energy and feeds it to the transducer, which converts the energy into sound waves via high-speed mechanical vibrations. The most efficient and commonly used transducers are electromechanical, and function based on the piezoelectric

or magnetostrictive effect (Bermúdez-Aquirre et al., 2011; Knorr et al., 2004; Mason & Lorimer, 1988). The generated sound waves are then radiated into the surrounding system by an emitter.

Typical laboratory scale emitter configurations can be categorized into ultrasonic baths and ultrasonic horns (Bermúdez-Aquirre et al., 2011). In the bath configuration, transducers are directly attached to the walls of a bath vessel filled with water. A separate reaction vessel is placed in the bath, and the sample inside is ultrasonicated through the water bath and vessel walls. The horn configuration, on the other hand, involves placing an ultrasound-emitting horn, or probe, directly into the reaction vessel. The sound-emitting tip of the probe, a sonotrode, then radiates ultrasonic waves into the sample medium. Different configurations are shown in Figure 9.

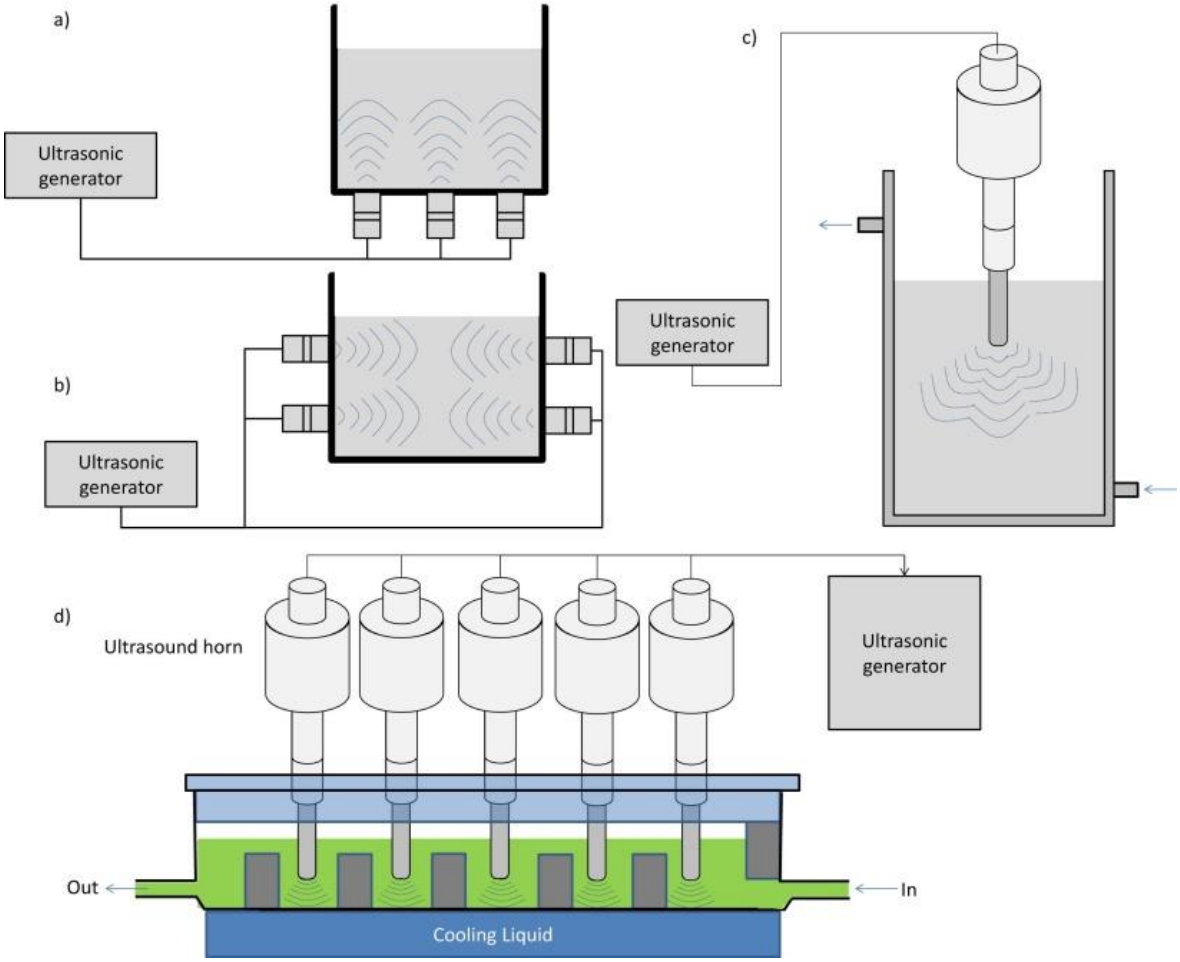

Figure 9 Ultrasonic emitter configurations: a) and b) Ultrasonic bath; c) Ultrasonic horn; d) Multi-horn with continuous operation. (Tiwari et al., 2015)

In comparison to ultrasonic baths, horn configurations are capable of emitting significantly higher amounts of ultrasonic power not only because the sonotrode is directly immersed into the sample, but also because the horn functions as a mechanical amplifier. Consequently, however, the sonotrode itself is subjected to the intense conditions of acoustic cavitation. Titanium alloys are typically used in horn manufacturing because they are chemically inert, have high fatigue strength, and do not excessively contribute to acoustic attenuation (Mason & Lorimer, 1988). Degree of sound amplification depends on the shape of the horn used, and intensity of sound emitted is determined by the area of sonotrode tip (Equation 1). Basic horn shapes are shown in Figure 10 and main advantages and disadvantages of ultrasonic baths and horns in Table 5.

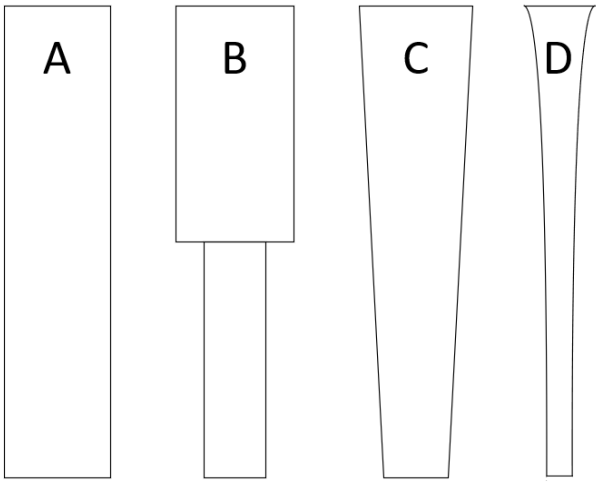

Figure 10 Basic ultrasonic horn shapes. A: Cylindrical; B: Stepped; C: Conical; D: Exponential taper.

Table 5 Advantages and disadvantages of ultrasonic bath and horn configurations. (Chemat et al., 2017; Mason & Lorimer, 1988)

	Ultrasonic bath	**Ultrasonic horn**
Advantages	- More uniform energy distribution - Simple and low-cost solution - Multiple samples may be processed simultaneously	- Potential to use higher powered ultrasound - Sonication intensity adjustable by horn shape
Disadvantages	- Limited in power - Ultrasonic attenuation by water bath and reactor walls - Ultrasonic intensity affected by location of reaction vessel in the bath	- Possible erosion of sonotrode leading to decreased performance and release of metal particles to the sample - Uneven energy distribution: high intensity near the horn tip may produce unwanted radical species

4.3 Considerations in UAE upscaling

In the wide variety of laboratory scale UAE experiments reported in literature (Pingret et al., 2013; Shirsath et al., 2012), equipment used include ultrasonic baths, ultrasonic horns, and more recently, specialized reactors that aim to overcome the negatives of these setups by the attachment of transducers directly on the walls of a jacketed reaction vessel. However, even though the results have been excellent in many cases, reports of successful large-scale tests are significantly less numerous, which hints at complications in the scale-up process. As listed by Gogate et al. (2015), knowledge from the fields of chemical engineering, material engineering, as well as acoustics is required for designing efficient large scale sonochemical reactors. Optimized reactor geometry and transducer setup are essential for the uniform ultrasonication of raw materials. In commercial use, it would also be desirable to achieve uniform processing in continuous operation.

4.3.1 Distribution of cavitational activity

In any sonochemical process, it is essential for cavitational activity to be evenly spread in the reaction vessel in order to avoid formation of dead zones and ensure high process efficiency (Gogate & Pandit, 2015). While this is relatively simple to achieve with laboratory

scale reactors due to small processing volumes, it is less so at pilot or industrial scale, where the importance of reactor geometry and transducer setup increases.

Several experimental methods have been proposed for the mapping of cavitation inside a reactor. Hydrophones or thermocouples can be set in different locations of the reactor to measure the distribution of acoustic pressure or temperature, respectively, which correlate to the intensity of cavitation at a given location (Gogate & Pandit, 2015). With a sufficient amount of measurements, an understanding of the distribution of cavitation may then be gained. Another method involves the use of regular aluminum foil (Avvaru & Pandit, 2009; Servant et al., 2001). In this method, the foil is fixed in the reactor and subsequently perforated by cavitation. The extent of damage at different positions on the foil then corresponds to cavitational activity.

Sonochemiluminescence, meaning the emission of light from a chemical reaction initiated by ultrasound, has also been used to investigate cavitational activity. Luminol, for example, is a well-known chemiluminescent reagent that emits blue light when oxidized by OH^- radicals produced by ultrasonication in an alkaline aqueous solution (Gogate & Pandit, 2015). Therefore, experiments can be done with such solutions and intensity of emitted light in different locations of the reactor can be observed with the help of photography (Servant et al., 2001). Another approach is to fix separate test tubes containing samples of a chemiluminescent reagent solution in different locations of the reactor (Hu et al., 2008). After ultrasonication, reagent samples which were subjected to more intense cavitation will emit more light, and the intensity of chemiluminescence can be measured and compared between the samples. A similar type of approach could be applicable for chemical dosimeters as well.

4.3.2 Change of reactor processing mode from batch to continuous

The advantages of continuous operation over batch operation, such as smaller equipment sizes, improved and more uniform product quality, lower downtimes, and less operating costs, are well known in the chemical process industry (Boodhoo & Harvey, 2013). Even so,

batch operation has been used in most of the UAE studies found in literature, likely due to its simplicity and economic feasibility in small scale applications.

Batch and continuous UAE were compared in pilot scale by Alexandru et al. (2013), who studied UAE of phenolics from clove buds with batch and flow reactors. Processing capacity with both configurations was 20 L in 45 min. Batch extraction was done in a mechanically agitated, cylindrical 25 L reactor equipped with an ultrasound-generating plate attached to the bottom. Continuous flow experiments were performed in a multi-horn flow reactor (Figure 9d) with four horns. The raw material suspension was pumped through the reactor one, two, or three times by adjustment of flow rate so that residence time was kept constant. It was found that multiple loops through the reactor gave higher extraction yields, and yields gained with three loops exceeded batch yields in all tests.

4.4 Solid-liquid separation

A natural product extraction procedure typically produces a slurry which consists of liquid solvent containing the extracted solutes and solid plant matter from which the solutes were retrieved. The next step is then to separate the solids from the mixture. In the case of sludges and slurries, conventional methods of solid-liquid separation include thermal drying and mechanical dewatering, such as compression and filtration (Mahmoud, 2013). However, mechanical methods struggle with fine particle sizes and remove only free water (Mahmoud, 2013), while thermal drying is energy-intensive and often inapplicable for natural product matrices due to degradation of the products. As such, separation methods assisted by phenomena such as electro-osmosis have been proposed.

4.4.1 Electro-osmotic dewatering

Electro-osmotic dewatering (EOD) is a solid-liquid separation method in which water is removed from a solid matrix by the application of an external electric field. The field is generated by packing the slurry in between of two electrodes and applying a direct current (DC) voltage between them. Negatively charged species in the solid matrix migrate towards

the cathode, and are thus released from the solids into the water. The electrodes are set up so that the cathode pulls water out of the system through a filter (Orsat et al., 1996).

Unlike conventional mechanical dewatering, EOD is able to remove some of the water bound inside solid particles, resulting in more effective water removal (Mahmoud, 2013). However, a major drawback of EOD is that as the top of the solid bed dries up, its electrical resistance increases greatly, and as a result plenty of water remains in the lower sections of the bed (Mujumdar & Yoshida, 2008). Therefore, EOD is usually combined with mechanical compression, which is capable of dewatering the bottom parts of the bed (Mujumdar & Yoshida, 2008; Menon et al., 2019; Orsat et al., 1996). This is illustrated in Figure 11.

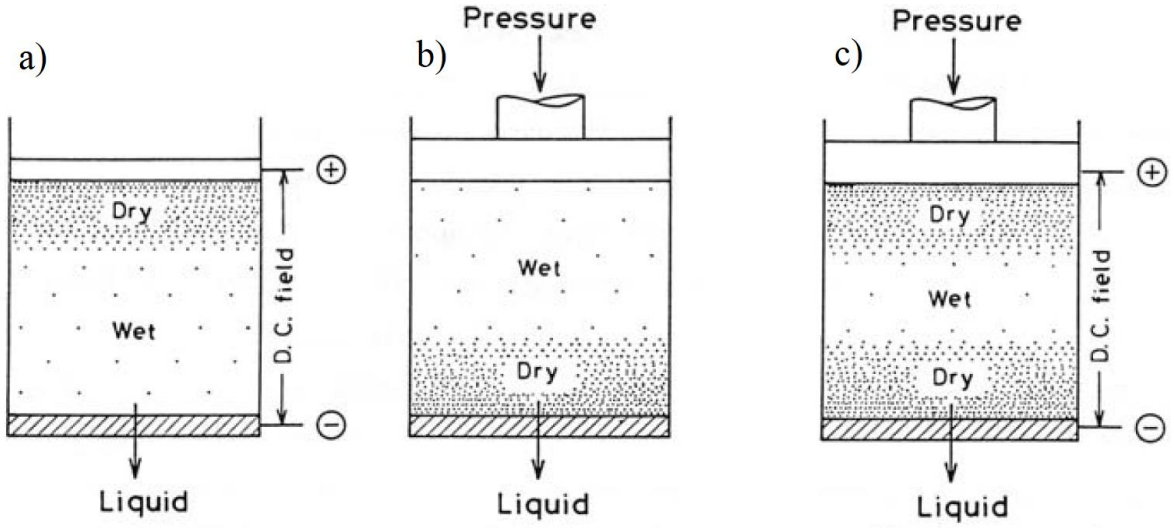

Figure 11 Displacement of moisture in a solid bed during dewatering. a) Electro-osmotic dewatering; b) Mechanical compression; c) Electro-osmotic dewatering combined with mechanical compression. Modified from Mujumdar & Yoshida (2008).

In a study by Menon et al. (2019), EOD was used in the drying of yogurt, orange pulp, and egg whites. It was found that with compared to thermal drying, over 80 % reductions in energy consumption and carbon emissions could be achieved. Similar results, with energy consumption reductions of up to 60 times, were reported by Ng et al. (2011) in a study where EOD combined with mechanical compression was used for food waste.

4.5 Process configurations

In the 21st century, several novel ultrasonication configurations have already been designed with scalability and continuous operation in mind and demonstrated in pilot scale. This paints a promising picture for the future of ultrasound as a method of process intensification, as the technology has already been proven in a plethora of applications in laboratory scale, and scale-up has thus far been the limiting factor for large scale applications.

4.5.1 Multi-frequency flow cell and longitudinal horn setups

Sivakumar et al. (2002) developed a dual-frequency system which had a volume of 1.5 L and consisted of a flow cell flanked by three transducers on each side. The transducers of one side operated with a frequency of 25 kHz and the ones on the other side with a frequency of 40 kHz. The system was used for sonochemical degradation of *p*-nitrophenol, and it was concluded that the dual-frequency setup was more effective than traditional horn and bath, as well as the same flow cell operated with a single frequency of either 25 or 40 kHz. Gogate et al. (2003) took this idea further and developed a triple frequency flow cell system with a capacity of 7.5 L and a total of 18 transducers. The system was tested in the sonochemical decomposition of potassium iodide and degradation of formic acid with frequencies of 20, 30, and 50 kHz, and it was found that using all three frequencies combined gave the best results. Schematic of a triple frequency flow cell is shown in Figure 12.

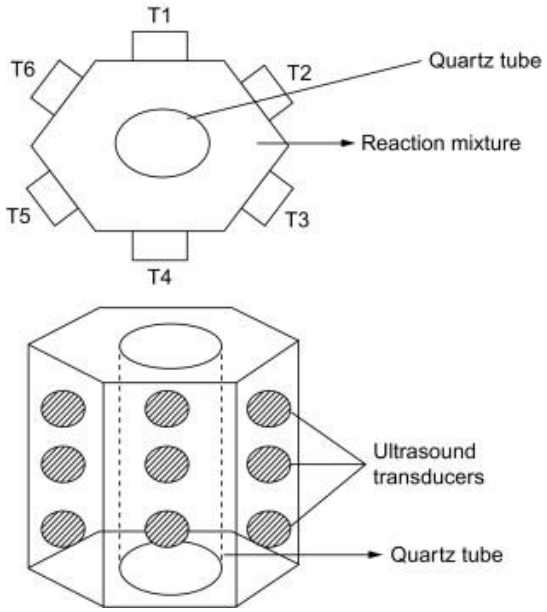

Figure 12 Schematic of a triple frequency flow cell. T = set of three transducers. (Gogate & Pandit, 2015; Gogate et al., 2003)

Bhirud et al. (2004) took a different type of approach and designed a reactor with a longitudinally vibrating ultrasonic horn at the bottom (Figure 13). The system had a capacity of 7 L and, operated at 36 kHz, was tested in the degradation of formic acid. The results were compared with previous experiments with other ultrasonication configurations. This comparison is shown in Figure 14.

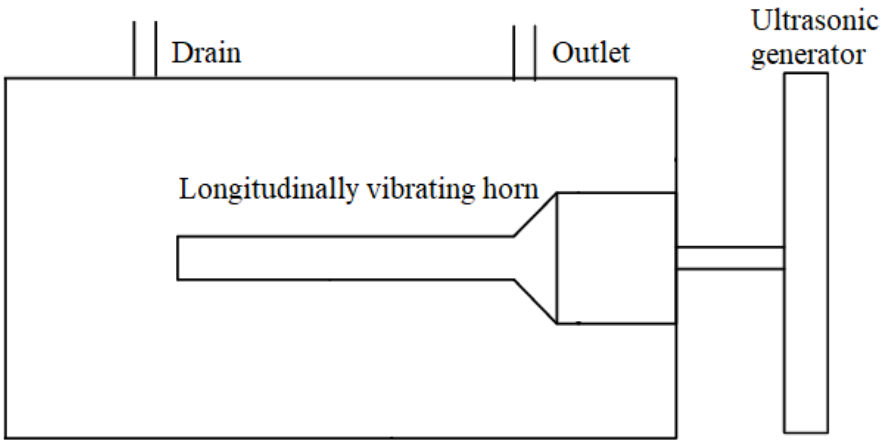

Figure 13 Topside view schematic of a reactor with a longitudinally vibrating horn. Drain and outlet are at different heights to allow for continuous operation. Modified from Bhirud et al., 2004.

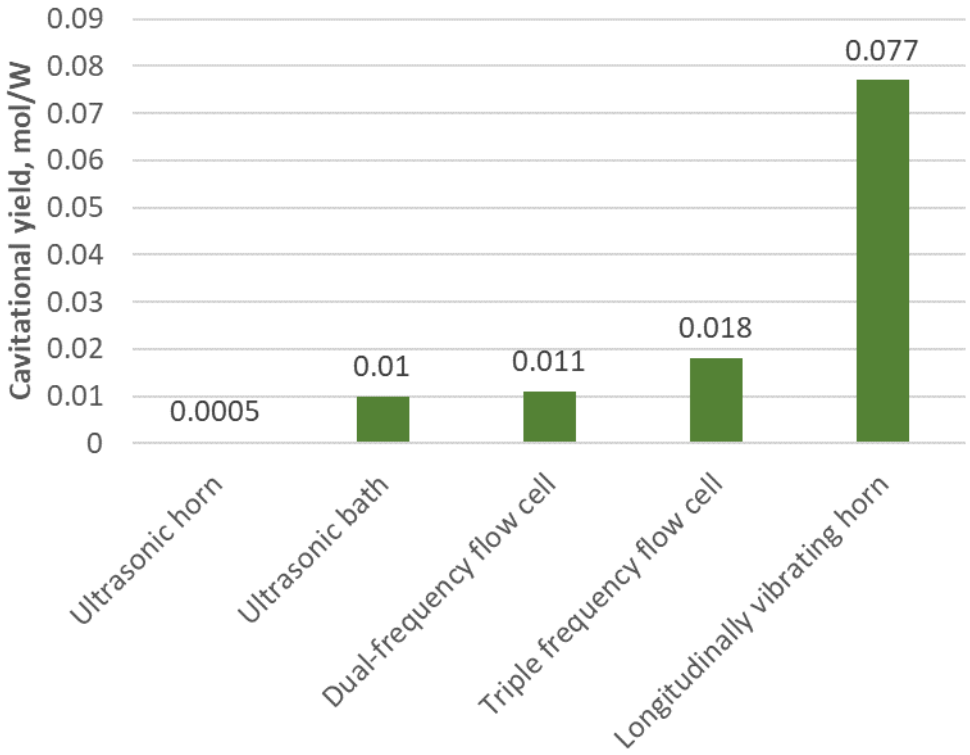

Figure 14 Efficiency of formic acid degradation with different ultrasonication configurations. Initial acid concentration was 500 ppm and sonication time was 1 h. Cavitational yield = net degradation of formic acid [mol/L] divided by density of supplied electric power for ultrasound generation [W/L]. Data from Bhirud et al., 2004.

As is evident from Figure 14, the longitudinal horn setup shows excellent results for formic acid degradation in comparison to bath, horn, and flow cell setups. However, it is worthwhile to consider that the longitudinal horn has a relatively large vibrating surface area and thus low ultrasonic intensity, which may limit its use in applications with high intensity requirements. Another thing to note is that the ultrasonic bath configuration used in the experiments was not a traditional bath with a separate reaction vessel, but instead the reaction medium was contained directly in the bath vessel, which effectively excluded attenuation due to reactor walls and bath water from the investigation.

Kumar et al. (2007) evaluated the cavitational distribution in the triple frequency flow cell and longitudinal horn setups by measuring acoustic pressure distribution with a hydrophone. In the tests it was found that both setups had similar pressure variations in the range of 10-

30 % throughout their respective sonication chambers. The results were highly promising in comparison to traditional ultrasonic horn setup, which has been measured to have pressure variations of 80-400 % near the horn tip alone (Kanthale et al., 2003). The study came to the conclusion that flow cells and longitudinal horns are suitable technologies for upscaling.

Sutkar et al. (2010) later replicated the experiments conducted by Kumar et al. (2007) and Kanthale et al. (2003) for traditional horn and longitudinal horn by numerical simulation using COMSOL Multiphysics -software. The simulation results were in accordance with experimental measurements – ultrasonic horn showed a high-intensity area that rapidly faded as distance to the horn tip increased, while longitudinal horn showed cavitational activity throughout the reactor.

The effectiveness, or lack thereof, of traditional horn setup was further investigated by Groznova (2014) in the form of modelling the flow velocity caused by acoustic cavitation and streaming in water and non-Newtonian carboxymethyl cellulose (CMC). The study found that in water, streaming mostly affected the area directly below the horn tip, with minor flow occurring along the reactor walls (Figure 15). In CMC, on the other hand, the acoustic pressure dissipated almost immediately upon exiting the horn (Figure 16). The simulation results were validated with experimental particle image velocimetry (PIV) measurements, which were well in line with the simulations.

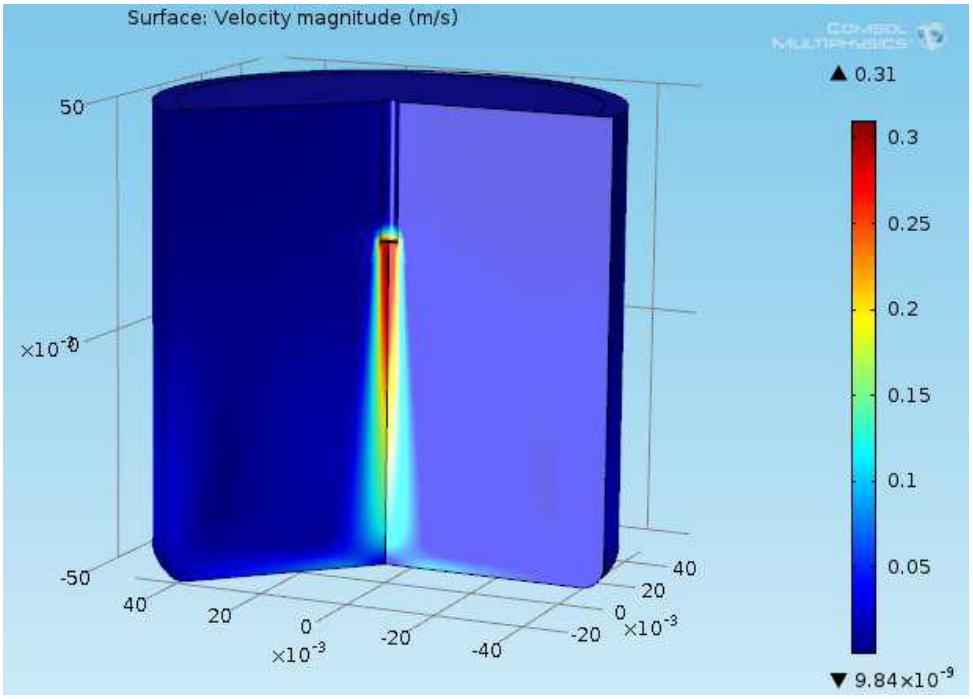

Figure 15 Simulation of flow velocity in water caused by ultrasonication with ultrasonic horn and calorimetric power of 7.18 W. (Groznova, 2014)

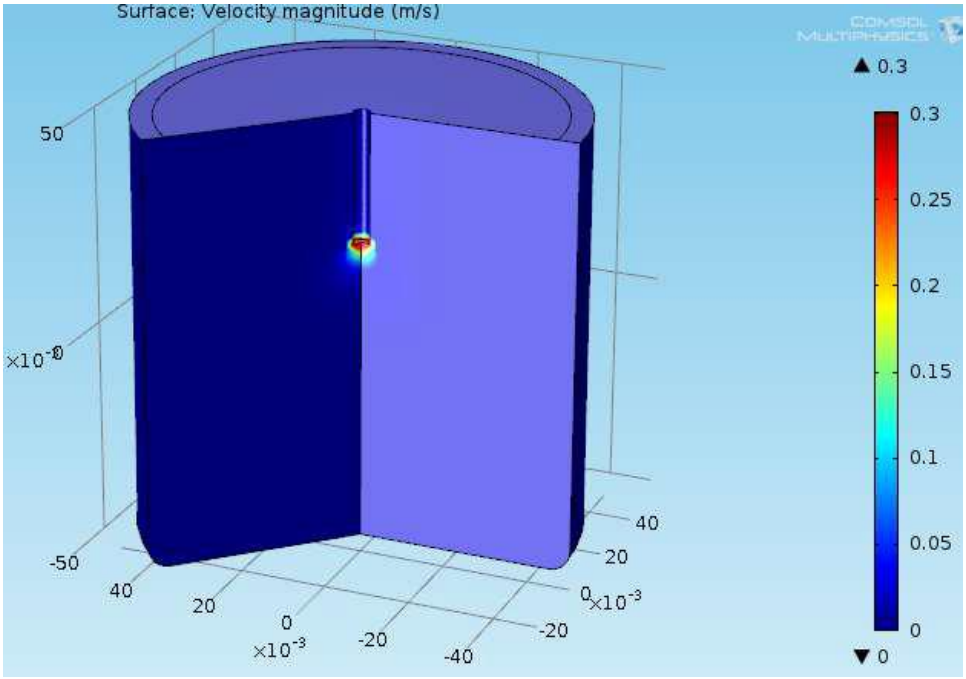

Figure 16 Simulation of flow velocity in carboxymethyl cellulose caused by ultrasonication with ultrasonic horn and calorimetric power of 7.18 W. (Groznova, 2014)

4.5.2 Pilot process examples

Nickel and Neis (2007) designed a 29 L flow reactor for high-intensity ultrasonic disintegration of bacterial cells from sewage sludge. The reactor is equipped with five horns, and its geometry ensures that the feed travels through areas close to the sonotrode tips (Figure 17). In experimental tests, the setup achieved a degree of cell disintegration of up to around 40 %, while the corresponding value was around 20 % a single horn in laboratory scale mixed vessel.

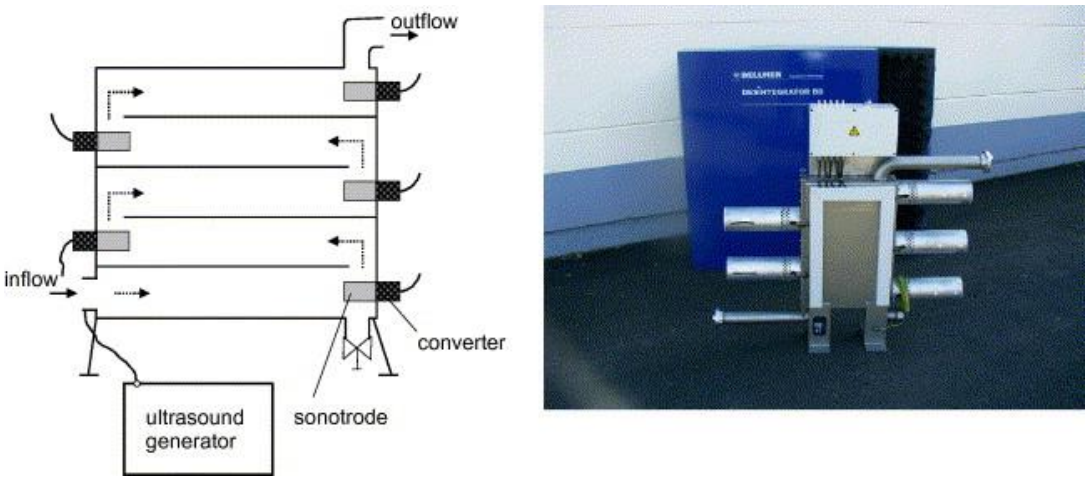

Figure 17 Schematic view and a photograph of a flow reactor equipped with five ultrasonic horns. (Nickel & Neis, 2007)

Cintas et al. (2010) presented a pilot scale ultrasonication flow reactor and used it for the synthesis of biodiesel. The ultrasonication chamber of this design has a volume of 0.5 L contains three transducers at the chamber walls and air cooling is used. The design also includes a 5 L mixing tank, from which the reactants are pumped into the sonication chamber. A schematic is shown in Figure 18.

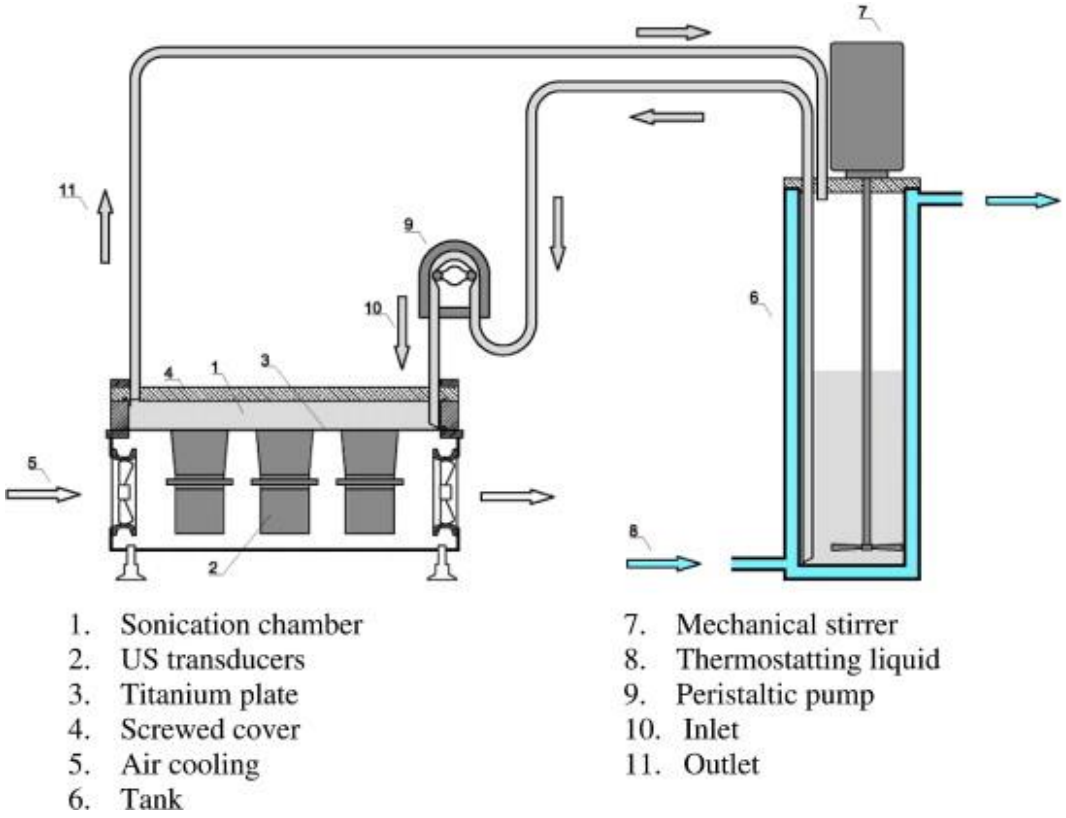

Figure 18 Schematic for a pilot scale ultrasound flow reactor. (Cintas et al., 2010)

4.5.3 Industrial examples and commercially available equipment

While there are a few examples of successful ultrasound application in the food industry, the companies involved do not, quite understandably, spread much technical information about their processes for everyone to see.

G. Mariani & C. S.p.A., a company based in Italy, produces extracts, infusions, and distillates with pleasant flavors and fragrances by UAE of aromatic herbs and spices. Reportedly, the use of ultrasound decreases the necessary amount of extraction cycles and therefore extraction time (G. Mariani & C. S.p.A., 2013). Another Italian company, Giotti, uses 500 L batch reactors for the UAE of plant matter in the production of alcoholic beverages, natural flavors, and emulsions for soft drinks (Mason et al., 2015). Yet another Italian company, Moliserb s.r.l, uses UAE of plant matter to produce extracts that are then used in the production of pharmaceuticals, cosmetics, and food flavorings (Moliserb s.r.l, 2003).

Hielscher Ultrasonic Technology (2020b) offers commercial ultrasonicators for industrial use. The design consists of a flow cell containing a longitudinally vibrating sonotrode. The units can handle maximum flow rates of 12.5 m^3/h and can be clustered for larger production volumes. Nominal ultrasonication powers of up to 16 kW are available. Industrial Sonomechanics LLC (2020) offers a more traditional design where the tip of an ultrasonic horn is placed in a small flow cell. With the design, processing rates from 0.05 to over 0.25 m^3/h can be handled, depending on the required ultrasonication time.

EXPERIMENTAL PART

5 AIM OF THE EXPERIMENTAL WORK

The main objective of the experimental part was to upscale a laboratory scale batch process for the UAE of valuable plant compounds into a continuously operating pilot reactor superior to conventional extraction processes. Extraction tests were first done at laboratory scale with the goal of selecting operating parameters for pilot scale experiments. The pilot scale experiments were then carried out in different conditions using two different reactor designs, and the UAE results were compared with conventional extraction results.

5.1 Selection of raw material and solvent

Though there were multiple potential options, the extraction process selected to be used in this work was the extraction of chlorophylls from fresh spinach. Chlorophylls, best known for their essential role in photosynthesis, are commonly applied as green food coloring additives, and have also shown potential for medical applications, such as cancer treatment (Mishra et al., 2011). Spinach was selected due to its soft leaf matrix, which is easily damaged by shear stress, and its high chlorophyll *a* and *b* contents. In degradation kinetics experiments, thermal degradation of chlorophylls has been observed at temperatures of over 60 °C (Weemaes et al., 1999; Corina & Buruleanu, 2017; Van Loey et al., 1998).

While chlorophylls are liposoluble and insoluble in water, they are soluble in ethanol and ethanol solutions (Henry, 2011). Ethanol has many favorable qualities as a solvent, as it is inexpensive, easily available, easy to handle, and on the list of Generally recognized as safe (GRAS) substances (U.S. Food and Drug Administration, 2019). For these reasons, ethanol solutions were selected for use as solvents in the extraction experiments.

6 MATERIALS AND METHODS

6.1 Materials

Analytical grade acetone (100 %, VWR) or ethanol (100 %, VWR) were used to dilute extract samples for analysis. Technical grade ethanol (92.4 %, Altia Industrial) was used to prepare the ethanol-based solvents used in extraction. Technical grade glycerol (97 %, VWR) was used to prepare the cooling fluid for the ultrasonication reactors. Tracer solution for residence time measurements was prepared using KCl (99.5 %, Riedel-de Haën). Spinach (*Spinacia oleracea*) leaves used in the extraction experiments originated from Spain, Italy, Sweden, and Finland, and were purchased from local grocery stores in Lappeenranta, Finland.

6.2 Experimental setup

6.2.1 Laboratory scale setup

Laboratory scale experiments were carried out in a jacketed cylindrical glass reaction vessel (SONOPULS KG 5: inner diameter 35 mm, inner height 95 mm). Ultrasound was produced by an ultrasound generator, Hielscher UP400St (f = 24 kHz, www.hielscher.com), and emitted using a cylindrical ultrasonic horn type sonotrode (Hielscher H22, d = 22 mm), the tip of which was submerged in the sample. Sample temperature was monitored with a temperature probe, which transmitted temperature data to the ultrasound generator. A nitrogen hose was fixed to the top of the vessel and used during experiments to provide nitrogen flow over the sample surface in order to maintain nitrogen atmosphere in the vessel,

preventing oxidation of the products. Temperature of the cooling water was maintained by a thermostat unit (LAUDA RC6CP, www.lauda.de). A schematic view and a photo of the laboratory setup are shown in Figures 19 and 20.

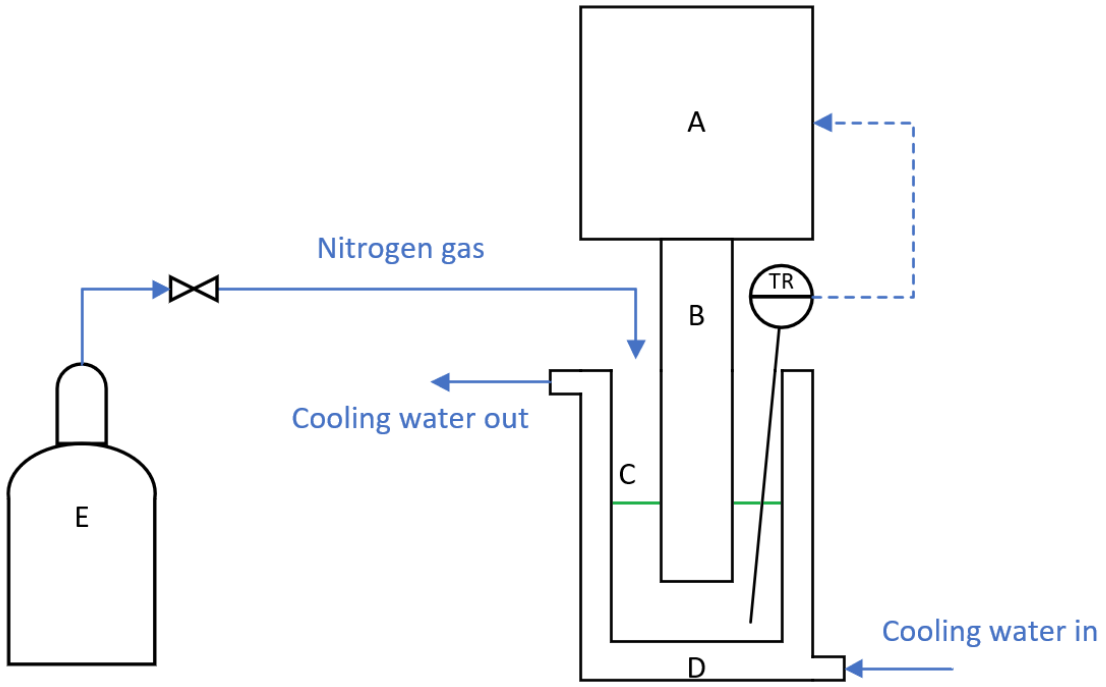

Figure 19 Schematic view of the laboratory UAE setup. A: Ultrasound generator; B: Cylindrical ultrasonic horn; C: Reaction vessel; D: Cooling jacket; E: Nitrogen gas tank; TR: Temperature recorder.

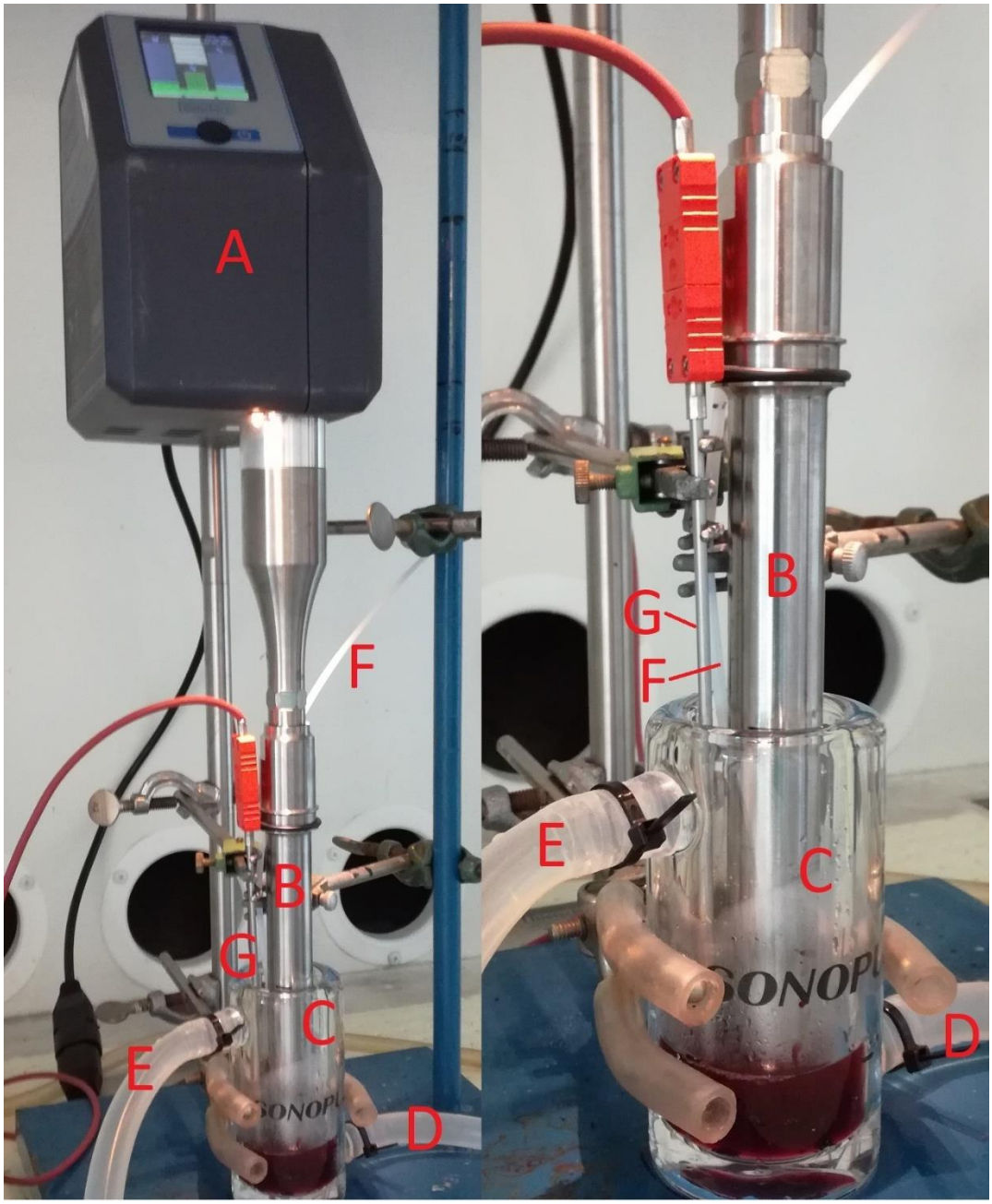

Figure 20 Photograph of the laboratory setup used (left) and a close-up on the reaction vessel (right). A: Ultrasound generator; B: Ultrasonic horn; C: Reaction vessel; D: Cooling jacket inlet; E: Cooling jacket outlet; F: Nitrogen hose; G; Temperature probe.

6.2.2 Pilot scale setup

In the pilot scale setup, a jacketed cylindrical glass vessel (V = 3 L, d = 15.9 cm, h = 25.2 cm) with a curved bottom functioned as the feed tank. Temperature of the feed tank was maintained via circulating water through the jacket of the tank. A thermostat (LAUDA ECO RE 630) controlled the temperature of the circulating water. In addition, the feed tank was equipped with a mechanical mixer, which was equipped with a pitched blade turbine (d = 9 cm) with four blades (2.4 x 3.0 x 0.4 cm) at 45° angle. A nitrogen hose was also fixed over the solution surface at the top of the feed tank.

The feed was pumped through the ultrasonication module using a hose pump (Flowrox LPP-D15, www.flowrox.com). The module was a cylindrical stainless steel tube (d_o = 14 cm, L = 101.6 cm) filled with circulating heat transfer fluid, a longitudinally vibrating sonotrode (Weber Sonopush Mono, d = 5 cm and L = 89.1 cm for the oscillating body, www.weber-ultrasonics.com), and a reaction tube made of stainless steel and coiled around the sonotrode. Ultrasound generator used was Weber Ultrasonics Sonic Digital MG2000-SD25, which radiates sound waves at 25 kHz, at nominal powers up to 2000 W. LAUDA WK4600 thermostat was used to maintain constant temperature in the flow cell module. Reactor and jacket outlets were equipped with temperature probes for monitoring purposes.

Two different ultrasonication module designs, henceforth referred to as modules A and B, were used in this work. The main difference between these designs was inner diameter of the coiled reaction tube, which was 18 mm for module A and 8 mm for module B. This caused differences in the volume of the reaction tube, which was 0.98 L for module A and 0.8 L for module B. In addition, the coiled reaction tube was closer to the sonotrode in module A. Finally, a minor difference between the modules was outlet orientation – in module A, inlet and outlet were on opposing sides of the ultrasonication module, but in module B the reaction tube was looped back to the inlet side after the ultrasonicated section. Surfaces of module A were also insulated with polyethylene foam. A schematic of module A and a flow diagram of the pilot process are shown in Figures 21 and 22.

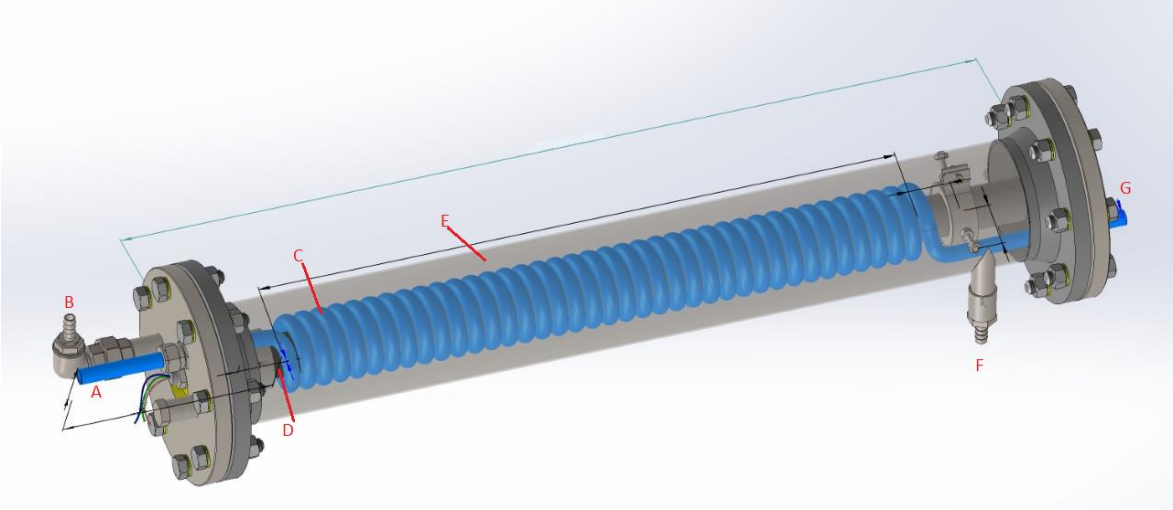

Figure 21 Schematic of ultrasonication module A. A: Reactor inlet, B: Jacket outlet, C: Reaction tube, D: Transducer, E: Reactor jacket, F: Jacket inlet, G: Reactor outlet.

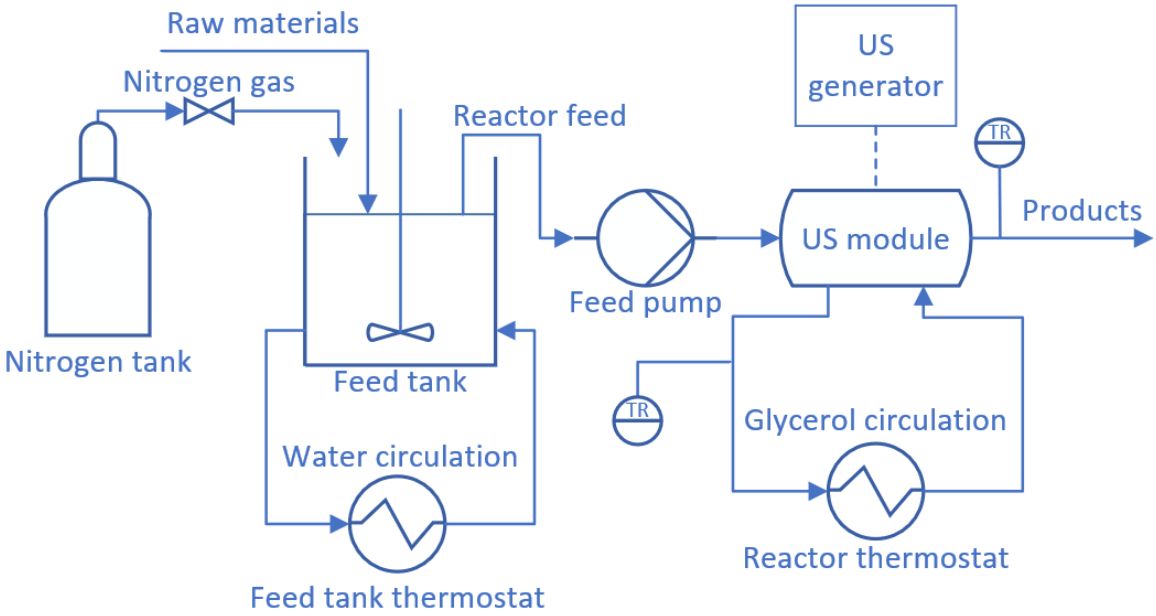

Figure 22 Flow diagram of the pilot UAE process.

Glycerol was used as the reactor heat transfer fluid due to its acoustic impedance being higher than that of water (see Table 3), thus resulting in higher sound energy transmittance through steel: As calculated according to Equation (6), 23.5 % of sound energy is transmitted through a phase boundary between pure glycerol to steel, while the corresponding value for water-steel systems is 12 %. However, as the 97 % glycerol used had a high freezing point (18.6 °C) and viscosity (1412 mPa·s at 20 °C), it was diluted 4:1 with water in order to

prevent sluggish flow and crystallization in the jacket. This resulted in a solution of 78 wt% glycerol, with an approximate freezing point and viscosity of -20 °C and 49 mPa·s at 20 °C, respectively (Dean, 1999; Takamura et al., 2012).

6.3 Experimental procedures of applied methods

After the pilot modules were assembled, their operation was first tested with flow rate measurements. Performance of the feed pump was simultaneously evaluated. Residence times were measured for module A with and without ultrasound, and the results were compared to earlier experiments for module B conducted by Ezeanowi et al. (2020). A raw material pretreatment procedure was also established, and the effect of storage time on disintegrated spinach was investigated. Extraction tests were then done first with laboratory scale equipment and later with pilot equipment. In addition, calorimetric measurements were done with the laboratory scale setup, and calorimetric powers were later estimated for the pilot modules based on temperature data from the extraction experiments. The calorimetric results are presented in Appendix 1.

6.3.1 Measurement of pump flow rate

Stability of the pump performance was evaluated by pumping tap water through the modules with at different pumping speeds. Pump motor speed was controlled by a variable-frequency drive, which was used to adjust motor frequency in the range of 0-100 Hz. The volumetric flow rates were measured by collecting and weighing the outflow over a set time within 1-5 minutes. Each experiment was repeated three times with both modules A and B. The temperature of water was kept at 18 ± 2 °C, and as such density of 998.6 kg/m^3 was used in mass-to-volume conversion.

6.3.2 Residence time measurements

Using the measured pump flow rates, residence times with different pump settings were calculated for the modules. The residence times were then confirmed by experimental step tracer measurements. Residence times were measured for module A with three different pump motor frequencies; 16 Hz, 8 Hz, and 4 Hz, which produced the corresponding volumetric flow rates of 0.2, 0.1, and 0.06 L/min, respectively. The measurements were done by first pumping water through the module, followed by a rapid change from water feed to 0.01 M KCl tracer solution with simultaneous monitoring of the outflow conductivity using a conductivity probe controlled by a multimeter station (Consort C3310). The conductivity and temperature probes were placed in a separate measurement vessel, which collected reactor outflow. The vessel had a drainage hole near the bottom for continuous sample replacement.

The measurements were repeated twice by first replacing water in the module with KCl and waiting for the conductivity to settle to a constant value, and subsequently by switching the feed back to water and monitoring conductivity until KCl was replaced. In addition to regular measurements, residence times were also measured for module A with ultrasonication at nominal acoustic energy densities of 1530 and 1020 W/L. The experiments with ultrasound were stopped after water was replaced with KCl solution to minimize the ultrasound usage times. A schematic of the experimental setup is shown in Figure 23.

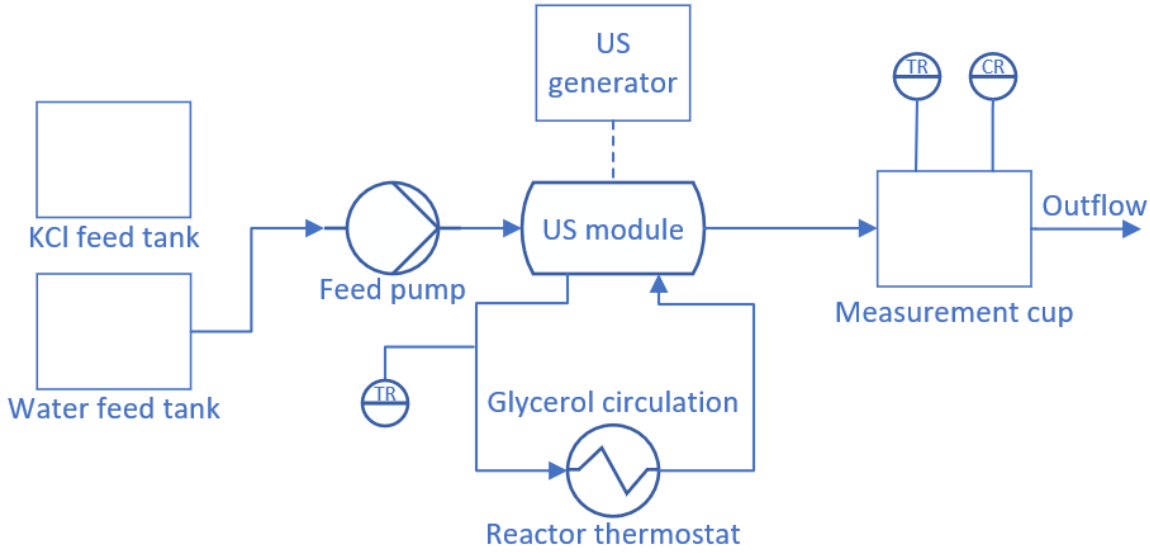

Figure 23 Schematic of the experimental setup in the residence time measurements. Experiments were begun with feed hose in the water tank, and the hose was rapidly switched to the KCl feed tank at a documented time to start the step tracer experiment. CR: Conductivity recorder.

Reynolds numbers were calculated from the experimental results using Equation (7).

$$Re = \frac{\rho v d_i}{\mu} \tag{7}$$

Where	Re	Reynolds number, -
	ρ	Fluid density, kg/m^3
	v	Flow velocity, m/s
	d_i	Inner diameter, m
	μ	Dynamic viscosity, Pa·s

Cumulative residence time distributions (RTD) were calculated using Equation (8). For the experiments where step responses were negative as KCl solution was replaced by water, washout functions were defined as using tracer concentrations, which correspond to the measured conductivities, as shown in Equations (9-10). (Fogler, 2005; Nauman, 2004)

$$F(t) = \frac{C(t)}{C_{\max}} \quad (8)$$

$$W(t) = \frac{C(t)}{C_0} \quad (9)$$

$$W(t) = 1 - F(t) \quad (10)$$

Where $F(t)$ Cumulative residence time distribution, -

$C(t)$ Outlet tracer concentration, mol/m^3

C_{max} Concentration of the tracer solution, mol/m^3

C_0 Initial tracer concentration in feed solution, mol/m^3

$W(t)$ Washout function, -

Using the relationship between cumulative RTDs and washout functions shown in Equation (9), the washout functions were converted to RTDs and plotted. The RTDs were then in turn converted to washout functions, and the mean residence times were calculated by numerical integration of the washout function curves. Numerical integration was done using the trapezoidal rule (Equation 10), from which Equation (11) can be derived. (Levenspiel, 1999; Råde & Westergren, 1995).

$$\int_a^b f(x)dx \approx (b-a) \cdot \frac{f(a)+f(b)}{2} \quad (10)$$

$$t_{\mathrm{m}} = \sum_{i=0}^{t} (t_{i+1} - t_i) \cdot \frac{F(t_{i+1})+F(t_i)}{2} \quad (11)$$

From the RTDs, dead times (t_d), ramp rates (r_I), and process time constants (τ_P) were determined for each experiment. Dead time refers to the time it takes to detect any change in the measured process variable at process outlet after adjustments to process inlet, ramp rate describes the speed at which the adjusted process variable approaches its final value, and process time constant is the time required on top of dead time for the process variable to reach 63.2 % of its final value. Graphical determination of these variables is shown in Figure 24 (Stephanopoulos, 1984).

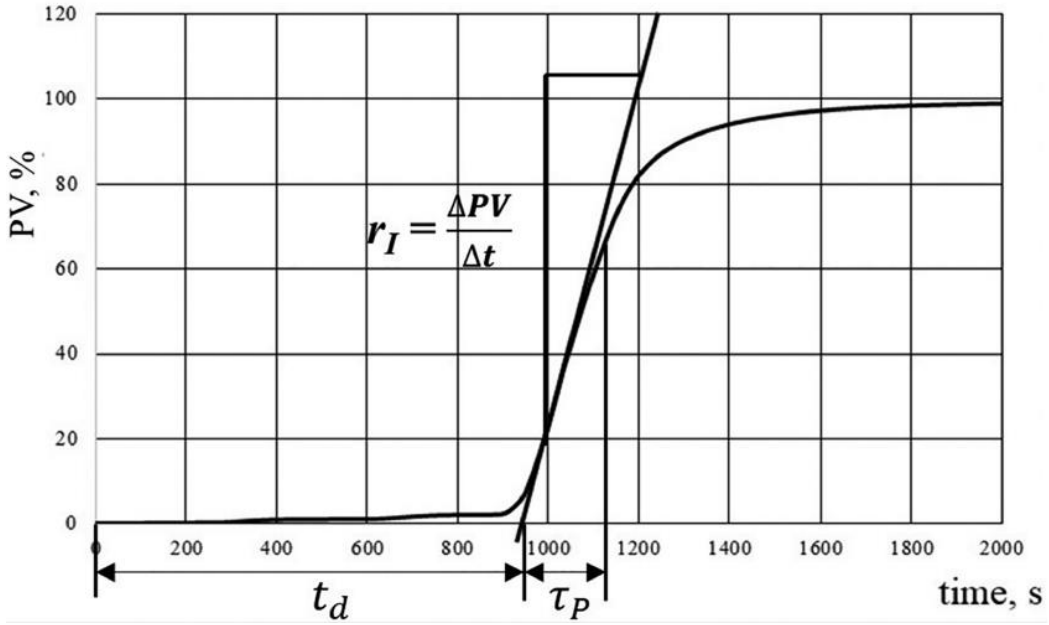

Figure 24 Graphical determination of dead time (t_d), ramp rate (r_I), and process time constant (τ_P) from a cumulative residence time distribution. PV = Process variable. (Stephanopoulos, 1984; Figure from Ezeanowi et al., 2020)

6.3.3 Raw material pre-treatment

As the chlorophyll in fresh green vegetables, including spinach, degrades in a matter of days if stored at ambient room temperatures (Manolopoulou & Varzakas, 2016; Yamauchi & Watada, 1991), purchased fresh spinach batches were placed under refrigeration upon arrival. Extractive degradation in spinach was also investigated experimentally as described in chapter 6.3.4. Prior to extraction experiments, spinach leaves were rinsed to remove remaining dirt and subjected to a manual disintegration procedure, in which the leaves were first cut by hand to 1-2 cm^2 pieces. The pieces were then fed to a centrifugal juicer (Wilfa Squeezy JEB-800S), which simultaneously shredded the leaves and separated free water from them. After two passes through the juicer, the spinach pulp was screw pressed and disintegrated further using a kitchen size shredder (Wilfa Essential MC3B-400S) for five seconds two times, with a thorough mixing in between. The disintegrated spinach batches were stored under refrigeration in vacuum-sealed plastic bags.

6.3.4 Quantification of extractive degradation in spinach

Degradation of extractives in pretreated spinach samples was investigated experimentally. Two vacuum packed batches were stored under refrigeration for up to 16 days and samples were regularly taken for use in conventional extraction experiments. Extraction was done in a sealed glass vessel with a nitrogen atmosphere. The sample was agitated with a magnetic stirrer at 500 rpm, and the vessel was covered in aluminum foil to protect the sample from all light sources. In the experiments, R/S was 0.1, total volume was 50 mL, solvent was 25 vol% aqueous ethanol, and extraction time was 4 h. The experiments were done at ambient temperature, but sample temperatures had been slightly elevated to 23-24 °C by end of the experiments, likely due to heat loss from the mixing unit.

6.3.5 Extraction experiments at laboratory scale

The laboratory scale experiments were started by switching on the reaction vessel jacket thermostat and weighing raw materials and solvent. Raw materials were placed into the vessel, after which the sonotrode and temperature probe were lowered into the vessel. In addition, a nitrogen hose was mounted at the top of the vessel to blow over the sample surface. The ultrasound generator was switched on and the desired power was set.

Once the preparations were complete, a nitrogen flow rate of 15 cm^3/min was started and the solvent was added into the vessel. Ultrasonication was then started and continued for 15 minutes. During the experiment, sample temperature and electric power of ultrasonication were automatically measured and recorded. After the experiment, the sample was centrifuged for 10 min at 4000 rpm, after which the liquid extract was separated from the solids.

In the lab scale experiments, total sample volume was 15 mL and nominal electric powers of ultrasonication ranged between 20 and 80 W. Due to the resulting high ultrasound intensities (5-21 W/cm^2) and acoustic energy densities (1333-5333 W/L), extraction temperature was not a controllable parameter with the lab scale setup. Instead, the cooling water was set to 5 °C in an attempt to keep the sample in near-ambient temperatures.

6.3.6 Extraction experiments with pilot equipment

The pilot extraction preparations were started by switching on reactor and feed tank thermostats and allowing the temperatures to reach the value set for the experiment. The required amount of solvent was then measured and placed in the feed tank for temperature adjustment. The module was also pre-filled with the solvent, and the raw materials were weighed.

The experiment began by starting nitrogen flow of 23 L/min at the top of the feed tank. Feed tank agitator was then started and set to 500 rpm, after which raw materials were added into the tank. Before the feed pump was switched on, the feed was mixed for 10 minutes to let the raw material particles homogenize and swell. Ultrasonication was started as soon as the pulp from feed tank entered the reaction tube, which took roughly 5 minutes depending on piping length.

During the experiment, volumetric flow rates through the module was monitored at regular intervals. Flow rates were measured by collecting module outflow into graduated cylinders for a known time, typically 1 minute. The collection of extract samples from reactor outlet was started as soon as the feed began to pass through the reaction tube, which was indicated by coloring in the outlet product. To evaluate extraction performance of the ultrasonication reactor, control samples were also taken from the feed tank, which can be considered as a conventional maceration reactor. During the experiment, reactor thermostat temperature and feed tank temperature, as well as electric power, amplitude, and frequency of ultrasound were monitored and recorded. In addition, process temperature was automatically recorded from reactor outlet and jacket outlet.

The extract samples, still containing solid raw materials, were filtered through a sieve and centrifuged for 10 min at 4000 rpm, after which the liquid phase was separated from the remaining solids. To prevent chlorophyll degradation, samples were stored away from heat and direct sunlight, and analyzed as soon as possible, within a few hours at latest.

6.4 Analytics

To evaluate the consistency and reproducibility of the manual disintegration, particle sizes were measured from spinach batches using image analysis. In addition, dry solids contents were also measured. Spinach extracts were analyzed using UV-Vis spectrophotometry.

6.4.1 Raw material particle size measurements

In the particle size measurement procedure, 200 mL of deionized water was first placed in a flat-bottomed white plastic vessel, and roughly 0.5-1 g of spinach pulp was mixed with the water to achieve even distribution of particles throughout the vessel bottom and minimize the stacking of the settling particles. In addition, a ruler was placed in the vessel to scale the recorded images. After the particles had settled, the vessel was photographed for image analysis. It was noticed that images from at least five samples of each batch should be taken from a single sample in order to sufficiently reduce noise in the data.

The images were loaded to ImageJ, which is an open source image processing software for scientific use (Rasband, 1997-2018). Particle sizes were then measured using a procedure in which the image scale was first determined using the ruler, and the images were then cropped to exclude nonrelevant sections. Afterwards, the images were converted to grayscale and subsequently thresholded to binary images, from which particle edges were clearly detected and their areas were evaluated. An example of this process is shown in Figure 25.

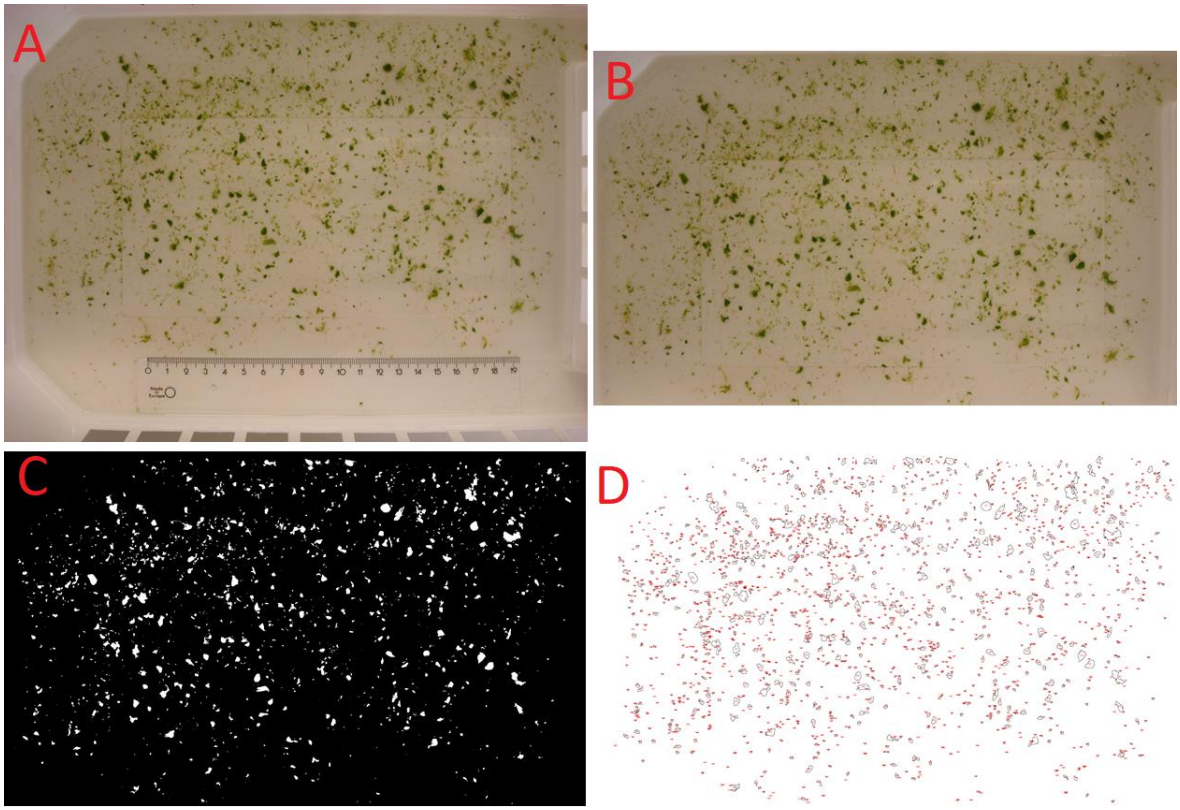

Figure 25 Image analysis procedure. A: Original photograph; B: Cropped image with the scale applied; C: Thresholded binary image showing white particles on black background; D: Detected particle edges, showing determined areas of the particles.

Using the calculated particle areas, the volumes of the particles were estimated. To this end, particles were estimated to have uniform thickness, which was determined for each particle by calculating the diameter of a circle with an equal area to that of the particle Equation (12).

$$d_{\mathrm{CE}} = 2\sqrt{\frac{A_{\mathrm{p}}}{\pi}} \tag{12}$$

Where d_{CE} Diameter of a circle with an equal area to the particle, m

A_{p} Area of the particle, m^2

This diameter was used as the particle thickness, which effectively approximated the particles as thin cylinders with constant thickness. However, a thickness limit of 1 mm,

which roughly corresponds to the thickness of a fresh spinach leaf, was set and used for largest particles. Particle volumes were then calculated using Equation (13).

$$V_{\mathrm{p}} = A_{\mathrm{p}} \cdot l_{\mathrm{p}} \tag{13}$$

Where V_{p} Particle volume, m^3

l_{p} Particle thickness, m

The particle size distributions were calculated based on particle number, area, and volume using Equations (14-16) (Richardson et al., 2002). In these distributions, the particles were divided into 20 size classes between 0 and 10 mm, at intervals of 0.5 mm.

$$f_{n,i} = \frac{n_{\mathrm{p},i}}{\sum n_{\mathrm{p},i}} \tag{14}$$

$$f_{A,i} = \frac{A_{\mathrm{p},i}}{\sum Ap_{,i}} \tag{15}$$

$$f_{V,i} = \frac{V_{\mathrm{p},i}}{\sum V_{\mathrm{p},i}} \tag{16}$$

Where $f_{n,i}$ Fraction of particle number in size class i, -

n_{p} Number of particles, -

$f_{A,i}$ Fraction of particle area in size class i, -

$f_{V,i}$ Fraction of particle volume in size class i, -

Finally, the mean volume diameters, which represent the diameter of a sphere with a volume to that of the particle, were calculated for the particles using Equation (17) (Richardson et al., 2002).

$$d_V = \sqrt[3]{\frac{\sum(n_i d_i^3)}{\sum n_i}} \tag{18}$$

Where d_V Mean volume diameter of the particle, m

From these analyses, it was determined that different spinach batches had similar PSDs and their mean volume diameters were in the range of 1.21 ± 0.18 mm. An example set of distributions is shown in Figure 26.

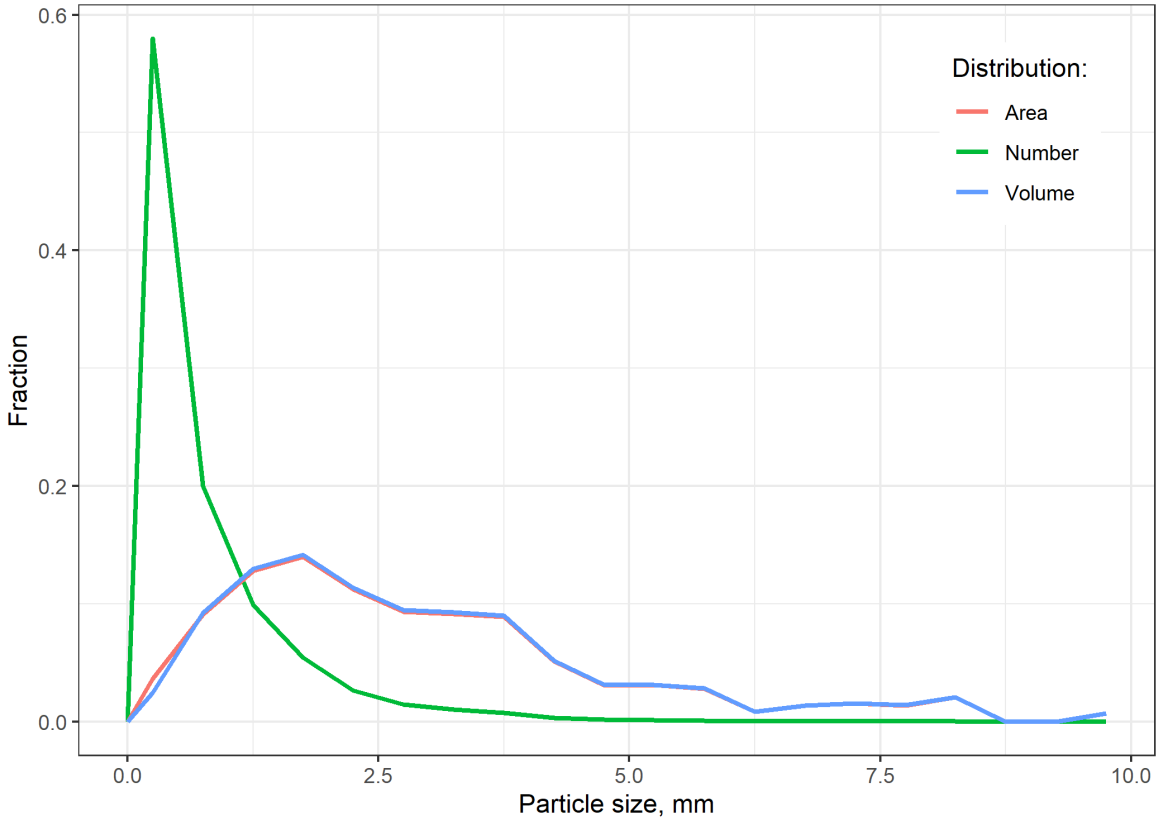

Figure 26 Typical PSDs for a spinach batch pre-treated using the described procedure.

6.4.2 Dry solids content measurements

The dry solids content measurements were done by drying 1-2 g of spinach pulp in an oven at 100 °C for 4 hours, which was tested to be more than sufficient for complete drying of the samples. The dry solids contents were then calculated with Equation (18).

$$Dry\ solids\ content = \frac{m_{\mathrm{d}}}{m_{\mathrm{w}}} \cdot 100\% \quad (18)$$

Where m_{d} Mass of dried sample, kg

m_{w} Mass of fresh sample, kg

The solids contents for the pre-treated spinach batches were determined to be in the range of 9.5 ± 2.0 %. Measured moisture content in spinach was thus 90.5 ± 2.0 %.

6.4.3 Extract concentration measurements

After the separation of extracts from solid raw materials, the concentrations of extracted chlorophyll *a*, chlorophyll *b*, and total carotenoids were analyzed from the spinach extract samples using a UV-Vis spectrophotometer (Agilent Cary 8454) and a method presented by Lichtenthaler and Buschmann (2001). The solvents and dilution factors used were selected so that they were applicable with the presented method. In laboratory scale experiments, samples were diluted 1:21 with analytical grade ethanol, after which they consisted of 95 % ethanol. Absorbances were then analyzed at 664, 649, 470, and 750 nm, of which 664 nm corresponds to chlorophyll *a*, 669 nm to chlorophyll *b*, 470 nm to total carotenoids. Absorbances at 750 nm were used for baseline correction. In the pilot experiments, some sample concentrations were lower and in order to avoid excessive dilution, the samples were diluted 1:5 with analytical grade acetone instead. This resulted in 80 % acetone solutions, and shifted absorption maxima to 663, 647, and 470 nm. The samples that were cloudy after dilution were centrifuged for 5 min at 4000 rpm.

Baseline correction was done by subtracting absorbance at 750 nm from the other absorbances, and concentrations were then calculated for 95 % ethanol solutions using Equations (19-21) and 80 % acetone solutions using Equations (22-24).

$$\frac{C_a}{\text{mg/L}} = 13.36 \cdot A_{664} - 5.19 \cdot A_{649} \quad (19)$$

$$\frac{C_b}{\text{mg/L}} = 27.43 \cdot A_{649} - 8.12 \cdot A_{664} \quad (20)$$

$$\frac{C_{car}}{\text{mg/L}} = \frac{1000 \cdot A_{470} - 2.13 \cdot C_a - 97.64 \cdot C_b}{209} \quad (21)$$

Where C_a Chlorophyll *a* concentration

A_{663} Sample absorbance at 664 nm, -

A_{647} Sample absorbance at 649 nm, -

C_b Chlorophyll *b* concentration

C_{car} Total carotenoid concentration

A_{470} Sample absorbance at 470 nm, -

$$\frac{C_a}{\text{mg/L}} = 12.25 \cdot A_{663} - 2.79 \cdot A_{647} \quad (22)$$

$$\frac{C_b}{\text{mg/L}} = 21.5 \cdot A_{647} - 5.1 \cdot A_{663} \quad (23)$$

$$\frac{C_{car}}{\text{mg/L}} = \frac{1000 \cdot A_{470} - 1.82 \cdot C_a - 85.02 \cdot C_b}{198} \quad (24)$$

Where A_{663} Sample absorbance at 663 nm, -

A_{647} Sample absorbance at 647 nm, -

7 RESULTS AND DISCUSSION

7.1 Pump performance

Measured volumetric flow rates are shown in Figure 27 and calculated residence times in Table 6.

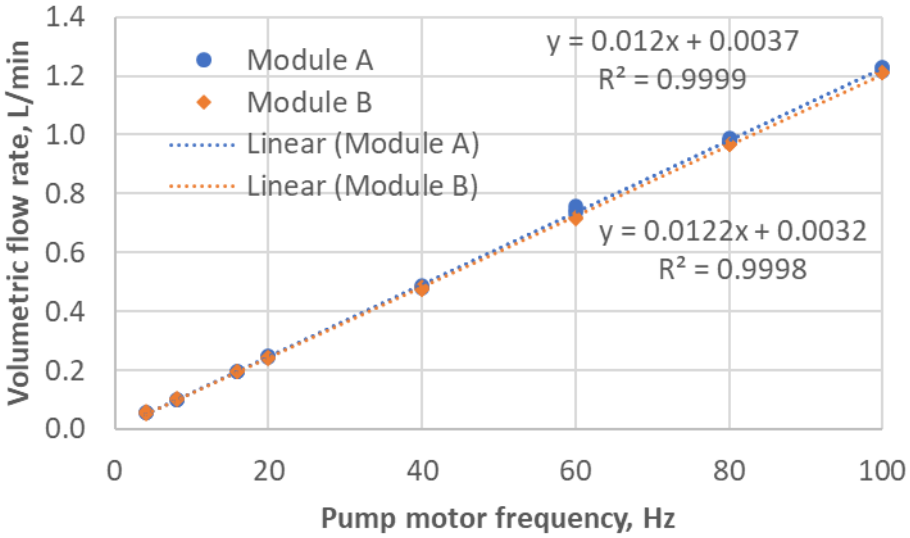

Figure 27 Volumetric flow rates with the two different ultrasonication modules using pump motor frequencies of 4-100 Hz with Flowrox LPP-D15 hose pump.

Table 6 Calculated residence times with the two modules using different pump motor frequencies.

Pump motor frequency, Hz	**Flow rate, L/min**	**τ(Module A), min**	**τ(Module B), min**
4	0.06	17.2	14.2
8	0.10	9.7	7.9
16	0.20	5.0	4.1
20	0.24	4.0	3.3
40	0.48	2.0	1.7
60	0.72	1.3	1.1
80	0.97	1.0	0.8
100	1.21	0.8	0.7

Based on the results shown in Figure 27, it was concluded that the pump performance was stable and linear at even low settings up until 4 %, after which there was no practical change in the flow rate. The highest attainable residence times for water were therefore 17 and 14 minutes for modules A and B, respectively.

7.2 Residence time distribution

The measured cumulative residence time distributions for module A are shown in Figure 28. The graphs are plotted so that $t = 0$ is the moment when the feed solution was changed.

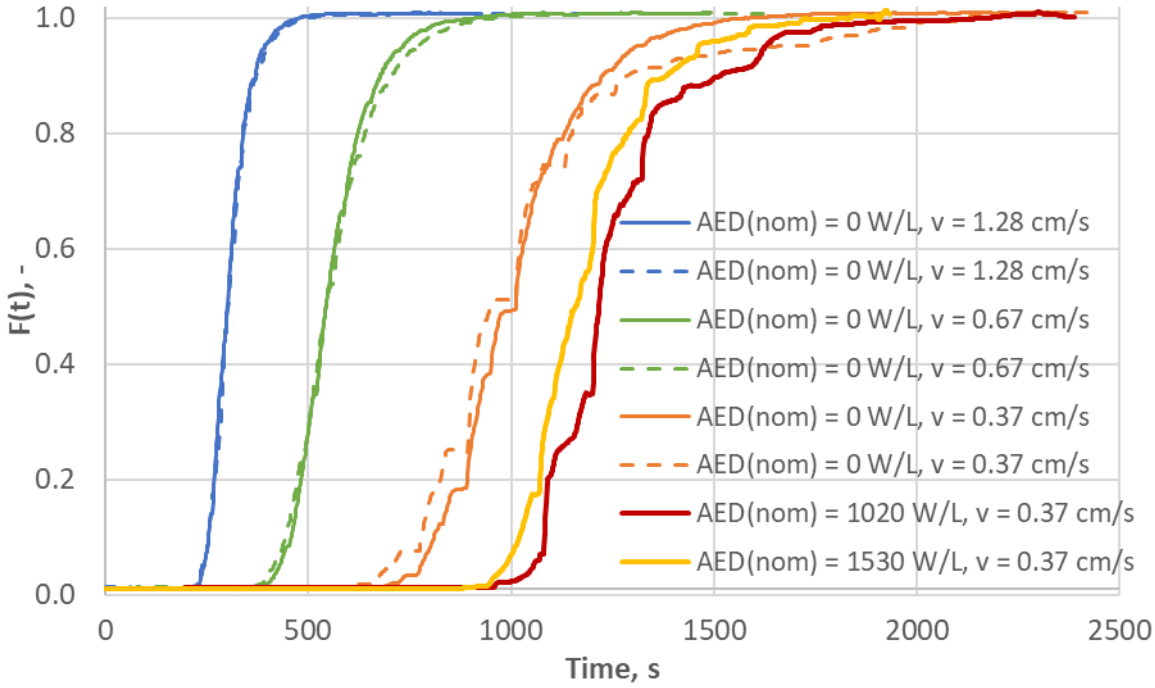

Figure 28 Measured cumulative residence time distributions for module A. Dashed lines denote distributions measured as washout functions. Inner diameter of the module was 18 mm. Reynolds numbers were 230, 120, and 67 for flow velocities of 1.28, 0.67, and 0.37 cm/s, respectively. Corresponding residence times were 5.0, 9.7, and 17.2 min. AED(nom) = nominal acoustic energy density.

Figure 28 shows not only that decreasing the flow rate increased residence time as expected, but also that ultrasonication increased residence times further, which is in contrast to the results of Ezeanowi et al. (2020), where ultrasonication decreased residence times. This could be attributed to the low flow velocities and increased mixing in the reaction tube; As the coiled tube design required the fluid to alternate between upward and downward travel, it is possible that at low flow rates, the tube was not completely filled with the fluid at the apex point of the cycle where travel direction shifted from upward to downward. It is thus

possible that the mixing effect of ultrasound led to slightly more complete filling of the reaction tube.

The figure also shows that the RTDs were sharp and stable with the higher flow rates, which indicates high stability in pump performance. The RTDs at v = 0.37 cm/s, however, seem to show leveling in the graphs. This is possibly a result of uneven pump flow rate, which is a common occurrence with peristaltic pumps running at low speeds (Cole-Parmer, 2020). In addition, as the tracer was not fed directly into reactor inlet, the measurements involved pumping the tracer through the pump and piping as well. This may have increased the effects of pulsation further. Another contributor may be limitations in the measurement setup, as the measuring cup itself likely had an unstable residence time at such a torpid flow rate.

The measured flow rates and mean residence times for module A are compared to their calculated values in Table 7. For each experiment, the time at which 95 % of the final concentration value was reached was also calculated.

Table 7 Comparison between calculated and measured flow rates and mean residence times for module A.

AED_{nom}, W/L	Q(calc.), L/min	Q(meas.), L/min	τ_m(calc.), min	τ_m(meas.), min	$t_{mix95\%}$, min
0	0.195	0.197	5.0	5.2	6.8
0	0.195	0.197	5.0	5.2	6.8
0	0.102	0.101	9.7	9.4	12.4
0	0.102	0.101	9.7	9.5	13.1
0	0.057	0.056	17.2	16.9	22.3
0	0.057	0.056	17.2	17.2	29.3
1020	0.057	0.058	17.2	21.0	27.3
1530	0.057	0.050	17.2	19.8	25.2

Table 7 shows that the measured flow rates and mean residence times were generally well in line with the calculated ones. In addition, it is noteworthy that even though ultrasonication increased the residence times, it had no conclusive effect on the measured flow rates. With low flow rates, the time needed to reach 95 % of final concentration also varied heavily.

Ezeanowi et al. (2020) earlier performed dynamics monitoring experiments with and without ultrasound in module B. In these experiments, a cascade of three identical modules, with a

total volume of 2.4 L was used. The ramp rates, dead times, and process time constants for these experiments as well as the experiments done with module A are shown in Table 8.

Table 8 Determined ramp rates, dead times, and process time constants for the two modules with different measured flow rates. Flow velocities and residence times were calculated from the flow rates. Data for module B is from Ezeanowi et al. (2020) using a cascade of three identical modules with a total volume of 2.4 L.

Module	**AED_{nom}, W/L**	**Q, L/min**	**v, cm/s**	**τ, min**	**r_I, s^{-1}**	**t_d, s**	**τ_P, s**
A	0	0.197	1.29	5.0	0.0078	242	81
A	0	0.197	1.29	5.0	0.0080	243	79
A	0	0.101	0.66	9.7	0.0041	431	154
A	0	0.101	0.66	9.7	0.0038	426	166
A	0	0.056	0.37	17.6	0.0023	770	274
A	0	0.056	0.37	17.6	0.0019	724	332
A	1020	0.058	0.38	17.0	0.0026	1012	242
A	1530	0.050	0.33	19.4	0.0026	989	242
B	0	0.210	7.0	15.0	0.0036	540	173
B	1200	0.210	7.0	15.0	0.0043	540	144
B	1900	0.210	7.0	15.0	0.0048	580	141
B	0	0.160	5.3	11.4	0.0038	940	166
B	1200	0.160	5.3	11.4	0.0039	880	164
B	1900	0.160	5.3	11.4	0.0041	940	174

From Table 8 it can be seen that decreasing the flow rates resulted in increased dead times and process time constants. For module A, dead times were further increased by ultrasonication, but process time constants decreased instead. For module B, ultrasonication did not seem to have any significant effects when Q = 0.16 L/min, but it did decrease process time constants when Q = 0.21 L/min. Also, due to differences in reaction tube diameters, module B had much higher flow velocities than module A. The ramp rates were plotted as a function of flow rate in Figure 29 and as a function of acoustic energy density in Figure 30.

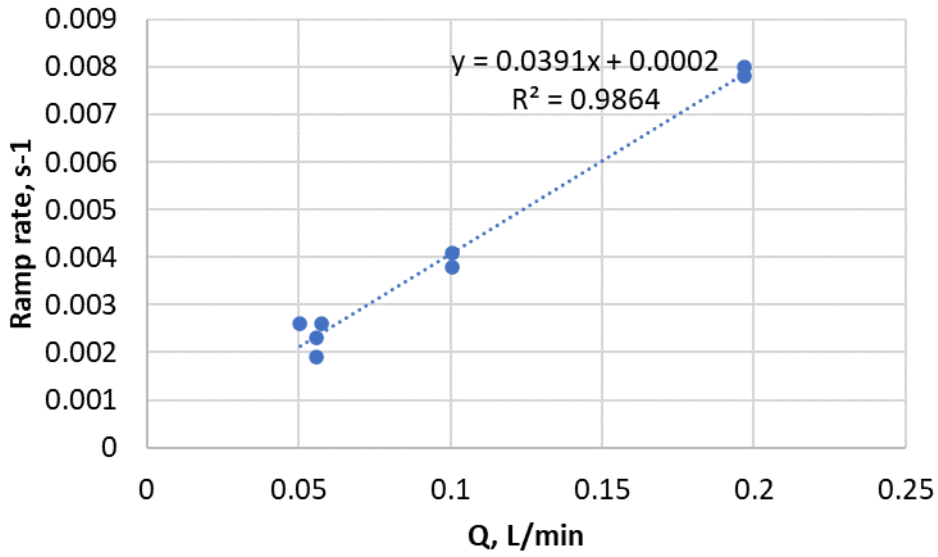

Figure 29 Ramp rate as a function of volumetric flow rate for module A.

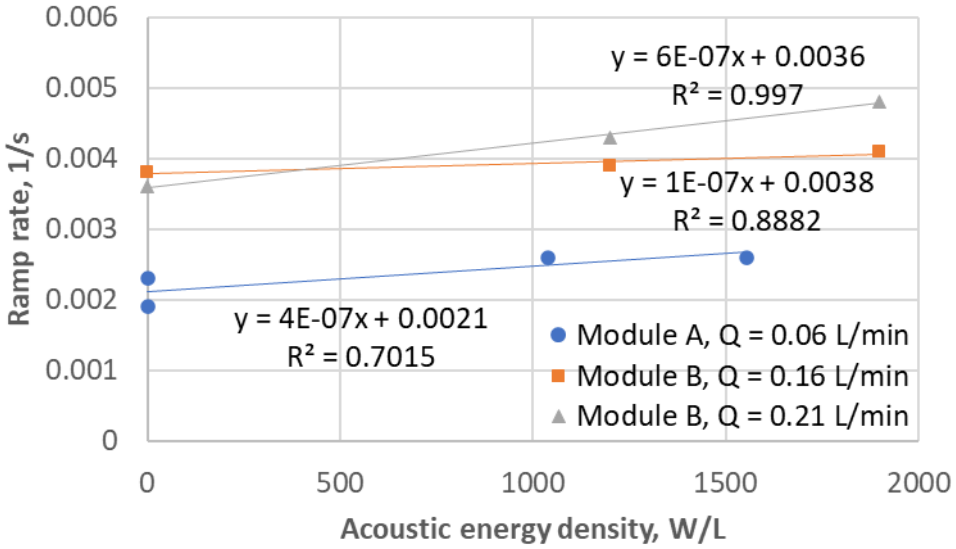

Figure 30 Ramp rates as a function of acoustic energy density for modules A and B. Data for module B from Ezeanowi et al., 2020.

Figure 29 shows that volumetric flow rate had a clear correlation with ramp rate with module A. From Figure 30, on the other hand, it can be seen that ultrasonication increased ramp rates slightly in all scenarios. This is likely a result of the increased mixing generated by ultrasound.

7.3 Extractive degradation in spinach

The results of the spinach storage experiments are shown in Figure 31.

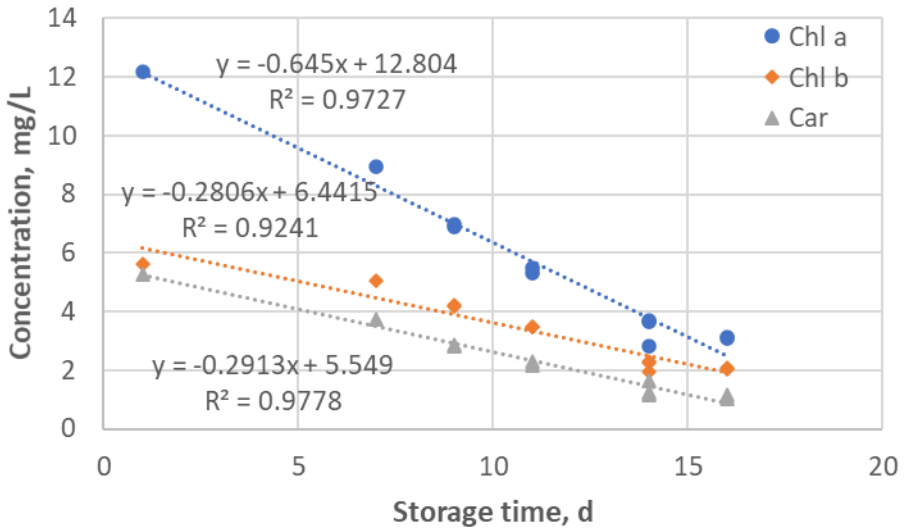

Figure 31 Degradation of chlorophyll *a* (Chl a), chlorophyll *b* (Chl b), and total carotenoids (Car) in spinach as a function of storage time. Disintegrated spinach samples were stored in vacuum bags under refrigeration. Extraction conditions were R/S = 0.1, t = 4 h, and T = 23-24 °C. Solvent was 25 vol% aqueous ethanol.

Figure 31 indicates that storage of pre-treated spinach had a clear effect on the extract concentrations, which degraded almost linearly during the tested timeframe.

7.4 Laboratory scale extraction

The laboratory scale experiments were begun by screening for an optimal ethanol concentration in the solvent. Extraction experiments were done with several different ethanol concentrations, using R/S of 0.1 and nominal acoustic energy density of 2667 W/L. The results are shown in Figure 32.

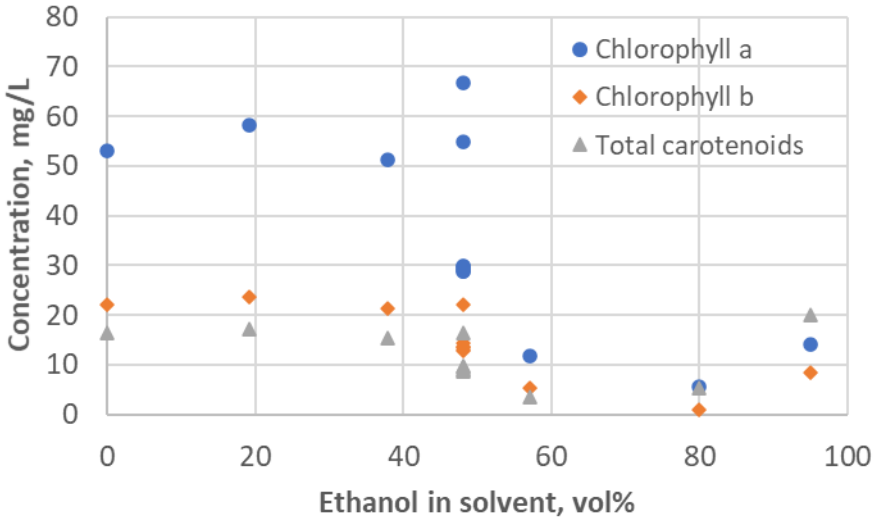

Figure 32 Screening for optimal ethanol concentration for the UAE of spinach with a laboratory scale ultrasonic horn at R/S = 0.1 and AED_{nom} = 2667 W/L.

In regular maceration of spinach, highest extract concentrations are achieved with concentrated ethanol (Derrien et al., 2017). However, Figure 32 shows that in the UAE experiments, ethanol concentration had a sweet spot at around 20 vol%, and the graph appears to have a trend resembling that of a third-degree polynomial function. The two samples with chlorophyll *a* concentrations of over 50 mg/L at 50 vol% ethanol were deemed as likely outlying values, as the other five samples at this concentration were almost identical to one another at 30 mg/L. Even so, as there was not a certain conclusion on the matter, ethanol concentration of 50 vol% was selected for further investigation along with pure water and concentrations of around 20 vol%.

A full factorial design of experiments (DOE) was then created using MODDE Pro -software (v12.1) to further investigate the effects of ethanol concentration, as well as R/S ratio and nominal US power, on the extraction of the compounds from spinach. The tested values were 0.1, 0.5, and 1.0 for R/S ratio, 0, 25, and 50 vol% for ethanol concentration, and 40, 60, and 80 W for nominal US power. The DOE is shown in Table 9.

Table 9 Laboratory scale DOE for investigating the effects of R/S ratio, ethanol concentration, and nominal acoustic energy density on spinach UAE experiments.

Trial No	R/S	Ethanol, vol%	P_{nom}, W	AED_{nom}, W/L
1	0.1	25	40	2667
2	0.1	50	40	2667
3	0.1	0	40	2667
4	0.1	25	60	4000
5	0.1	25	80	5333
6	0.1	50	60	4000
7	0.1	50	80	5333
8	0.1	0	60	4000
9	0.1	0	80	5333
10	0.5	0	60	4000
11	0.5	0	80	5333
12	0.5	25	60	4000
13	0.5	25	80	5333
14	0.5	50	60	4000
15	0.5	50	80	5333
16	0.5	25	60	4000
17	0.5	25	60	4000
18	1	0	60	4000
19	1	0	80	5333
20	1	25	60	4000
21	1	25	80	5333
22	1	50	60	4000
23	1	50	80	5333

As the sample volume was kept at 15 mL in all tests, changing the R/S ratio affected the mass of solid spinach and therefore the total mass of extractives fed into the extraction system, which was taken into account during the calculation of the results from this DOE. As such, all raw material samples were assumed to contain the average amounts of chlorophyll *a* and *b* for spinach, which are, respectively, 0.7 and 0.25 wt% on a dry basis (Schwartz & von Elbe, 1983). Carotenoids were assumed to consist solely of β-carotene and lutein, resulting in an average total carotenoid amount of 114.13 mg/100 g of fresh spinach (Khoo et al., 2011). Using these values, fractions extracted were calculated using Equation 25.

$$E = \frac{m_e}{m_0} \cdot 100\% \qquad (25)$$

Where E Fraction extracted, %

m_e Mass of extracted compound, kg

m_0 Initial mass of extracted compound in raw material, kg

During the experiments it was observed that as R/S was increased above 0.1 and the reaction mixture subsequently thickened, sonication alone was not capable of properly agitating the reaction mixture, as there was little free liquid present. The following figures are presented only for chlorophyll *a*, as the displayed trends were nearly identical for chlorophyll *b* and total carotenoids as well. The effect of R/S on the extraction of chlorophyll *a* is shown in Figure 33.

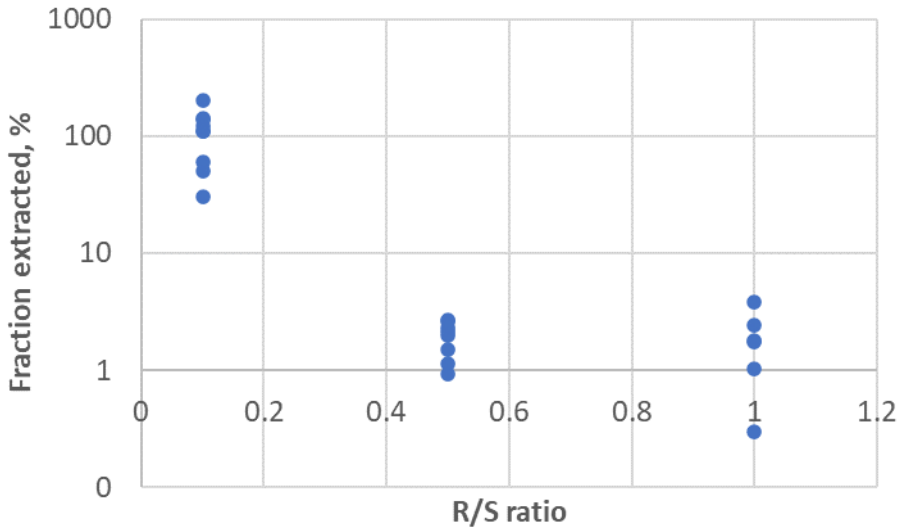

Figure 33 Effect of R/S ratio on the extraction of chlorophyll *a* from spinach in laboratory scale. In the experiments solvent ethanol concentrations were 0, 25, or 50 vol%, and nominal AEDs were 2667, 4000, or 5333 W/L. Average values from literature were used in the calculation as total extractive concentrations in the raw material (Schwartz & von Elbe, 1983; Khoo et al., 2011). Fractions extracted of over 100 % are likely a result of deviation between actual total extractive concentrations and literature values.

Figure 33 clearly demonstrates that R/S ratio dominated the experimental results, regardless of the values of ethanol concentration or US power. This is most likely due to insufficient mixing in the reaction vessel, which was observed during the experiments. R/S of 0.1 was therefore selected for use in the extraction experiments.

From the DOE, trial points with R/S 0.1 were examined further. Figure 34 shows the effects of nominal US power and ethanol concentration on fraction of chlorophyll *a* extracted.

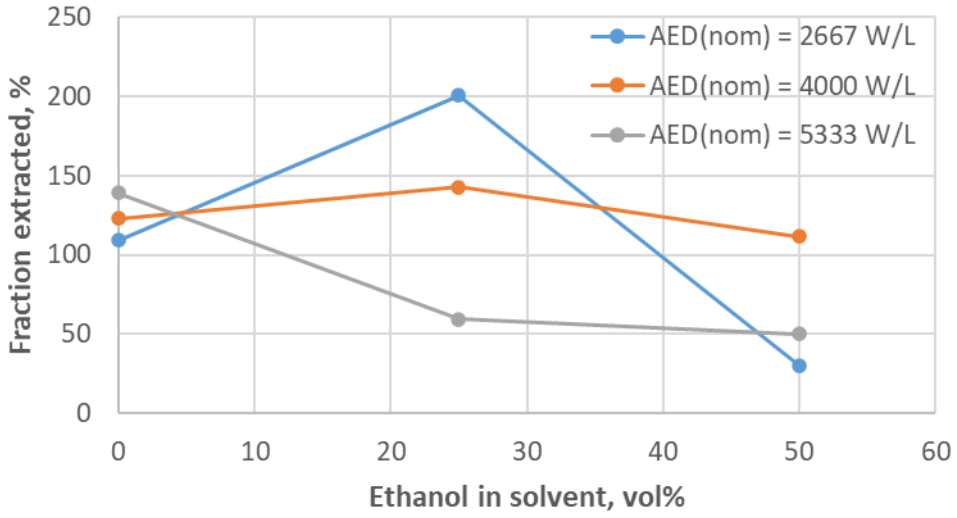

Figure 34 Effects of nominal acoustic energy density and ethanol concentration on chlorophyll *a* extraction from spinach in laboratory scale. R/S ratio was 0.1. Average values from literature were used in calculation as total extractive concentrations in the raw material (Schwartz & von Elbe, 1983; Khoo et al., 2011). Fractions extracted of over 100 % are likely a result of deviation between actual total extractive concentrations and literature values.

Based on Figure 34 it appears that increasing the US power benefited extraction with pure water but had an opposite effect with 25 vol% ethanol solution. A possible explanation for this is excessive disintegration of spinach by higher intensity ultrasound, which could lead to some of the extractives binding to the solids. In addition, it appears that increasing the ethanol content to 50 vol% had a hindering effect on the extraction, which was to be expected based on the results shown in Figure 32. Ethanol concentrations at around 25 vol% were thus selected for use in further tests.

As the results presented in Figure 34 suggest that with 25 vol% ethanol, increasing AED further from 2667 W/L does not have desirable results, a D-optimal screening DOE was created to gain more insight on the effects of US power on the extraction process. In this DOE, nominal AEDs were 1333, 2667, and 4000 W/L, ethanol concentrations used were 10, 15, 20, and 25 vol%, and R/S was 0.1. The experimental results of this DOE were analyzed using MODDE pro -software. The following variables were given as factors affecting the process: Ethanol concentration, average measured temperature, storage time of disintegrated raw materials, nominal AED, and measured average electrical AED. Response variables were measured concentrations of the spinach extractives. The trial points, factors, and responses are shown in Table 10.

Table 10 Second laboratory scale DOE, investigating the effect of US power on the UAE of spinach. R/S was 0.1 in all tests.

Trial No	Ethanol, vol%	T_{avg}, °C	Storage time, d	AED_{nom}, W	AED_{el}, W	C(chl a), mg/L	C(chl b), mg/L	C(car), mg/L
1	20	34.1	1	2667	3407	15.2	12.6	2.6
2	20	33.8	1	2667	3380	17.7	14	3.4
3	20	33.8	1	2667	3373	16.7	12.7	2.9
4	15	16.3	2	1333	2153	8.5	6.8	1.5
5	25	17.7	2	1333	2120	8.2	5.7	1.5
6	15	41.1	2	4000	4460	25.2	18.3	4.3
7	25	40.4	2	4000	4387	19	13	3.1
8	10	18.3	2	1333	2160	8.4	6.2	1.7

As shown in Table 10, the trends in nominal AED, measured electrical AED, and temperature were quite similar, and as they all were direct results of increasing the nominal power, it would have been redundant to include all of them in the model. Out of the three, measured electrical AED was selected as the predictor variable to represent the increase in US power.

The model was then fitted with partial least squares (PLS) regression, and insignificant factors were identified and removed using MODDE. Residual plots as well as observed vs predicted plots were drawn with MODDE. These plots are shown for chlorophyll *a* in Figures 35-36.

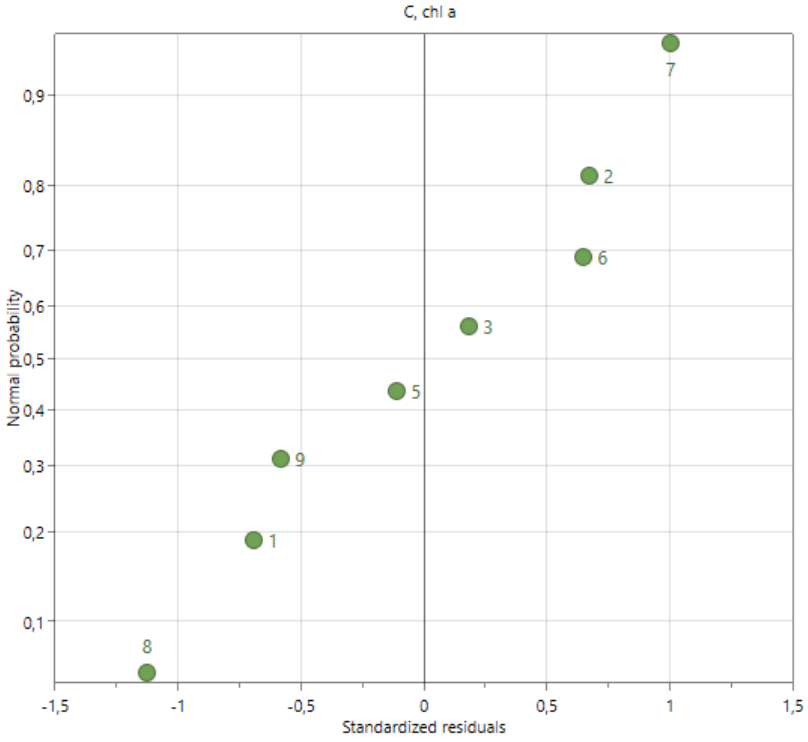

Figure 35 Initial residual plot for the UAE of chlorophyll *a* concentration in the second lab scale DOE. Conditions were: R/S = 0.1; ethanol in solvent = 15, 20, and 25 vol%; AED_{nom} = 1333, 2667, and 4000 W/L.

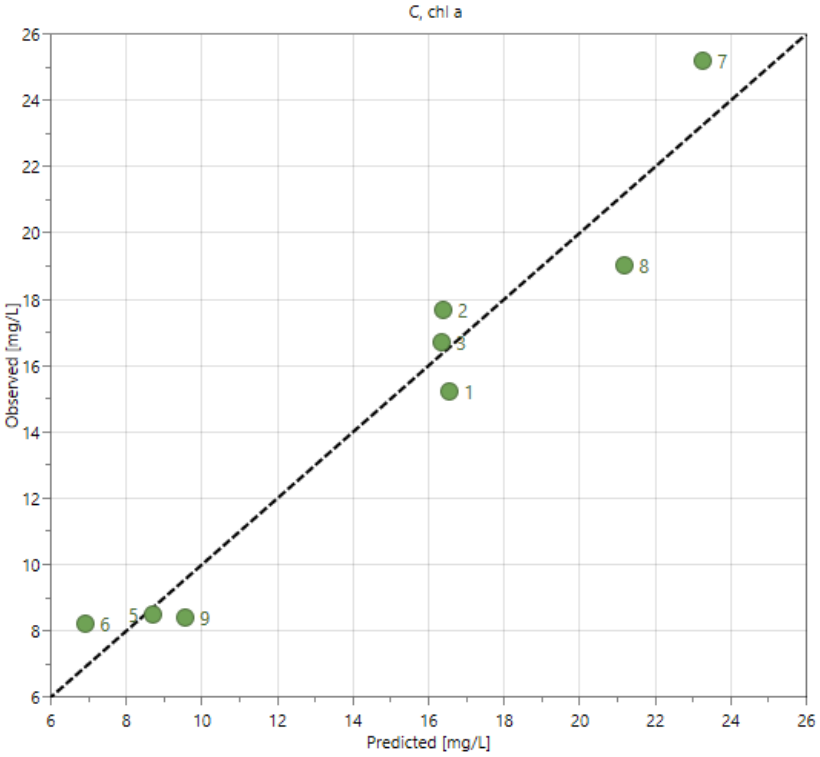

Figure 36 Initial observed vs predicted plot for the UAE of chlorophyll *a* concentration in the second lab scale DOE. Conditions were: R/S = 0.1; ethanol in solvent = 15, 20, and 25 vol%; AED_{nom} = 1333, 2667, and 4000 W/L. For this fit, R^2 = 0.94 and Q^2 = 0.71.

Based on the plots in Figures 35-36, no trial points were classified as outliers. The coefficient plot, displaying the scaled and centered impacts of the factors on the responses, is shown for chlorophyll *a* in Figure 37. This plot shows how impactful each factor was on the selected response, and whether the impact was positive or negative.

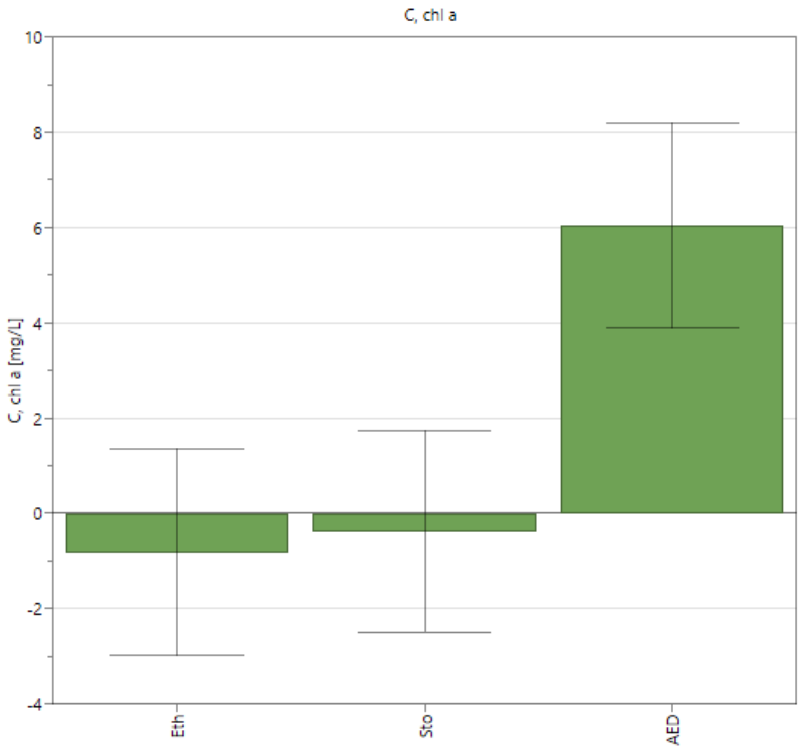

Figure 37 Coefficient plot for the UAE of chlorophyll *a* in the second laboratory scale DOE. Eth = ethanol content (10-25 vol%), Sto = storage time (1-2 d), AED = average measured electrical acoustic energy density (2120-4460 W/L).

The coefficients plot shows that an increase in US power had a significant positive effect on chlorophyll extraction. Storage time and further increase of ethanol content, on the other hand, are shown to variate on both positive and negative impacts, which makes them insignificant variables. This is likely due to the low differences between their respective values. As such, they were removed from the model, leaving measured electrical AED as the sole predictor variable. Final residual and observed vs predicted plots are shown for chlorophyll *a* in Figures 38-39. In the models, R^2 and Q^2 values were 0.92 and 0.87 for chlorophyll *a*, 0.86 and 0.79 for chlorophyll *b*, and 0.84 and 0.77 for carotenoids

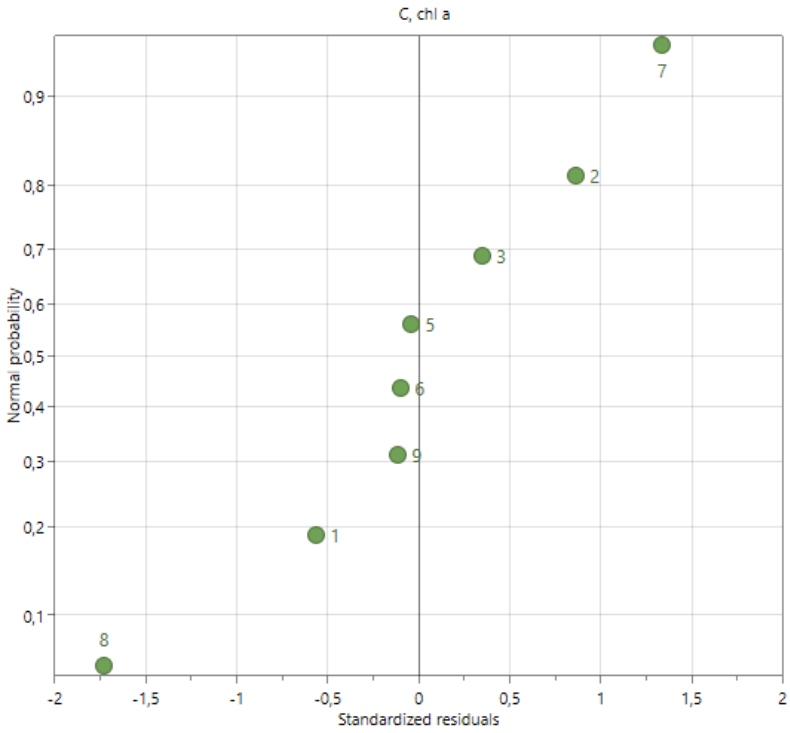

Figure 38 Final residual plot for the UAE chlorophyll *a* concentration in the second lab scale DOE. Conditions were: R/S = 0.1; ethanol in solvent = 15, 20, and 25 vol%; AED_{nom} = 1333, 2667, and 4000 W/L.

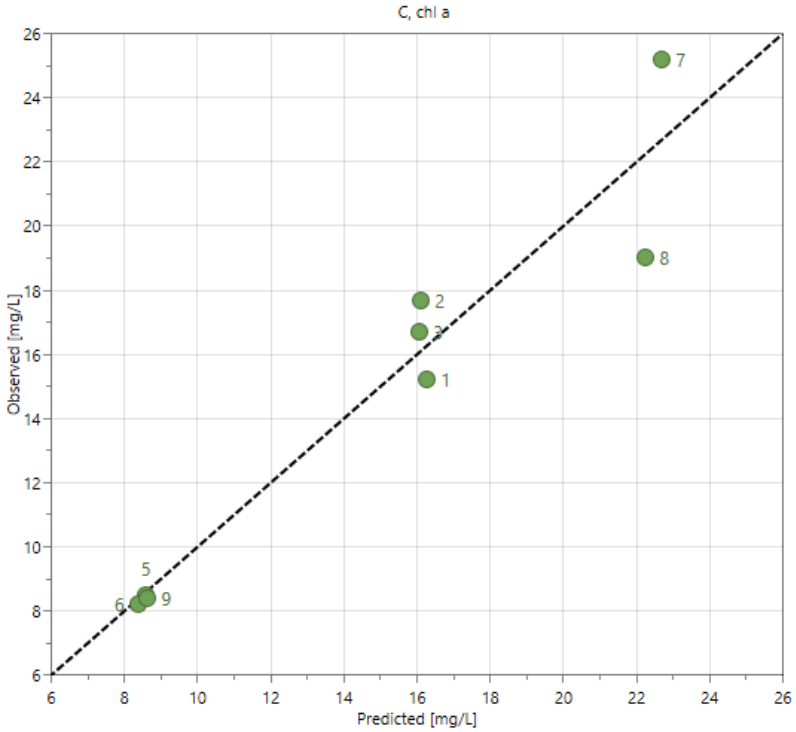

Figure 39 Final observed vs predicted plot for the UAE of chlorophyll *a* concentration in the second lab scale DOE. Conditions were: R/S = 0.1; ethanol in solvent = 15, 20, and 25 vol%; AED_{nom} = 1333, 2667, and 4000 W/L. For this fit, R^2 = 0.92 and Q^2 = 0.87.

As ultrasonic power was the only significant factor in the DOE, the effect of measured electrical AED on the extraction of chlorophyll *a* was plotted with MODDE and is shown in Figure 40.

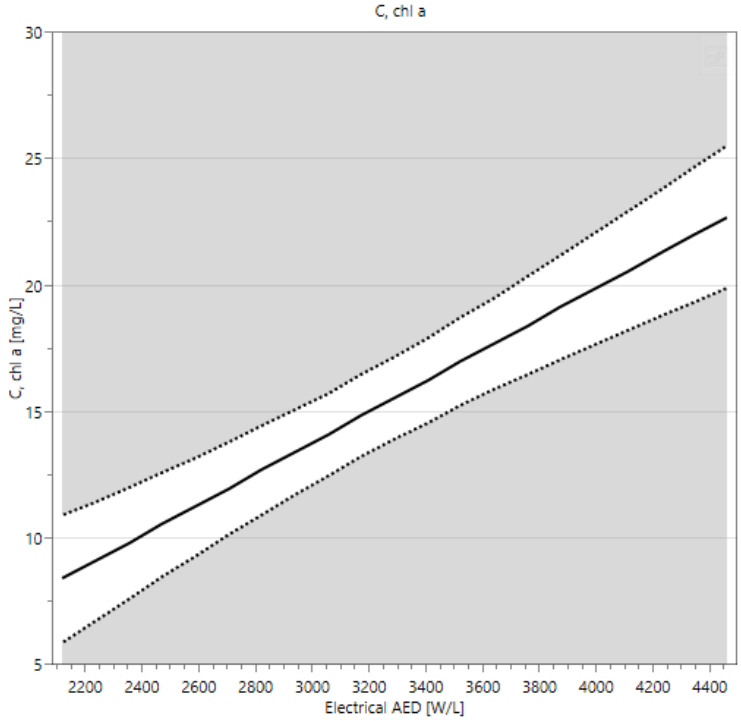

Figure 40 Effect of US power on UAE of chlorophyll *a* from spinach in second lab scale DOE. Solid line denotes prediction and dotted lines denote confidence interval. Effects of ethanol content and storage time were removed from the model.

As seen in Figure 40, an increase in electrical AED between 2000 and 4400 W/L benefited the extraction process at the tested conditions. However, as temperature control was not possible, process temperature increased almost linearly based on US power. It is therefore difficult to conclude how much of the observed extraction benefit is caused directly by the increase in US power, as higher temperatures may also improve extraction kinetics. Measured process temperatures were 18-41 °C.

7.5 Pilot scale extraction

Based on the results of the laboratory scale experiments, a full factorial DOE was made for the pilot scale extraction tests with module A. In the DOE, ethanol concentrations used were 15, 20, and 25 vol%, and extraction temperatures were 20, 30, and 40 °C. R/S ratio used was 0.1, nominal US power was 1500 W, which corresponds to a nominal AED of 1530 W/L, and nominal residence time in the ultrasonication tube was 17.2 min. The center point

experiment at 30 °C and 20 vol% ethanol was done four times in total, namely in trials number 2, 6, 7, and 8. The pilot DOE is shown in Table 11.

Table 11 DOE for pilot scale experiments with module A. R/S was 0.1, the nominal ultrasonication time was 17.2 min, nominal flow rate was 0.06 L/min, and the nominal AED was 1530 W/L.

Trial No	**Ethanol, vol%**	**T, °C**
1	20	20
2	20	30
3	20	40
4	15	40
5	25	40
6	20	30
7	20	30
8	20	30
9	15	30
10	25	30
11	15	20
12	25	20

As multiple extract samples were taken from both the feed tank and module outlet in each experiment, a method for the calculation of singular mean concentration values was established. To this end, mean concentration values for each extractive were first calculated between the outlet samples taken after complete feed breakthrough. Corresponding mean feed tank concentrations were then calculated from the feed tank samples taken during the timeframe the outlet samples were fed into the module, which was identified by subtracting nominal residence time of the entire pilot module, including the reaction tube, pump, and piping, from the outlet extraction times. The nominal residence time for module A setup was 27.8 min. This procedure is demonstrated in Figure 41 using the results of trial no. 7. In this example, only one sample is used as the average feed tank concentration, as no other feed tank samples hit the timeframe of outlet samples entering the module, and the first outlet sample is ignored, as feed breakthrough was not yet complete at the time of sampling.

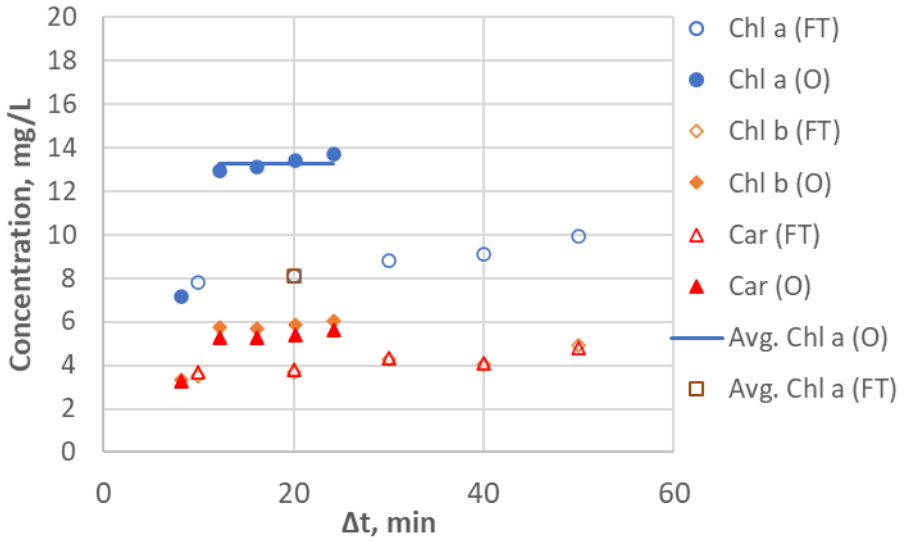

Figure 41 Determination of mean outlet and feed tank concentrations from pilot DOE trial no. 7. FT = feed tank; O = outlet; Δt = extraction time for feed tank samples, and extraction time minus nominal module residence time (27.8 min) for outlet samples. Extraction conditions were: R/S = 0.1; ethanol = 20 vol%; T = 30 °C; nominal AED = 1530 W/L, nominal flow rate = 0.06 L/min.

In order to compare the benefits gained from ultrasonication in each experiment, the results were calculated for each experiment by dividing the mean outlet concentrations with the mean inlet concentrations and presented as percentage values. These are shown in Figure 42.

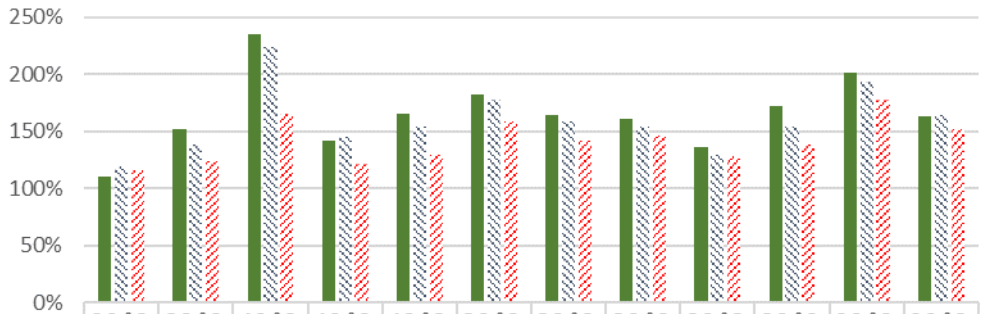

	20 °C, 20 vol%	30 °C, 20 vol%	40 °C, 20 vol%	40 °C, 15 vol%	40 °C, 25 vol%	30 °C, 20 vol%	30 °C, 20 vol%	30 °C, 20 vol%	30 °C, 15 vol%	30 °C, 25 vol%	20 °C, 15 vol%	20 °C, 25 vol%
c(O)/c(FT), chl a	110%	152%	235%	142%	166%	183%	164%	161%	136%	172%	201%	163%
c(O)/c(FT), chl b	120%	139%	225%	146%	155%	178%	159%	154%	129%	154%	194%	165%
c(O)/c(FT), car	117%	124%	166%	122%	130%	159%	143%	147%	128%	139%	178%	152%

Figure 42 Mean outlet concentrations divided by their respective mean feed tank concentrations for the pilot DOE. Module A was used in the experiments. Nominal AED was 1530 W/L, nominal flow rate was 0.06 L/min, and nominal residence time was 17.2 min. O = Outlet, FT = Feed tank; chl = Chlorophyll; car = Carotenoids.

Based on Figure 42, it appears that the most chlorophylls were extracted using ultrasonication at 40 °C and 20 vol% ethanol, while the best carotenoids extraction was achieved at 20 °C and 15 vol% ethanol. However, based on the differences in the four center point experiments at 30 °C and 20 vol% ethanol, it is evident that deviation in these results was quite high. This may result from the fact that differences in raw material types and storage times were not properly accounted for in the calculations, even though the use of non-dimensional concentrations should have mitigated their effects to some degree.

On top of the pilot DOE, several additional extraction experiments, testing both modules without the use of ultrasound, were done. Module A was tested with no ultrasound at 20, 30, and 40 °C while module B was tested at 40 °C with and without ultrasound. Ethanol concentration was 20 vol% in these tests. These results are shown in Figure 43.

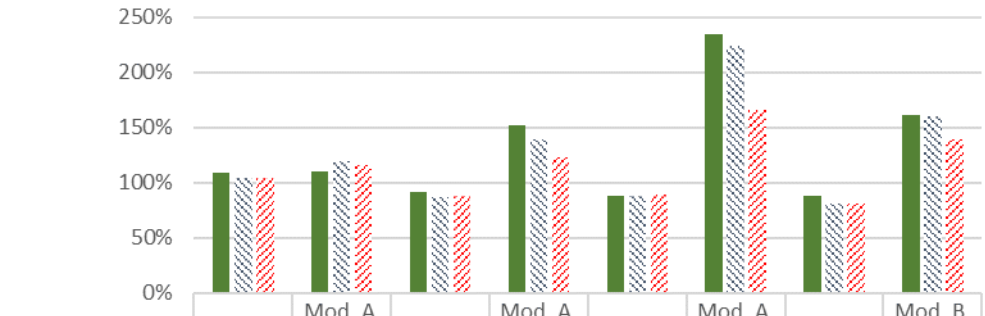

	Mod. A, 20 °C, US off	Mod. A, 20 °C, US 1520 W/L	Mod. A, 30 °C, US off	Mod. A, 30 °C, US 1520 W/L	Mod. A, 40 °C, US off	Mod. A, 40 °C, US 1520 W/L	Mod. B, 40 °C, US off	Mod. B, 40 °C, US 1520 W/L
c(O)/c(FT), chl a	109%	110%	92%	152%	89%	235%	89%	162%
c(O)/c(FT), chl b	105%	120%	87%	139%	88%	225%	82%	160%
c(O)/c(FT), car	105%	117%	88%	124%	89%	166%	81%	139%

Figure 43 Comparison of extraction experiments with modules A and B with and without ultrasound using 20 vol% ethanol. Nominal flow rate was 0.06 L/min, which corresponds to nominal residence times of 17.2 and 14.2 min for modules A and B, respectively. Mod = Module; US = nominal acoustic energy density; O = Outlet, FT = Feed tank; chl = Chlorophyll; car = Carotenoids.

The beneficial effect of ultrasound on the extraction process is underlined in the results shown in Figure 43. In addition, it can be seen that module B performed similarly to module A without ultrasound but fell behind in extraction efficiency once ultrasound was applied. This is a logical outcome of the differences in reactor pipe configurations, as a smaller fraction of the pulp volume in module B was adjacent to the transducer. In addition, due to pump speed limitations, module B was used with slightly shorter nominal mean residence times than module A (14 vs 17 min). Finally, another possible explanation is that different reaction tube diameters result in different mixing during ultrasonication.

7.5.1 Pilot DOE data analysis

The experimental results of the pilot DOE were analyzed with MODDE. The defined factors were solvent ethanol concentration, experiment temperature, storage time, and nominal AED. In addition, raw material type was added as a factor due to spinach availability issues. The mean concentration fractions shown in Figure 42 were used as the responses at first, but this caused high variation in the results. The responses were then changed to the mean

concentrations itself, and in order to include the effects of US into the model, each trial was entered twice – once using the calculated mean outlet concentrations (AED = 15), and again using the corresponding feed tank concentrations (US off) as the responses. The trial points, as they were fed into MODDE, are shown in Table 12.

Table 12 Experimental results of the pilot DOE with separate trials with extractive concentrations for samples with and without ultrasonication. In the experiments, inner diameter of the reaction tube was 18 mm, nominal flow rate was 0.06 L/min, and nominal residence time was 17.2 min.

Trial	Ethanol, vol%	T, °C	Storage time, d	Raw material	AED_{nom}, W/L	C(chl *a*), mg/L	C(chl *b*), mg/L	C(car), mg/L
1	20	20	12	Spinach	0	2.6	4.3	4.1
2	20	30	15	Spinach	0	1.9	1.1	1.4
3	20	40	12	Spinach	0	2.1	1.1	1.5
4	15	40	7	Spinach	0	4.9	2.3	2.3
5	25	40	1	Spinach	0	7.0	3.1	3.2
6	20	30	2	Spinach	0	7.7	3.4	3.2
7	20	30	1	Spinach	0	8.1	3.7	3.8
8	20	30	1	Baby spinach	0	12.4	5.0	4.2
9	15	30	1	Baby spinach	0	12.6	5.1	3.9
10	25	30	1	Baby spinach	0	8.9	3.9	3.9
11	15	20	1	Baby spinach	0	9.7	3.8	3.8
12	25	20	1	Baby spinach	0	9.4	3.8	4.2
13	20	20	12	Spinach	1530	2.9	5.1	4.8
14	20	30	15	Spinach	1530	2.9	1.6	1.7
15	20	40	12	Spinach	1530	4.9	2.5	2.4
16	15	40	7	Spinach	1530	6.9	3.4	2.8
17	25	40	1	Spinach	1530	11.6	4.9	4.2
18	20	30	2	Spinach	1530	14.0	6.0	5.1
19	20	30	1	Spinach	1530	13.3	5.8	5.4
20	20	30	1	Baby spinach	1530	20.0	7.8	6.1
21	15	30	1	Baby spinach	1530	16.6	6.4	4.8
22	25	30	1	Baby spinach	1530	15.4	6.1	5.3
23	15	20	1	Baby spinach	1530	19.4	7.5	6.7
24	25	20	1	Baby spinach	1530	15.3	6.2	6.3

The model was then fitted with PLS. Residual plots and observed vs predicted plots drawn with MODDE are shown for each of the responses in Figures 44-49.

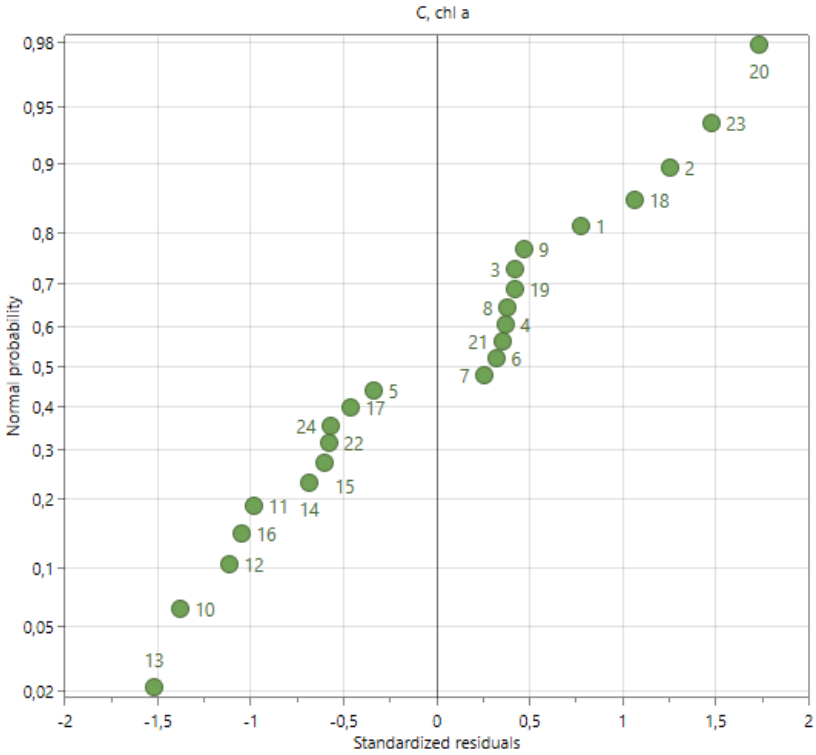

Figure 44 Initial residual plot for the UAE of chlorophyll *a* in the pilot DOE. Conditions were: R/S = 0.1; ethanol = 15, 20, or 25 vol%; T = 20, 30, or 40 °C; nominal AED = 0 or 1530 W/L; raw material storage time = 1-15 d; raw material = spinach or baby spinach.

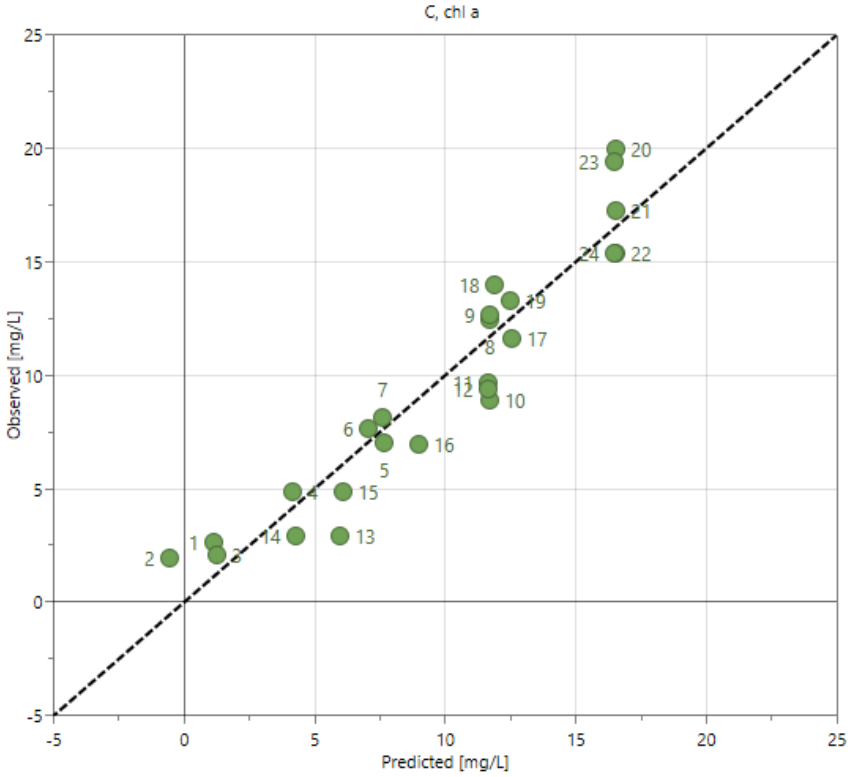

Figure 45 Initial observed vs predicted plot for the UAE of chlorophyll *a* in the pilot DOE. Conditions were: R/S = 0.1; ethanol = 15, 20, or 25 vol%; T = 20, 30, or 40 °C; nominal AED = 0 or 1530 W/L; raw material storage time = 1-15 d; raw material = spinach or baby spinach. For this fit, R^2 = 0.89 and Q^2 = 0.84.

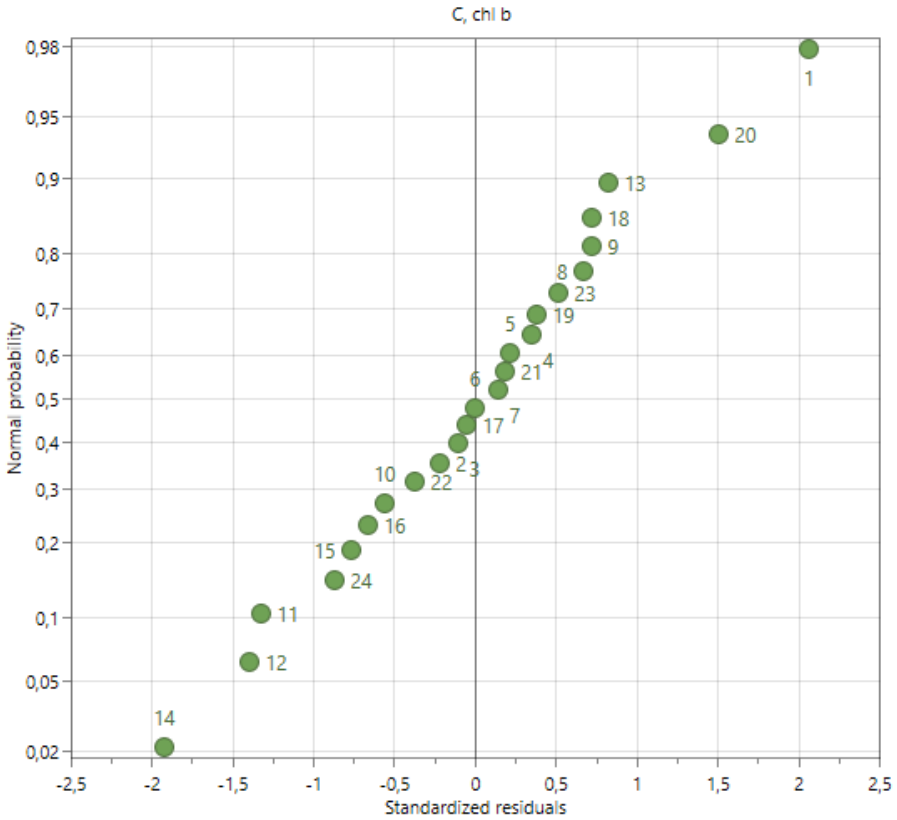

Figure 46 Initial residual plot for the UAE of chlorophyll *b* in the pilot DOE. Conditions were: R/S = 0.1; ethanol = 15, 20, or 25 vol%; T = 20, 30, or 40 °C; nominal AED = 0 or 1530 W/L; raw material storage time = 1-15 d; raw material = spinach or baby spinach.

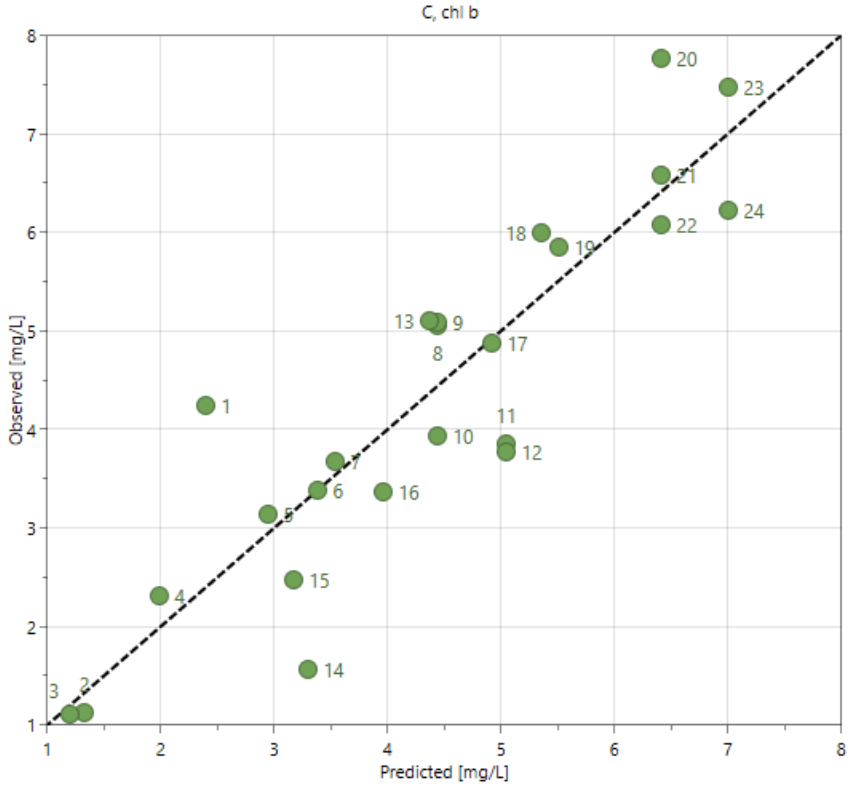

Figure 47 Initial observed vs predicted plot for the UAE of chlorophyll *b* in the pilot DOE. Conditions were: R/S = 0.1; ethanol = 15, 20, or 25 vol%; T = 20, 30, or 40 °C; nominal AED = 0 or 1530 W/L; raw material storage time = 1-15 d; raw material = spinach or baby spinach. For this fit, R^2 = 0.81 and Q^2 = 0.70.

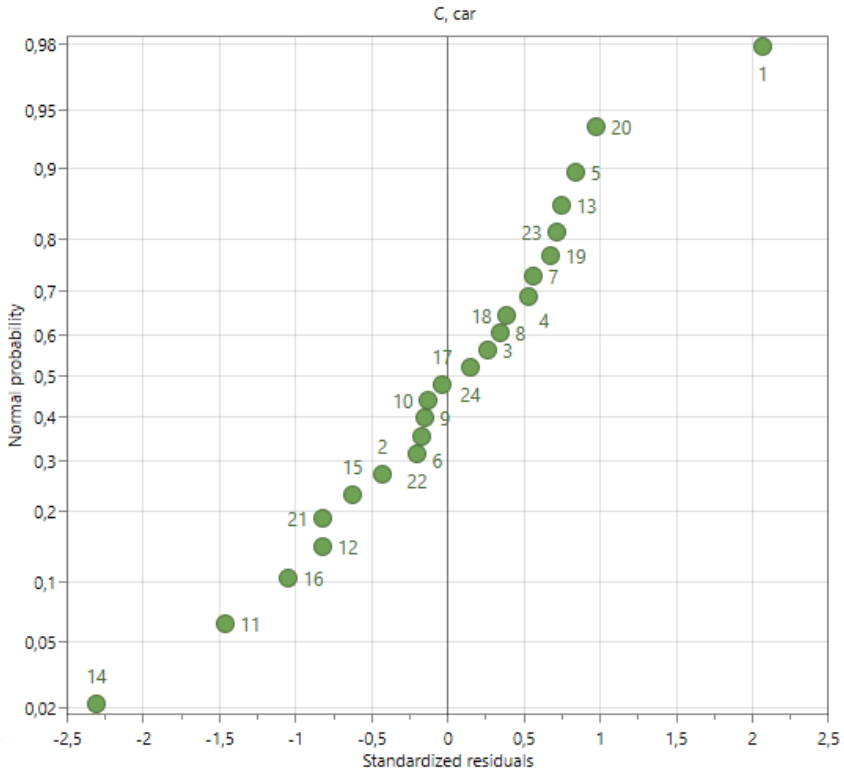

Figure 48 Initial residual plot for the UAE of carotenoids in the pilot DOE. Conditions were: R/S = 0.1; ethanol = 15, 20, or 25 vol%; T = 20, 30, or 40 °C; nominal AED = 0 or 1530 W/L; raw material storage time = 1-15 d; raw material = spinach or baby spinach.

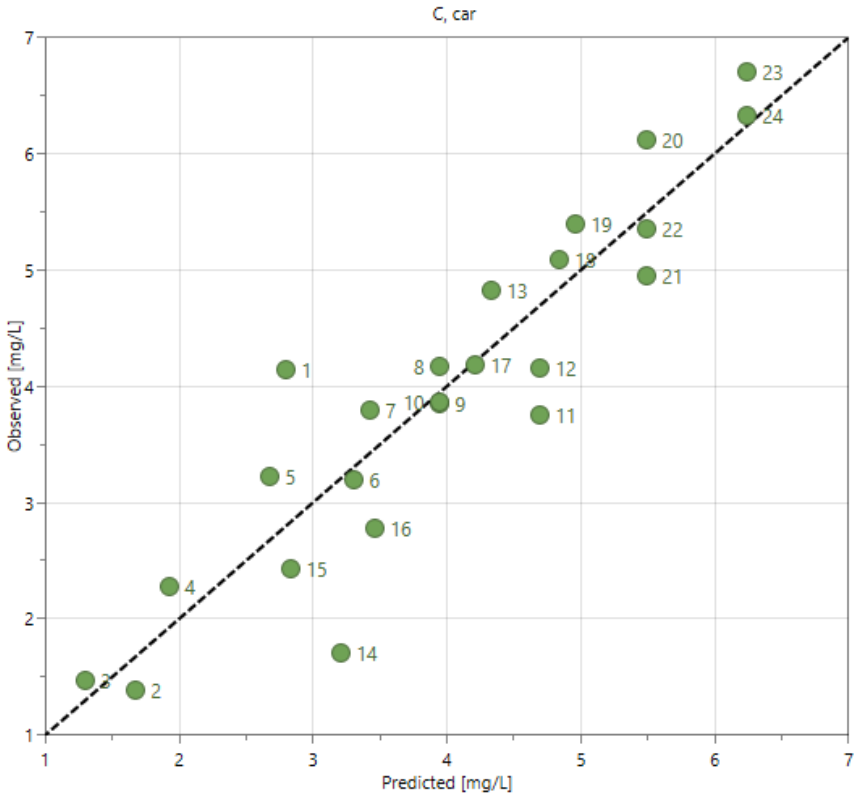

Figure 49 Initial observed vs predicted plot for the UAE of carotenoids in the pilot DOE. Conditions were: R/S = 0.1; ethanol = 15, 20, or 25 vol%; T = 20, 30, or 40 °C; nominal AED = 0 or 1530 W/L; raw material storage time = 1-15 d; raw material = spinach or baby spinach. For this fit, R^2 = 0.84 and Q^2 = 0.74.

Based on Figures 44-49, trials number 1, 13, 14, and 20 were removed from the model as outliers, as they deviated significantly from the fit. Coefficient plots for the three responses are displayed in Figures 50-52.

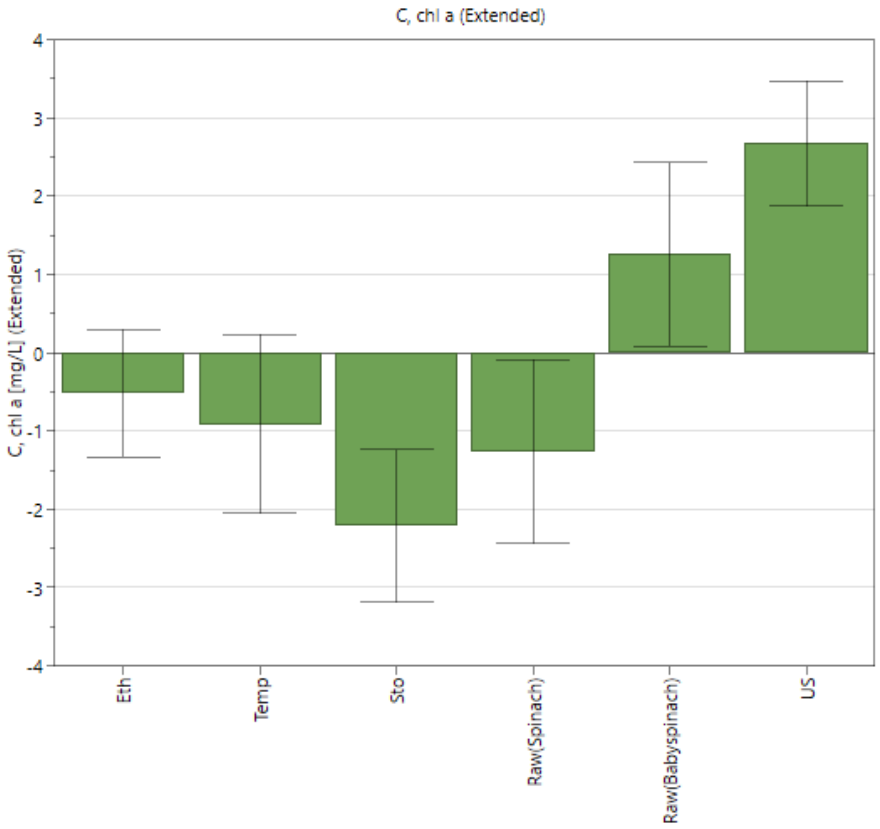

Figure 50 Initial coefficient plot for the UAE of chlorophyll *a* in the pilot scale DOE. Eth = Ethanol in solvent (15-25 vol%); Temp = process temperature (20-40 °C); Sto = storage time (1-15 d); Raw = raw material type (spinach or baby spinach); US = nominal ultrasonication power (0 or 1530 W/L).

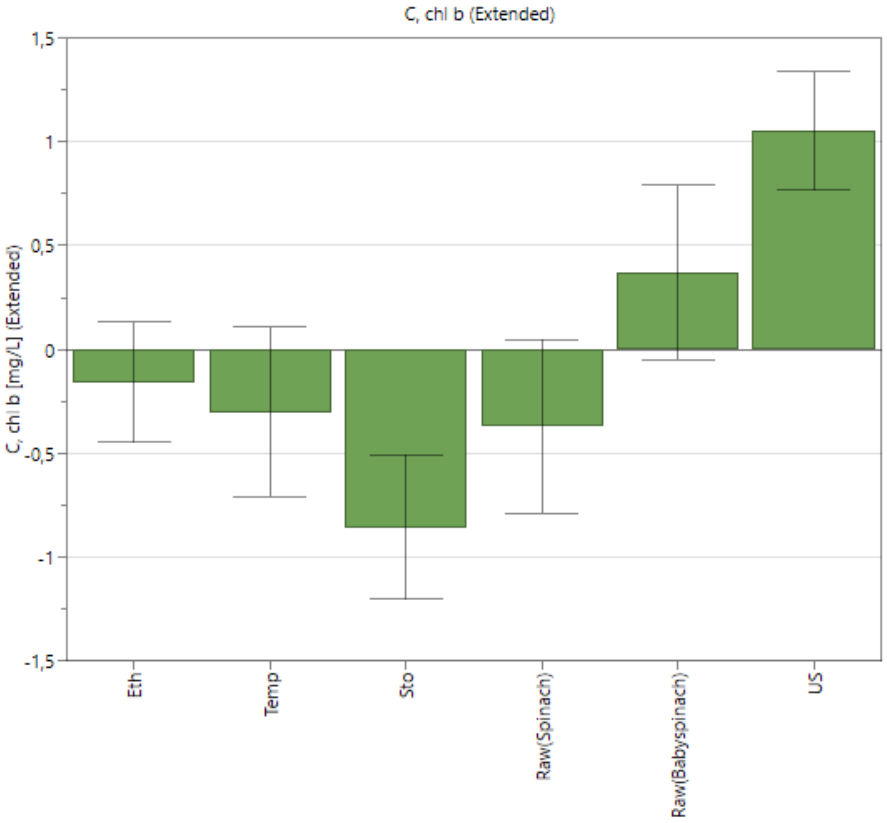

Figure 51 Initial coefficient plot for the UAE of chlorophyll *b* in the pilot scale DOE. Eth = Ethanol in solvent (15-25 vol%); Temp = process temperature (20-40 °C); Sto = storage time (1-15 d); Raw = raw material type (spinach or baby spinach); US = nominal ultrasonication power (0 or 1530 W/L).

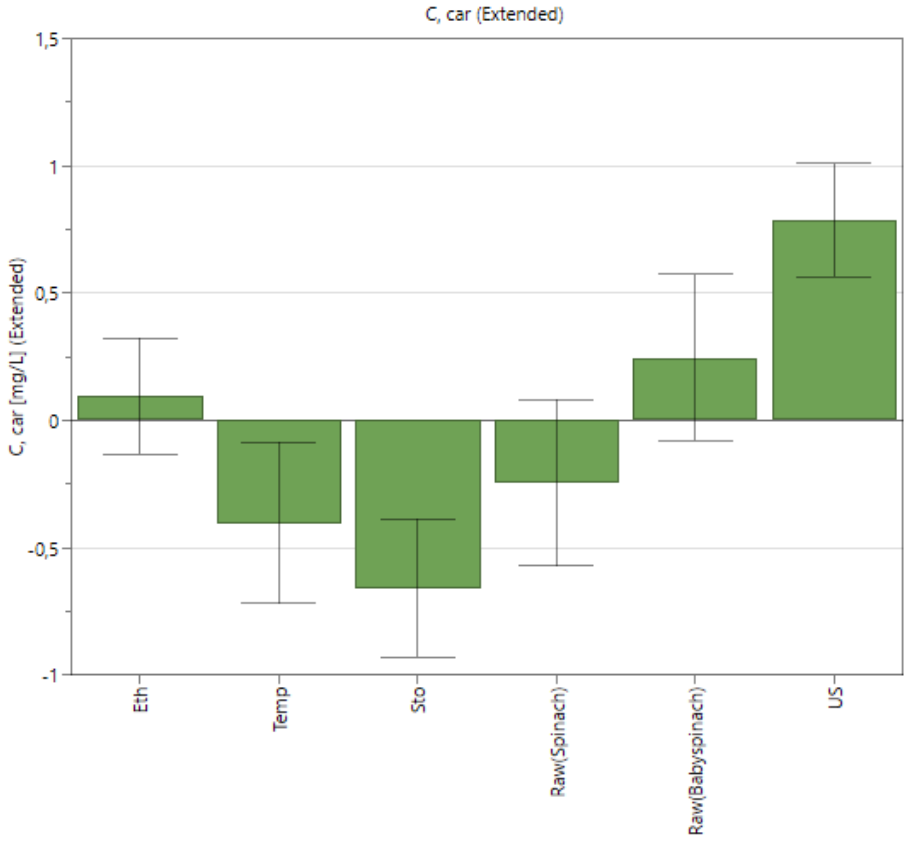

Figure 52 Initial coefficient plot for the UAE of carotenoids in the pilot scale DOE. Eth = Ethanol in solvent (15-25 vol%); Temp = process temperature (20-40 °C); Sto = storage time (1-15 d); Raw = raw material type (spinach or baby spinach); US = nominal ultrasonication power (0 or 1530 W/L).

Figures 50-52 show that changes in ethanol concentration between 15-25% in the solvent appeared inconsequential with all responses, and ethanol concentration then removed from the model. The effects of interaction factors and quadratic factors were investigated, and it was found that adding an interaction factor between temperature and ultrasound (T*US) benefited the model. As a result, R^2 and Q^2 values of the fits were improved to 0.93 and 0.89 for chlorophyll *a*, 0.94 and 0.90 for chlorophyll *b*, and 0.97 and 0.95 for carotenoids. Final residual plots and observed vs predicted plots for the responses are shown in Figures 53-58.

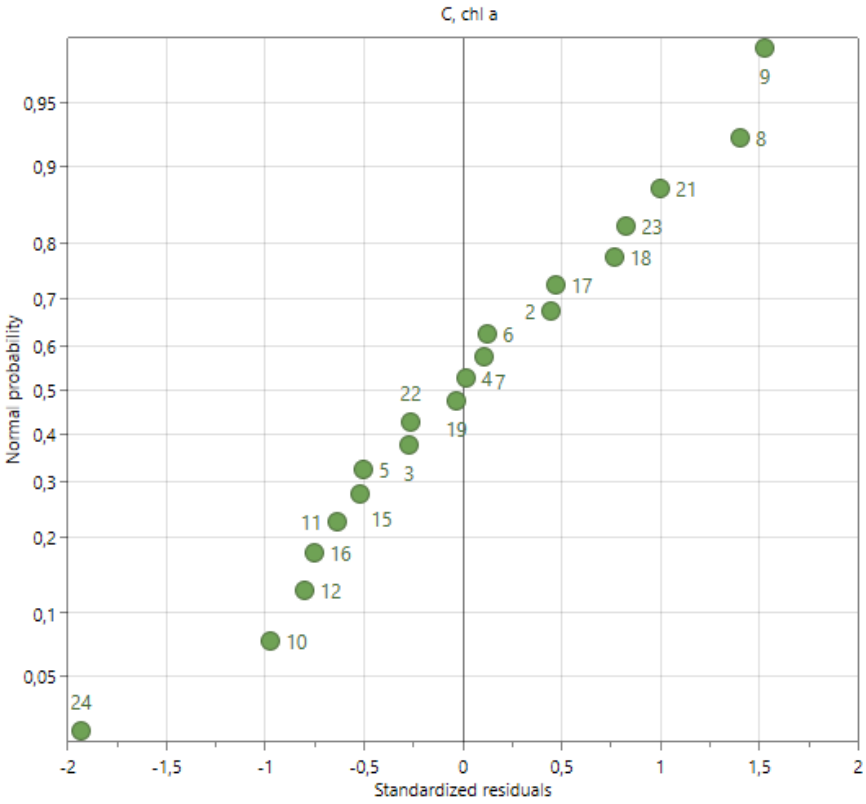

Figure 53 Final residual plot for the UAE of chlorophyll *a* in the pilot DOE. Conditions were: R/S = 0.1; ethanol = 15, 20, or 25 vol%; T = 20, 30, or 40 °C; nominal AED = 0 or 1530 W/L; raw material storage time = 1-15 d; raw material = spinach or baby spinach.

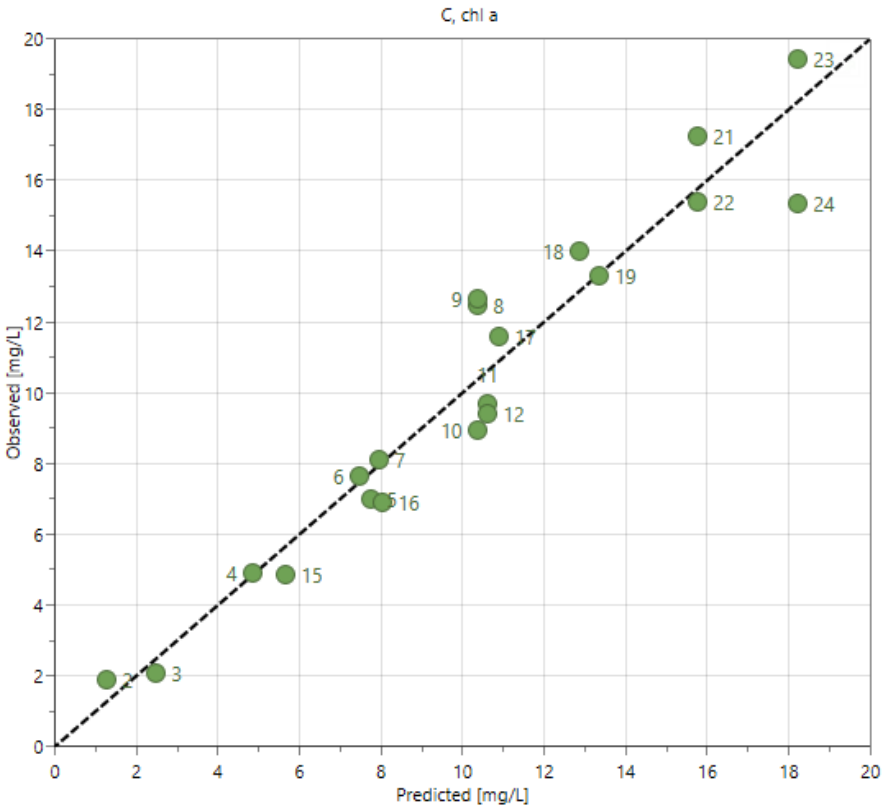

Figure 54 Initial observed vs predicted plot for UAE of chlorophyll *a* in the pilot DOE. Conditions were: R/S = 0.1; ethanol = 15, 20, or 25 vol%; T = 20, 30, or 40 °C; nominal AED = 0 or 1530 W/L; raw material storage time = 1-15 d; raw material = spinach or baby spinach. For this fit, R^2 = 0.93 and Q^2 = 0.89.

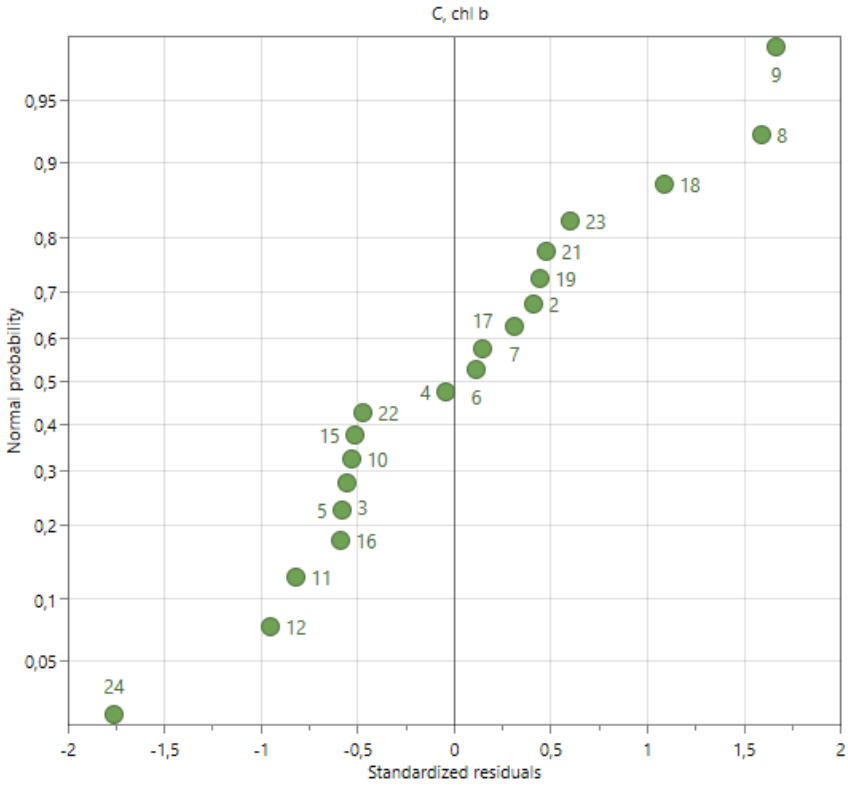

Figure 55 Final residual plot for the UAE of chlorophyll *b* in the pilot DOE. Conditions were: R/S = 0.1; ethanol = 15, 20, or 25 vol%; T = 20, 30, or 40 °C; nominal AED = 0 or 1530 W/L; raw material storage time = 1-15 d; raw material = spinach or baby spinach.

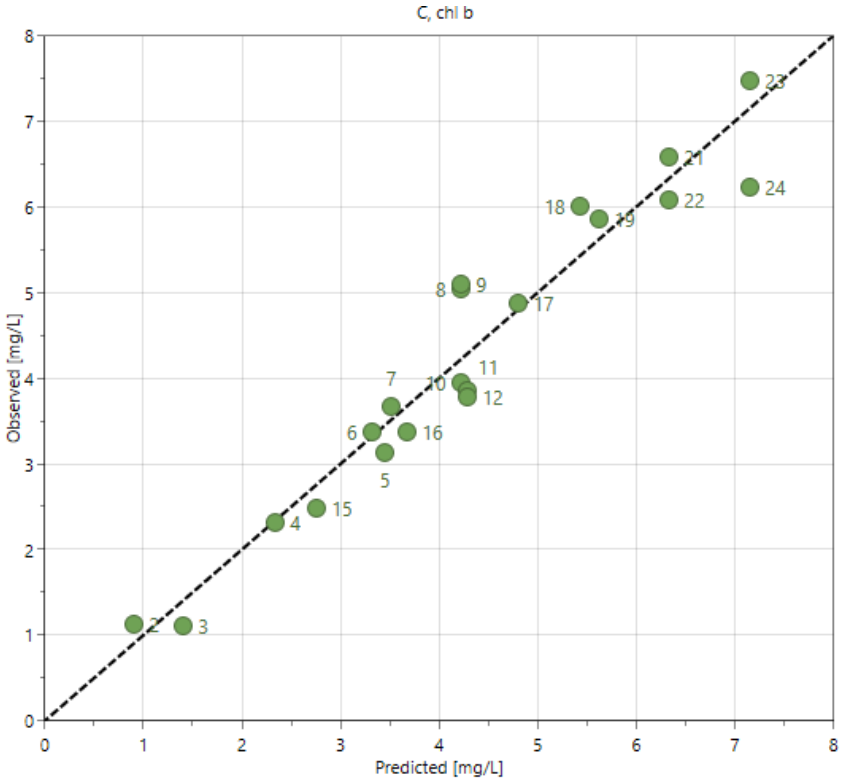

Figure 56 Final observed vs predicted plot for UAE of chlorophyll *b* in the pilot DOE. Conditions were: R/S = 0.1; ethanol = 15, 20, or 25 vol%; T = 20, 30, or 40 °C; nominal AED = 0 or 1530 W/L; raw material storage time = 1-15 d; raw material = spinach or baby spinach. For this fit, R^2 = 0.94 and Q^2 = 0.80.

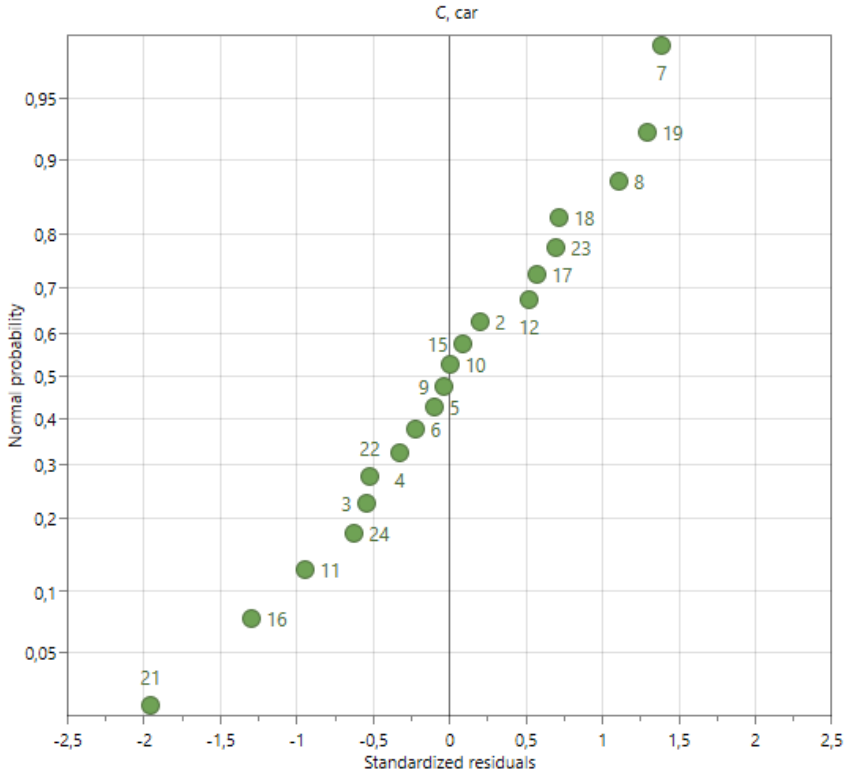

Figure 57 Final residual plot for the UAE of carotenoids in the pilot DOE. Conditions were: R/S = 0.1; ethanol = 15, 20, or 25 vol%; T = 20, 30, or 40 °C; nominal AED = 0 or 1530 W/L; raw material storage time = 1-15 d; raw material = spinach or baby spinach.

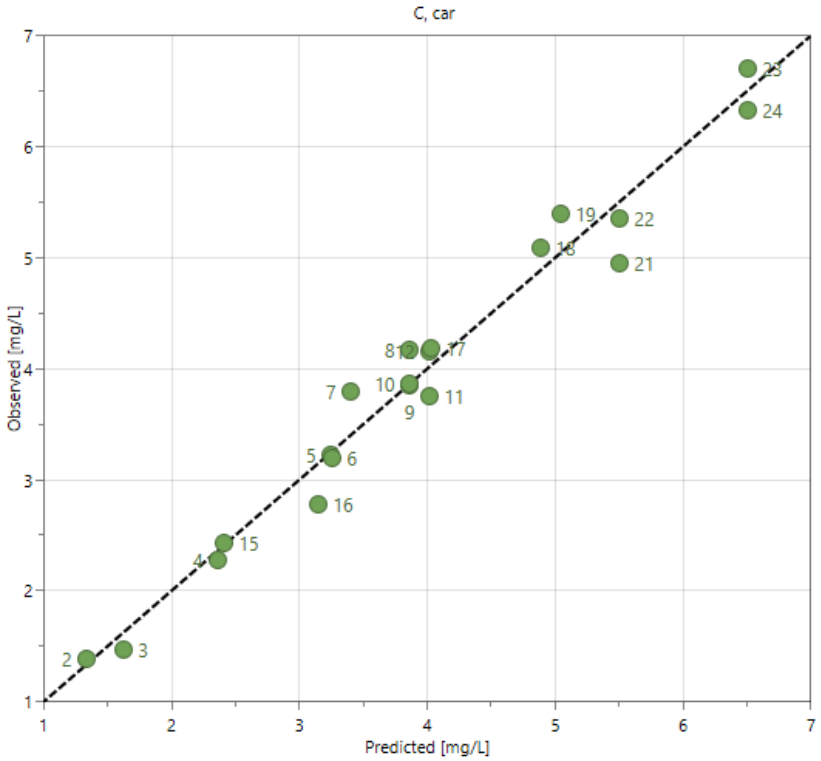

Figure 58 Final observed vs predicted plot for the UAE of carotenoids in the pilot DOE. Conditions were: R/S = 0.1; ethanol = 15, 20, or 25 vol%; T = 20, 30, or 40 °C; nominal AED = 0 or 1530 W/L; raw material storage time = 1-15 d; raw material = spinach or baby spinach. For this fit, R^2 = 0.97 and Q^2 = 0.95.

Based on Figures 53-58, trials 24 and 21 have the poorest fits to the model. However, it was decided to not remove any more data points in order to avoid overfitting. Final coefficient plots are shown in Figures 59-61.

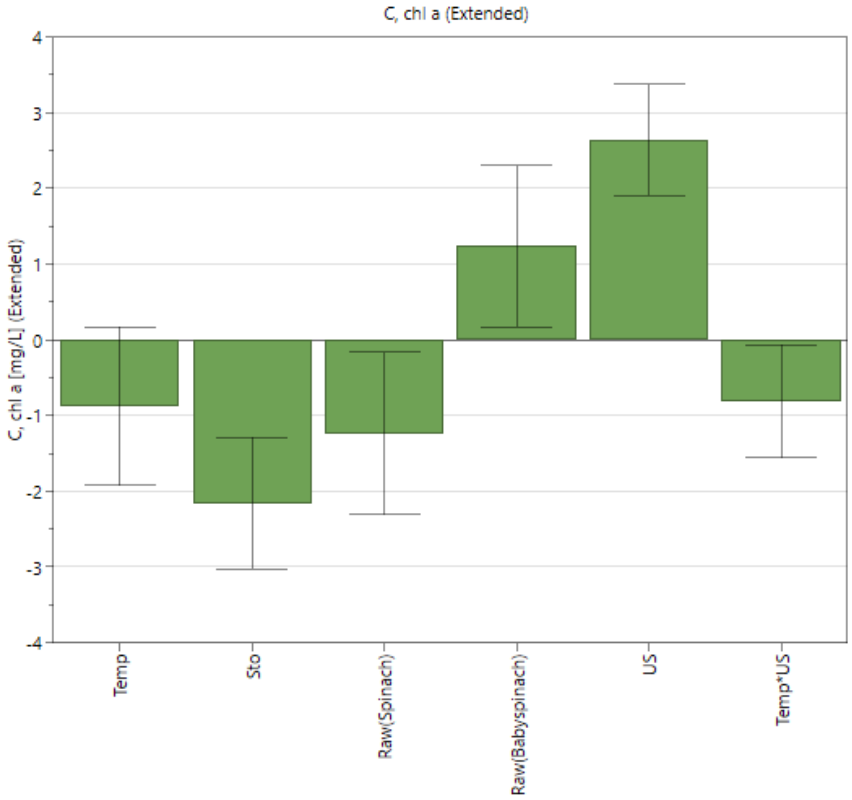

Figure 59 Final coefficient plot for the UAE of chlorophyll *a* in the pilot scale DOE. Temp = process temperature (20-40 °C); Sto = storage time (1-15 d); Raw = raw material type (spinach or baby spinach); US = nominal ultrasonication power (0 or 1530 W/L).

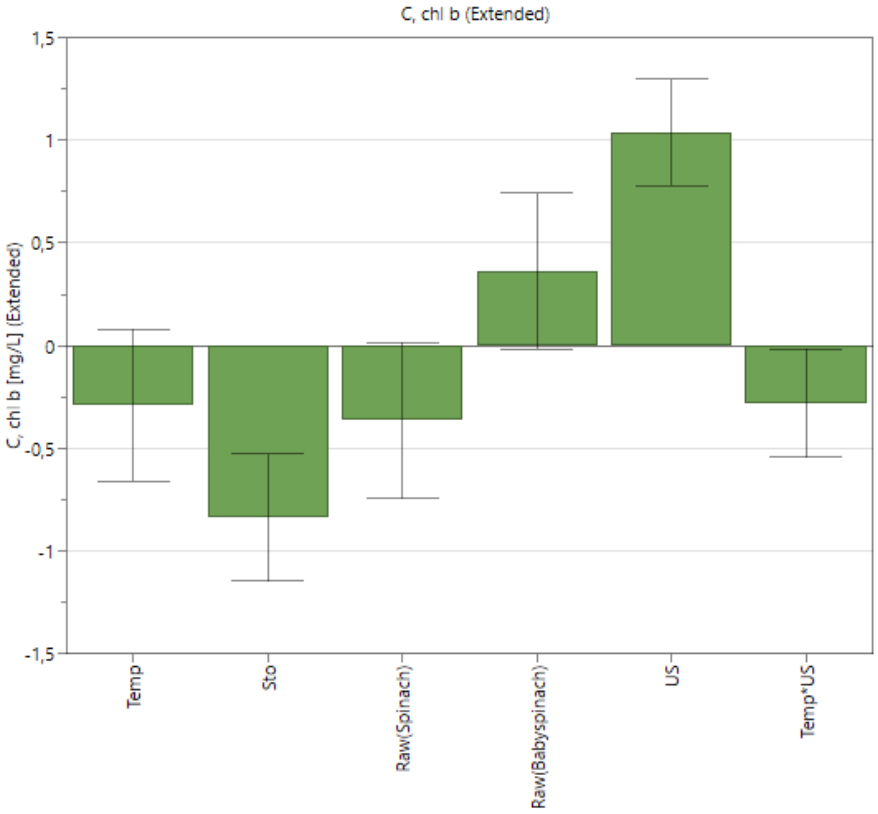

Figure 60 Final coefficient plot for the UAE of chlorophyll *b* in the pilot scale DOE. Temp = process temperature (20-40 °C); Sto = storage time (1-15 d); Raw = raw material type (spinach or baby spinach); US = nominal ultrasonication power (0 or 1530 W/L).

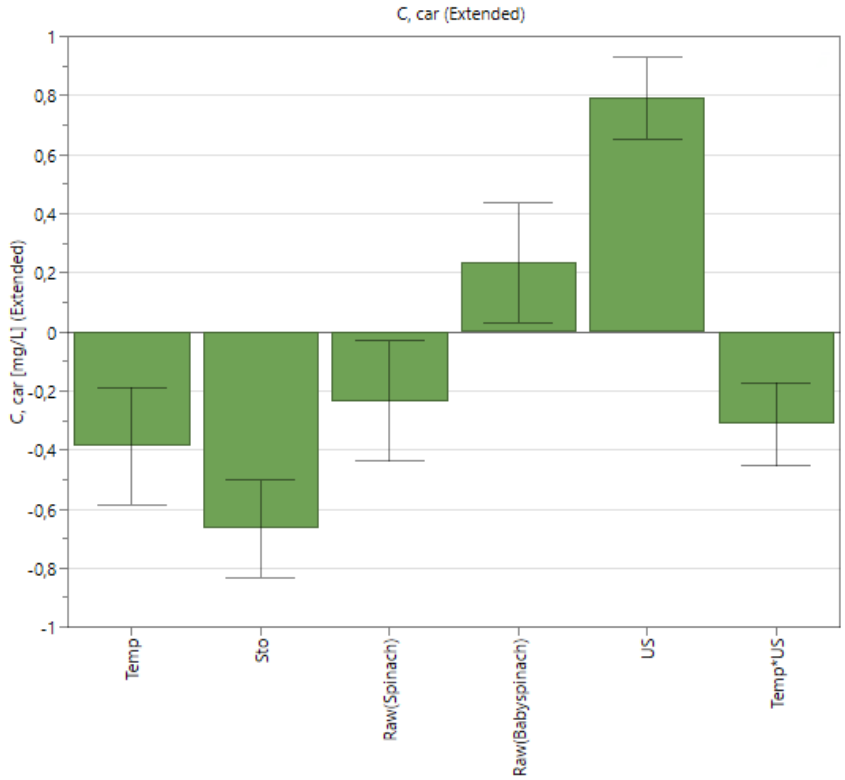

Figure 61 Final coefficient plot for the UAE of carotenoids in the pilot scale DOE. Temp = process temperature (20-40 °C); Sto = storage time (1-15 d); Raw = raw material type (spinach or baby spinach); US = nominal ultrasonication power (0 or 1530 W/L).

Figures 59-61 indicate that, as expected, ultrasonication benefited the extraction greatly and extended storage of the raw materials was detrimental due to degradation of the extractives. In addition, the different raw materials used affected extraction in favor of baby spinach. This seems logical, as baby spinach leaves are simply spinach leaves harvested at a less mature stage, and chlorophyll levels have been reported to be higher in younger leaves (Drews, 1996). Increase in process temperature, on the other hand, seemed to result in worse extraction performances, most clearly with carotenoids. Contour plots for ultrasonication vs storage time were drawn with MODDE and are shown in Figures 62-64.

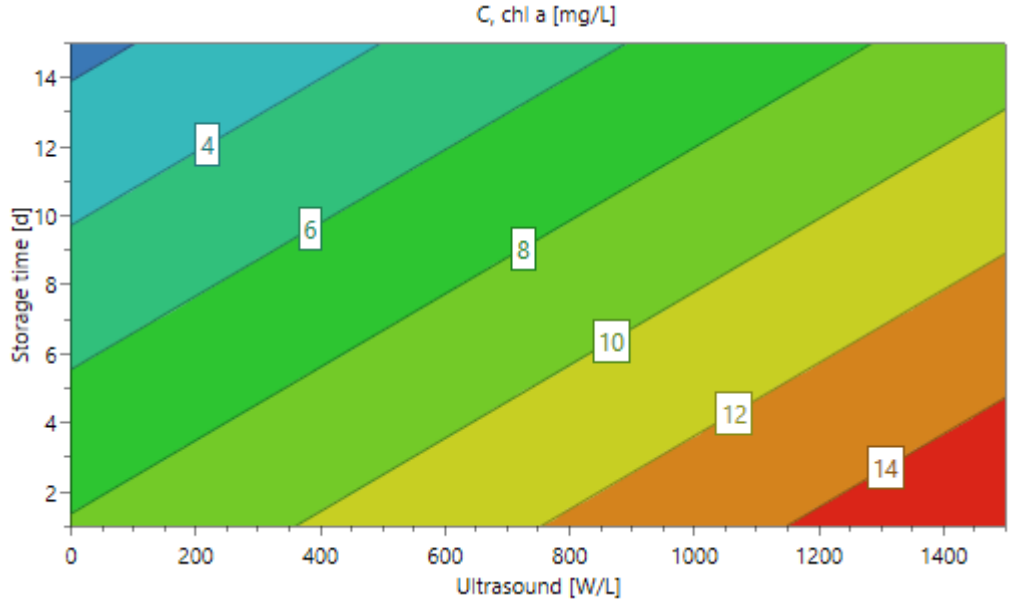

Figure 62 Contour plot showing the effects of raw material storage time and ultrasound power on chlorophyll *a* extraction in the pilot DOE. Constants: T = 20 °C, raw material = spinach.

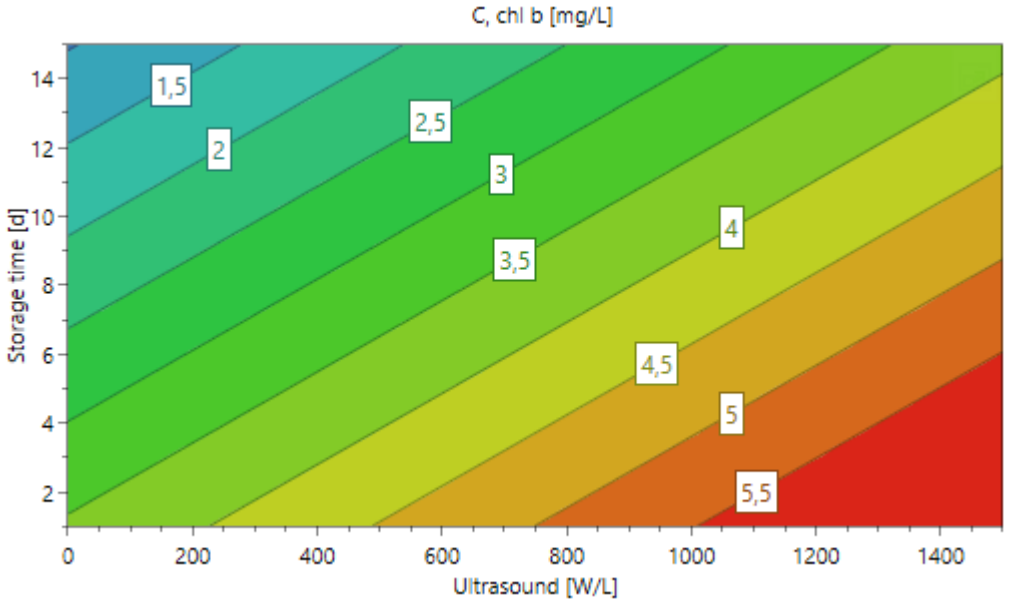

Figure 63 Contour plot showing the effects of raw material storage time and ultrasound power on chlorophyll *b* extraction in the pilot DOE. Constants: T = 20 °C, raw material = spinach.

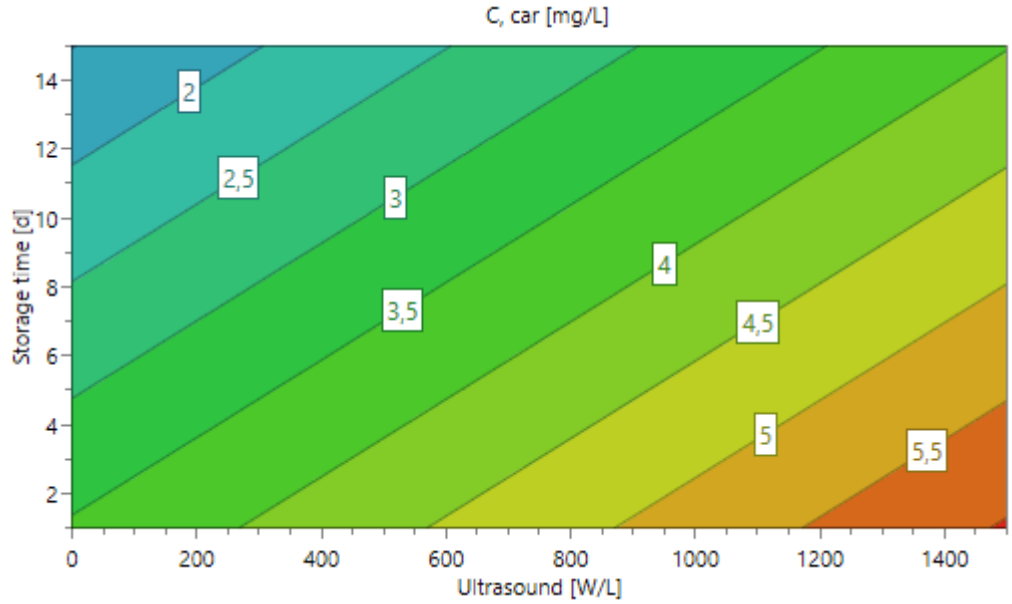

Figure 64 Contour plot showing the effects of raw material storage time and ultrasound power on carotenoid extraction in the pilot DOE. Constants: T = 20 °C, raw material = spinach.

Figures 62-64 clearly show that ultrasonication improved the extraction, while extended storage times were detrimental. Contour plots for ultrasonication vs temperature are shown in Figures 65-67.

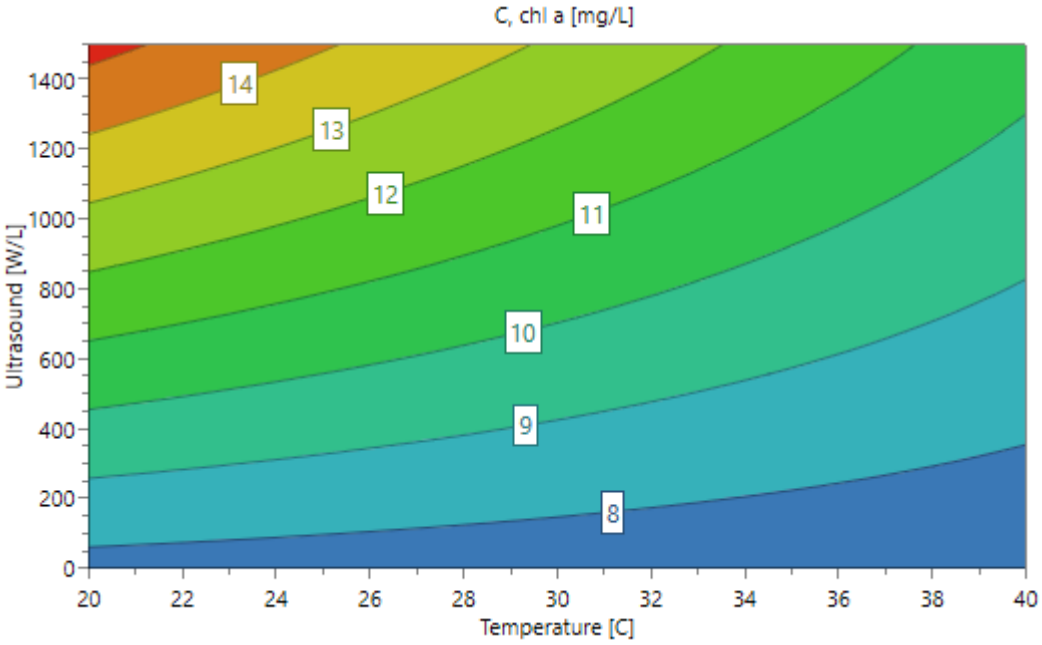

Figure 65 Contour plot showing the effects and ultrasound power and process temperature on chlorophyll *a* extraction in the pilot DOE. Constants: storage time = 2 d, raw material = spinach.

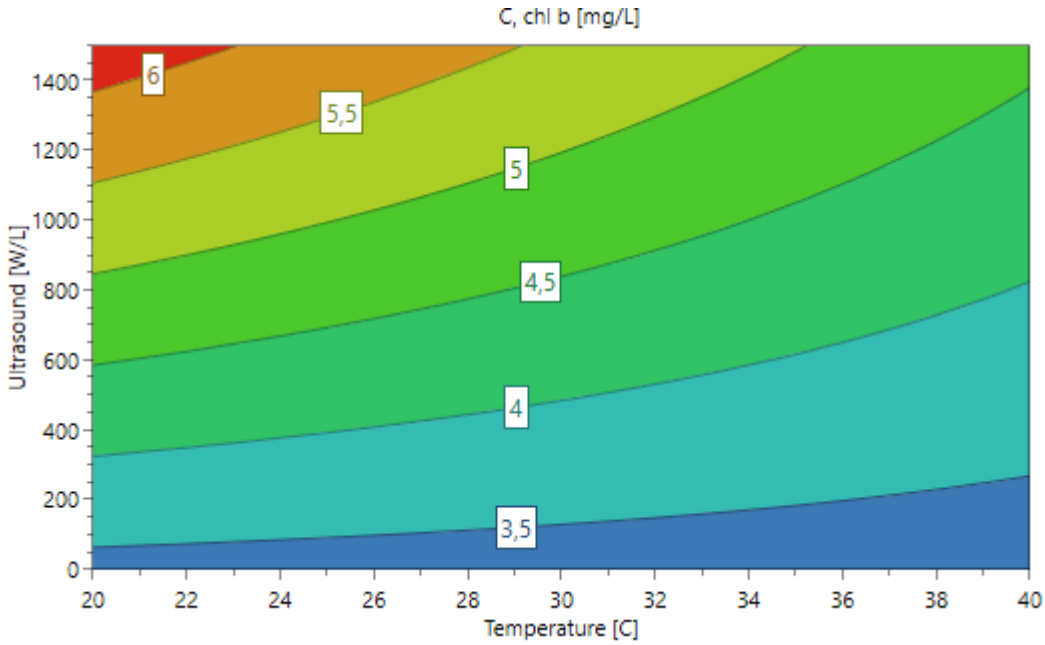

Figure 66 Contour plot showing the effects and ultrasound power and process temperature on chlorophyll *b* extraction in the pilot DOE. Constants: storage time = 2 d, raw material = spinach.

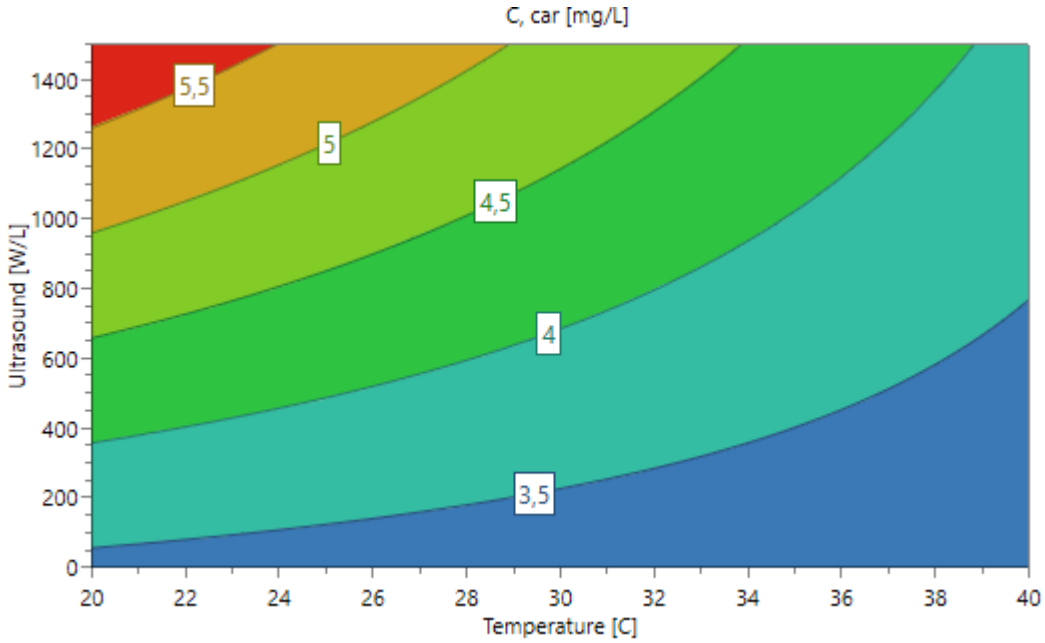

Figure 67 Contour plot showing the effects and ultrasound power and process temperature on carotenoid extraction in the pilot DOE. Constants: storage time = 2 d, raw material = spinach.

Figures 65-67 visualize how increase in process temperature between 20 and 40 °C appeared to be detrimental to the extraction process. This was surprising, as the temperature increase was expected to improve extraction speed, but product degradation was expected to be slow or nonexistent at temperatures of 40 °C and lower. At this stage it is unclear whether the decrease in extraction performance at higher temperatures was a result of product degradation or changes in solvent properties.

7.6 Scale-up outcomes

With the ultrasonic horn setup used in laboratory scale experiments, high US intensities and acoustic energy densities could be reached. The longitudinal sonotrodes used in the pilot modules have lower levels of intensity by design, as the area of the vibrating part of the sonotrode is large. However, the use of longitudinal vibrations should result in much more even cavitational distribution in the reactor, which is highly important in UAE processes.

In the pilot modules, most of the ultrasonic energy never reached the feed slurry inside the reaction tube due to scattering on the glycerol-steel as well as steel-feed phase boundaries, and it is very possible that there was never any acoustic cavitation in the feed slurry. Despite this, ultrasonication was shown to have highly beneficial effects on the extraction process. This could be a result of ultrasound induced micromixing caused by sound waves that reached inside the reaction tube, and even if the effect was small, it may have added up multiplicatively throughout the tube length. In addition, acoustic cavitation in the jacket likely affected the reaction tube from the outside, which may have resulted in brief hot spots on the tube wall and increased mixing in the feed slurry by impacts on the tube wall. Finally, as the reaction tube was coiled around the sonotrode, some of the reflected ultrasonic waves likely penetrated the tube wall from another location.

In the laboratory scale tests, it was found that the UAE process performed best with ethanol concentrations of around 20 vol%, even though concentrated ethanol has been reported to be ideal in conventional extraction experiments (Derrien et al., 2017). This is likely a result of interaction phenomena between ultrasound and the solvent. The effect of extraction temperature, however, remained inconclusive. In laboratory scale tests, temperature control

was not possible due to high acoustic energy densities and insufficient heat removal, and as a result, increasing US power also increased process temperature almost linearly. Increasing US power also increased extraction yield, and it was not possible to differentiate between the effects of US power and temperature on the yield. At pilot scale, where temperature control was possible, general trend was that temperature increase was seemingly detrimental to the extraction yield. In some cases, such as at 20 vol% ethanol, higher temperatures still seemed to increase the yield. Additional experiments should be conducted at different temperatures to reach a conclusion on this matter.

During the experiments at low pump speeds, the module outlet flow rates were observed to fluctuate. The pump may have been a bit too large for the modules used, as peristaltic hose pumps are generally not designed for operation at minimum speeds and increasing pump speed would have shortened residence times too much. This issue could be fixed by lengthening the reaction pipe or by operating several modules in a cascade.

All in all, the scale-up work shown could be described as successful, even though some open questions remain to be answered. By definition, the continuous pilot process also needs continuous raw material processing and extract separation, which were not implemented at this stage.

8 CONCLUSIONS

In this work, the UAE of chlorophylls and carotenoids from spinach and its upscaling from laboratory scale to pilot scale was investigated. The literature part focused on the principles, technologies, and scale-up issues related to UAE. In the experimental part, a laboratory scale batch process for the UAE of natural products was upscaled into pilot scale and converted to continuous operation. The extraction experiments were done using spinach leaves as the raw material and aqueous ethanol solutions as the solvent. A traditional ultrasonic horn setup was used at laboratory scale and two different tubular ultrasonication modules were used at pilot scale.

The extraction results showed that chlorophyll *a*, chlorophyll *b*, and carotenoids were successfully extracted from spinach leaves. The application of ultrasound clearly improved the extraction process with the pilot modules. Notably, the use of ultrasound was shown to be beneficial even though the ultrasound source was separated from the reaction solution by the walls of a steel pipe, which resulted in only a small fraction of the emitted acoustic energy reaching the processed solution due to reflection. Even better results could potentially be achieved with a reactor design where high-powered ultrasound is emitted directly into the solution, though in order to avoid damaging the products via overheating, ultrasonication times might then have to be reduced by pulsed sonication or decreased residence times.

In future work, more effort should be made to standardize the raw material supply, possibly by forming a direct agreement with a local supplier, and to use the materials with minimal delay. As natural products tend to be prone to degradation, this type of solution could help in minimizing the quality differences between raw material batches. In addition, the continuous pilot UAE process shown still lacks automated raw material pre-treatment as well as extract separation steps. From the perspective of commercial operation, however, these steps must likely be tailored separately for different extraction applications depending on raw material consistency, hardness, and texture, as well as the optimal extent of the treatment.

REFERENCES

Aboelsoud, N., 2009. Herbal medicine in ancient Egypt. *Journal of Medicinal Plants Research*, **4**(2), pp. 82-86.

Aggarwal, S. & Jain, T., 2019. Modern pretreatment techniques for phytochemical extraction. *Nutrition & Food Science*, **49**(3), pp. 441-454.

Alexandru, L., Cravotto, G., Giordana, L., Binello, A., and Chemat, F., 2013. Ultrasound-assisted extraction of clove buds using batch- and flow-reactors: A comparative study on a pilot scale. *Innovative Food Science & Emerging Technologies*, **20**, pp. 167-172.

Amarillo, M., Pérez, N., Blasina, F., Gambaro, A., Leone, A., Romaniello, R., Xu, X-Q, and Juliano, P., 2019. Impact of sound attenuation on ultrasound-driven yield improvements during olive oil extraction. *Ultrasonics Sonochemistry*, **53**, pp. 142-151.

Avvaru, B. & Pandit, A., 2009. Oscillating bubble concentration and its size distribution using acoustic emission spectra. *Ultrasonics Sonochemistry*, **16**(1), pp. 105-115.

Azwanida, N., 2015. A Review on the Extraction Methods Use in Medicinal Plants, Principle, Strength and Limitation. *Medicinal & Aromatic Plants*, **4**(3), pp. 1-6.

Barba, F., Parniakov, O., Pereira, S., Wiktor, S., Grimi, N., Boussetta, N., Saraiva, J., Raso, J., Martin-Belloso, O., Witrowa-Rajchert, D., Lebovka, N., and Vorobiev, E., 2015. Current applications and new opportunities for the use of pulsed electric fields in food science and industry. *Food Research International*, **77**, part 4, pp. 773-798.

Bendicho, C., De La Calle, I., Pena, F., Costas M., Cabaleiro, N., and Lavilla, I., 2012. Ultrasound-assisted pretreatment of solid samples in the context of green analytical chemistry. *TrAC Trends in Analytical Chemistry*, **31**, pp. 50-60.

Berk, Z., 2009. *Food Process Engineering and Technology*. Amsterdam: Academic Press, pp. 259-261.

Bermúdez-Aguirre, D., Mobbs, T., and Barbosa-Cánovas, G., 2011. Ultrasound Applications in Food Processing. In: H. Feng, G. Barbosa-Cánovas, and J. Weiss, eds., *Ultrasound Technologies for Food and Bioprocessing*. 1st ed, New York: Springer, pp. 69-77.

Belwal, T., Ezzat, S., Rastrelli, L., Bhatt, I., Daglia, M., Baldi, A., Devkota, H., Orhan, I., Patra, J., Das, G., Anandharamakrishnan, C., Gomez-Gomez, L., Nabavi, S.F., Nabavi, S.M., and Atanasov, A., 2018. A critical analysis of extraction techniques used for botanicals: Trends, priorities, industrial uses and optimization strategies. *TrAC Trends in Analytical Chemistry*, **100**, pp. 82-102.

Bertucco, A. & Franceschin, G., 2008. Supercritical Fluid Extraction of Medicinal and Aromatic Plants: Fundamentals and Applications. In: S. Handa, S. Khanuja, G. Longo, and D. Rakesh, eds., *Extraction Technologies for Medicinal and Aromatic Plants*. 1st ed. [pdf] Trieste: ICS-UNIDO. Available at: https://www.unido.org/sites/default/files/2009-10/Extraction_technologies_for_medicinal_and_aromatic_plants_0.pdf [Accessed 31.01.2020]

Beutler, J., 2009. Natural Products as a Foundation for Drug Discovery. *Current Protocols in Pharmacology*, **46**, 9.11.1-9.11.21.

Bhirud, U., Gogate, P., Wilhelm, A., and Pandit, A., 2004. Ultrasonic bath with longitudinal vibrations: a novel configuration for efficient wastewater treatment. *Ultrasonics Sonochemistry*, **11**(3-4), pp. 143-147.

Boodhoo, K. & Harvey, A., 2013. Process Intensification: An Overview of Principles and Practice. In: K. Boodhoo & A. Harvey, eds., *Process Intensification for Green Chemistry: Engineering Solutions for Sustainable Chemical Processing*. Chichester: John Wiley & Sons, pp. 3-30.

Chemat, F., Rombaut, N., Sicaire, A-G., Meullemiestre, A., Fabiano-Tixer, A-S., Abert-Vian, M., 2017. Ultrasound assisted extraction of food and natural products. Mechanisms,

techniques, combinations, protocols and applications. A review. *Ultrasonics Sonochemistry*, **34**, pp. 540-560.

Chua, L., Latiff, N., and Mohamad, M., 2016. Reflux extraction and cleanup process by column chromatography for high yield of andrographolide enriched extract. *Journal of Applied Research on Medicinal and Aromatic Plants*, **3**(2), pp. 64-70.

Cintas, P., Mantegna, S., Gaudino, E., and Cravotto, G., 2010. A new pilot flow reactor for high-intensity ultrasound irradiation. Application to the synthesis of biodiesel. *Ultrasonics Sonochemistry*, **17**(6), pp. 985-989.

Cole-Parmer, 2020. *Reducing Pulsation in Peristaltic Pumping Systems.* [online] Available at: https://www.coleparmer.com/tech-article/reducing-pulsation-peristaltic-pumping [Accessed 16.07.2020]

Dean, J., 1999. *Lange's Handbook of Chemistry*. New York: McGraw-Hill, pp. 5.85, 5.138.

Derrien, M., Badr, A., Gosselin, A., Desjardins, Y., and Angers, P., 2017. Optimization of a green process for the extraction of lutein and chlorophyll from spinach by-products using response surface methodology (RSM). *LWT – Food Science and Technology*, **79**, pp. 170-177.

Drews, H., 1996. *Analysis of Free Sugars and Chlorophyll in Spinach From A Local Retail Market*. Master's thesis. University of Tennessee.

Ezeanowi, N., Pajari, H., Laitinen, A., and Koiranen, T., 2020. Monitoring the Dynamics of a Continuous Sonicated Tubular Cooling Crystallizer. *Crystal Growth & Design*, **20**(3), pp. 1458-1466.

Fay, B. & Rinker, M., 1996. The thermoacoustic effect and its use in ultrasonic power determination. *Ultrasonics*, **34**(2-5), pp. 563-566.

Feng, R., Zhao, Y., Zhu, C., and Mason, T., 2002. Enhancement of ultrasonic cavitation yield by multi-frequency sonication. *Ultrasonics Sonochemistry*, **9**(5), pp. 231-236.

Fogler, H., 2005. *Elements of chemical reaction engineering*. Boston: Prentice Hall PTR, pp. 867-881.

Francony, A. & Pétrier, C., 1996. Sonochemical degradation of carbon tetrachloride in aqueous solution at two frequencies: 20 kHz and 500 kHz. *Ultrasonics Sonochemistry*, **3**(2), pp. S77-S82.

Generalic, E., 2018. *Soxhlet extractor*. [online] Croatian-English Chemistry Dictionary & Glossary. Available at: https://glossary.periodni.com/glossary.php?en=Soxhlet+extractor [Accessed 31.01.2020]

GMC, 2013. *Departments*. [online] Available at: https://www.gmariani.it/en/azienda/reparti#herb-extraction-ultrasound [Accessed 25.02.2020]

Gogate, P., Mujumdar, S., and Pandit, A., 2003. Large-scale sonochemical reactors for process intensification: design and experimental validation. *Journal of Chemical Technology and Biotechnology*, **78**(6), pp. 685-693.

Gogate, P. & Pandit, A., 2004. Sonochemical reactors: scale up aspects. *Ultrasonics Sonochemistry*, **11**(3-4), pp. 105-117.

Gogate, P. & Pandit, A., 2015. Design and scale-up of sonochemical reactors for food processing and other applications. In: A. Gallego-Juárez & K. Graff, eds., *Power Ultrasonics: Applications of High-Intensity Ultrasound*. 1st ed, Cambridge: Elsevier, pp. 728-752.

Groznova, A., 2014. *Modelling of ultrasound assisted mixing in Newtonian and non-Newtonian liquids*. Master's thesis. Lappeenranta University of Technology.

Henry, B., 2011. Colourings. In: J. Smith & L. Hong-Shum, eds., *Food Additives Data Book*. 2nd ed, Oxford: Wiley-Blackwell, pp. 182-183.

Hielscher Ultrasound Technology, 2020a. *Ultrasonic Cavitation in Liquids*. [online] Available at: https://www.hielscher.com/ultrasonic-cavitation-in-liquids-2.htm [Accessed 27.01.2020]

Hielscher Ultrasound Technology, 2020b. *UIP16000 – Most Powerful Ultrasonic Processor*. [online] Available at: https://www.hielscher.com/i16000_p.htm [Accessed 28.07.2020]

Hu, Y., Zhang, Z., and Yang, C., 2008. Measurement of hydroxyl radical production in ultrasonic aqueous solutions by a novel chemiluminescence method. *Ultrasonics Sonochemistry,* **15**(5), pp. 665-672.

Industrial Sonomechanics LLC, 2020. *ISP-3000 Industrial-Scale Processor*. [online] Available at: https://www.sonomechanics.com/3000_w_industrial-scale_processor/ [Accessed 28.07.2020]

Izewska, J. & Rajan, G., 2005. Radiation dosimeters. In: E. Podgorsak, ed., *Radiation oncology physics: A handbook for teachers and students*. 1st ed. Vienna: International Atomic Energy Agency, pp. 94-98.

Jordens, J., Bamps, B., Gielen, B., Braeken, L., Van Gerven, T., 2016. The effects of ultrasound on micromixing. *Ultrasonics Sonochemistry*, **32**, pp. 68-78.

Kanthale, P., Gogate, P., Pandit, A., and Wilhelm, A., 2003. Mapping of an ultrasonic horn: link primary and secondary effects of ultrasound. *Ultrasonics Sonochemistry*, **10**(6), pp. 331-335.

Khaiat, A., 2002. Botanical extracts. *Journal of Toxicology: Cutaneous and Ocular Toxicology*, **21**(1-2), pp. 109-118.

Khoo, H., Prasad, K., Kong, K., Jiang, Y., and Ismail, A., 2011. Carotenoids and Their Isomers: Color Pigments in Fruits and Vegetables. *Molecules*, **16**, pp. 1710-1738.

Kikuchi, T. & Uchida, T., 2011. Calorimetric method for measuring high ultrasonic power using water as a heating material. *Journal of Physics: Conference Series*, **279**.

Knorr, D., Zenker, M., Heinz, V., and Lee, D-U., 2004. Applications and potential of ultrasonics in food processing. *Trends in Food Science & Technology*, **15**(5), pp. 261-266.

Koda, S., Kimura, T., Kondo, T., and Mitome, H., 2003. A standard method to calibrate sonochemical efficiency of an individual reaction system. *Ultrasonics Sonochemistry*, **10**(3), pp. 149-156.

Krause, J. & Tobin, G., 2013. Discovery, Development, and Regulation of Natural Products. In: M. Kulka, ed., *Using Old Solutions to New Problems – Natural Drug Discovery in the 21st Century*. 1st ed. Rijeka: InTech, pp. 3-5.

Kumar, A., Gogate, P., and Pandit, A., 2007. Mapping the efficacy of new designs for large scale sonochemical reactors. *Ultrasonics Sonochemistry*, **14**(5), pp. 538-544.

Levenspiel, O., 1999. *Chemical Reaction Engineering*. 3rd ed. New York: John Wiley & Sons, pp. 260-273.

Lichtenthaler, H. and Buschmann, C., 2001. Chlorophylls and Carotenoids: Measurement and Characterization by UV-VIS Spectroscopy. *Current Protocols in Food Analytical Chemistry*, 1(1), Unit F4.3.1 – F4.3.8.

Mahmoud, A., Olivier, J., Vaxelaire, J., and Hoadley, A., 2013. Advances in Mechanical Dewatering of Wastewater Sludge Treatment. In: S. Sharma & R. Sanghi, eds., *Wastewater Reuse and Management*. 1st ed, Dordrecht: Springer, pp. 253-261, 271-290.

Malathi, N., Sahoo, P., Praveen, K., and Murali, N., 2013. A novel approach towards development of real time chemical dosimetry using pulsating sensor-based instrumentation. *Journal of Radioanalytical and Nuclear Chemistry*, **298**(2), pp. 963-972.

Manolopoulou, E. & Varzakas, T., 2016. Effect of Temperature in Color Changes of Green Vegetables. *Current Research in Nutrition and Food Science*, **4**(2), pp. 10-17.

Marathe, S., Jadhav, S., Bankar, S., and Singhal, R., 2017. Enzyme-Assisted Extraction of Bioactives. In: M. Puri, ed., *Food Bioactives – Extraction and Biotechnology Applications*. 1st ed, Cham: Springer International Publishing AG, pp. 171-174.

Martínez, J., Delso, C., Álvarez, I., and Raso, J., 2020. Pulsed electric field-assisted extraction of valuable compounds from microorganisms. *Comprehensive Reviews in Food Science and Food Safety*, **19**(2), pp. 530-552.

Mason, T., Chemat, F., and Ashokkumar, M., 2015. Power ultrasonics for food processing. In: A. Gallego-Juárez & K. Graff, eds., *Power Ultrasonics: Applications of High-Intensity Ultrasound*. 1st ed, Cambridge: Elsevier, pp. 815-821.

Mason, T. & Lorimer, J., 1988. *Sonochemistry: theory, applications and uses of ultrasound in chemistry*. Chichester: Ellis Horwood Limited, pp. 12, 25-26.

Menon, A., Mashyamombe, T., Kaygen, E., Nasiri, M., and Stojceska, V., 2019. Electro-osmosis dewatering as an energy efficient technique for drying food materials. *Energy Procedia*, **161**, pp. 123-132.

Mishra, V., Bacheti, R., and Husen, A., 2011. Medicinal Uses of Chlorophyll: A Critical Overview. In: H. Le & E. Salcedo, eds., *Chlorophyll: Structure, Function and Medicinal Uses*. 1st ed, New York: Nova Science Publishers, Inc., pp. 177-196.

Moliserb s.r.l, 2003. *This is Moliserb*. [online] Available at: http://www.moliserb.com/ [Accessed 25.02.2020]

Monnier, H., Wilhelm, A., and Delmas, H., 1999. Effects of ultrasound on micromixing in flow cell. *Chemical Engineering Science,* **55**(19), pp. 4009-4020.

Mujumdar, A. & Yoshida, H., 2008. Electro-Osmotic Dewatering (EOD) of Bio-Materials. In: E. Vorobiev & N. Lebovka, eds., *Electrotechnologies for Extraction from Food Plants and Biomaterials*. 1st ed, New York: Springer, pp. 128-130.

Nauman, E., 2004. Residence time distributions. In: E. Paul, V. Atiemo-Obeng, and S. Kresta, eds., *Handbook of Industrial Mixing: Science and Practice*. 1st ed, New Jersey: John Wiley & Sons, pp. 3-4.

Nasardin, N., Hanafiah, M., Zainon, M., Ibrahim, M., Zulkefle, A., and Rahman, A., 2018. Comparative Study on Steam Distillation and Hydro-Distillation Methods for Agarwood Oil Extraction. *International Journal of Applied Engineering Research,* **13**(8), pp. 6253-6256.

NDT Resource Center, 2006. *Reflection and Transmission Coefficients*. [online] Available at: https://www.nde-ed.org/EducationResources/CommunityCollege/Ultrasonics/Physics/reflectiontransmission.htm [Accessed 10.02.2020]

Ng, S., Plunkett, A., Stojceska, V., Ainswort, P., Lamont-Black, J., Hall, J., White, C., Glendenning, S., and Russell, D., 2011. Electro-Kinetic Technology as a Low-Cost Method for Dewatering Food By-Product. *Drying Technology*, **29**(14), pp. 1721-1728.

Nickel, K. & Neis, U., 2007. Ultrasonic disintegration of biosolids for improved biodegradation. *Ultrasonics Sonochemistry*, **14**(4), pp. 450-455.

Orsat, V., Raghavan, G., and Norris, E., 1996. Food processing waste dewatering by electro-osmosis. *Canadian Agricultural Engineering*, **38**(1), pp. 63-67.

Palma, M., Barbero, G., Piñeiro, Z., Liazid, A., Barroso, C., Rostagno, M., Prado, J, and Meireles, M., 2013. Extraction of Natural Products: Principles and Fundamental Aspects.

In: M. Rostagno & J. Prado, eds., *Natural Product Extraction: Principles and Applications*. 1st ed. Cambridge: The Royal Society of Chemistry, pp. 78-82.

Parvizian, F., Rahimi, M., and Azimi, N., 2012. Macro- and micromixing studies on a high frequency continuous tubular sonoreactor. *Chemical Engineering and Processing: Process Intensification*, **57-58**, pp. 8-15.

Pangarkar, V., 2008. Microdistillation, Thermomicrodistillation, and Molecular Distillation Techniques. In: S. Handa, S. Khanuja, G. Longo, and D. Rakesh, eds., *Extraction Technologies for Medicinal and Aromatic Plants*. 1st ed. [pdf] Trieste: ICS-UNIDO. Available at: https://www.unido.org/sites/default/files/2009-10/Extraction_technologies_for_medicinal_and_aromatic_plants_0.pdf [Accessed 31.01.2020]

Pétrier, C., Jeunet, A., Luche, J., and Reverdy, G., 1992. Unexpected frequency effects on the rate of oxidative processes induced by ultrasound. *Journal of the American Chemical Society*, **114**(8), pp. 3148-3150.

Pingret, D., Fabiano-Tixier., A-S., Chemat, F., 2013. Ultrasound-assisted Extraction. In: M. Rostagno & J. Prado, eds., *Natural Product Extraction: Principles and Applications*. 1st ed. Cambridge: The Royal Society of Chemistry, pp. 90-92, 100-106.

Popescu, E. & Buruleaun, C., 2017. Heat Degradation Kinetics of the Chlorophyll from Spinach and its Correlation with the Reflection Spectra. *Revista de Chimie*, **68**(4), pp. 830-834.

Rahimi, M., Safari, S., Faryadi, M., and Moradi, N., 2014. Experimental investigation on proper use of dual high-low frequency ultrasound waves-Advantage and disadvantage. *Chemicaln Engineering and Processing: Process Intensification*, **78**, pp. 17-26.

Rasband, W., 1997-2018. ImageJ, U. S. National Institutes of Health, Bethesda, Maryland, USA, https://imagej.nih.gov/ij/.

Regulation (EC) No 1334/2008 of the European Parliament and of the Council of 16 December 2008 on flavourings and certain food ingredients with flavouring properties for use in and on foods and amending Council Regulation (EEC) No 1601/91, Regulations (EC) No 2232/96 and (EC) No 110/2008 and Directive 2000/13/EC, 2008. *Official Journal of the European Union*, L354, pp. 34-50.

Richardson, J., Harker, J., Backhurst, J., and Coulson, J., 2002. *Coulson and Richardson's chemical engineering. Vol. 2, Particle technology and separation processes*. 5th ed. Oxford: Butterworth-Heinemann, pp. 10-14.

Råde, L. & Westergren, B., 1995. *Mathematics handbook for science and engineering*. 3rd ed. Lund: Studenrlitteratur.

Rudenko, O., Sarvazyan, A., and Emelianov, S., 1996. Acoustic radiation force and streaming induced by focused nonlinear ultrasound in a dissipative medium. *The Journal of the Acoustical Society of America*, **99**(5).

Saito, S., 2015. Ultrasound Field and Bubbles. In: F Grieser, P Choi, N Enomoto, H Harada, K Okitsu, and K Yasui, eds., *Sonochemistry and the Acoustic Bubble*. 1st ed. Amsterdam: Elsevier, pp. 17-30.

Schwartz, S. & von Elbe, J., 1983. Kinetics of chlorophyll degradation to pyropheophytin in vegetables. *Journal of Food Science*, **48**, pp. 1303-1306.

Selfridge, A., 1985. Approximate Material Properties in Isotropic Materials. *IEEE Transactions on Sonics and Ultrasonics*, **32**(3), pp. 381-394.

Servant, G., Laborde, J-L., Hita, A., Caltagirone, J-P., and Gérard, A., 2001. Spatio-temporal dynamics of cavitation bubble clouds in a low frequency reactor: comparison between theoretical and experimental results. *Ultrasonics Sonochemistry*, **8**(3), pp. 163-174.

Shirsath, S., Sonawane, S., and Gogate, P., 2012. Intensification of extraction of natural products using ultrasonic irradiations – A review of current status. *Chemical Engineering and Processing: Process Intensification*, **53**, pp. 10-23.

Singh, J., 2008. Maceration, Percolation and Infusion Techniques for the Extraction of Medicinal and Aromatic Plants. In: S. Handa, S. Khanuja, G. Longo, and D. Rakesh, eds., *Extraction Technologies for Medicinal and Aromatic Plants*. 1st ed. [pdf] Trieste: ICS-UNIDO. Available at: https://www.unido.org/sites/default/files/2009-10/Extraction_technologies_for_medicinal_and_aromatic_plants_0.pdf [Accessed 30.01.2020]

Sivakumar, M., Tatake, P., and Pandit, A., 2002. Kinetics of *p*-nitrophenol degradation: effect of reaction conditions and cavitational parameters for a multiple frequency system. *Chemical Engineering Journal*, **85**(2-3), pp. 327-338.

Stephanopoulos, G., 1984. *Chemical Process Control: An introduction to theory and practice*. London: Prentice Hall.

Suri, C., Takenaka, K., Yanagida, H., Kojima, Y., and Koyama, K., 2002. Chaotic mixing generated by acoustic streaming. *Ultrasonics*, **40**(1-8), pp. 393-396.

Suslick, K., 1994. The Chemistry of Ultrasound. In: D. Calhoun, ed., *Yearbook of Science and the Future 1994*. 1st ed. Chicago: Encyclopaedia Britannica, pp. 138-155.

Suslick, K. & Price, G., 1999. Applications of ultrasound to materials chemistry. *Annual Review of Materials Science*, **29**, pp. 295-326.

Suslick, K., Eddingsaas, N., Flannigan, D., Hopkins, S., and Xu, H., 2018. The Chemical History of a Bubble. *Accounts of Chemical Research*, **51**(9), pp. 2169-2178.

Sutkar, V., Gogate, P., and Csoka, L., 2010. Theoretical prediction of cavitational activity distribution in sonochemical reactors. *Chemical Engineering Journal*, **158**(2), pp. 290-295.

Takamura, K., Fischer, H., and Morrow, N., 2012. Physical properties of aqueous glycerol solutions. *Journal of Petroleum Science and Engineering*, **98-99**, pp. 50-60.

Takeuchi, T., Pereira, C., Braga, M., Maróstica Jr., M., Leal, P., and Meireles, M., 2009. Low-Pressure Solvent Extraction (Solid-Liquid Extraction, Microwave Assisted and Ultrasound Assisted) from Condimentary Plants. In: M. Meireles, ed., *Extracting Bioactive Compounds for Food Products: Theory and Applications*. 1st ed. Boca Raton: CRC Press – Taylor & Francis Group, p. 137.

Tandon, S. & Rane, S., 2008. Decoction and Hot Continuous Extraction Techniques. In: S. Handa, S. Khanuja, G. Longo, and D. Rakesh, eds., *Extraction Technologies for Medicinal and Aromatic Plants*. 1st ed. [pdf] Trieste: ICS-UNIDO.
Available at: https://www.unido.org/sites/default/files/2009-10/Extraction_technologies_for_medicinal_and_aromatic_plants_0.pdf [Accessed 30.01.2020]

Tiwari, B., 2015. Ultrasound: A clean, green extraction technology. *TrAC Trends in Analytical Chemistry*, **71**, pp. 100-109.

Toma, M., Fukutomi, S., Asakura, Y., and Koda, S., 2011. A calorimetric study of energy conversion efficiency of a sonochemical reactor at 500 kHz for organic solvents. *Ultrasonics Sonochemistry*, **18**(1), pp. 197-208.

U.S. Food and Drug Administration, 2019. *Direct Food Substances Affirmed as Generally Recognized as Safe*. 21 C.F.R. §184.1293.

Uhlenbrock, L., Sixt, M., Tegtmeier, M., Schulz, H., Hagels, H., Ditz, R., and Strube, J., 2018. Natural Products Extraction of the Future – Sustainable Manufacturing Solutions for Societal Needs. *Processes*, **6**(10), 177.

ULTRAWAVES GmbH, 2018. *Ultrasonic Disintegration*. [online] Available at: https://ultrawaves.de/technology/ultrasonic-disintegration [Accessed 29.01.2020]

Van Loey, A., Ooms, V., Weemaes, C., Van den Broeck, I., Ludikhuyze, L., Indrawati, Denys, S., and Hendrickx, M., 1998. Thermal and Pressure-Temperature Degradation of Chlorophyll in Broccoli (*Brassica oleracea* L. *italica*) Juice: A Kinetic Study. *Journal of Agricultural and Food Chemistry*, **46**, 5289-5294.

Vinatoru, M., Toma, M., and Mason, T., 1999. Ultrasonically assisted extraction of bioactive principles from plants and their constituents. In: T. Mason, ed., *Advances in Sonochemistry, Volume 5*. 1st ed. Stamford: JAI Press Inc., pp. 210-216.

Weemaes, C., Ooms, V., Van Loey, A., and Hendrickx, M., 1999. Kinetics of Chlorophyll Degradation and Color Loss in Heated Broccoli Juice. *Journal of Agricultural and Food Chemistry*, **47**, pp. 2404-2409.

Wen, C., Zhang, J., Zhang, H., Dzah, C., Zandile, M., Duan, Y., Ma, H., and Luo, X., 2018. Advances in ultrasound assisted extraction of bioactive compounds from cash crops – A review. *Ultrasonics Sonochemistry*, **48**, pp. 538-549.

Wood, R. & Loomis, A., 1927. XXXVIII. The physical and biological effects of high-frequency sound-waves of great intensity. *The London, Edinburgh, and Dublin Philosophical Magazine and Journal of Science*, **4**(22), pp. 417-436.

Yamauchi, N. & Watada, A., 1991. Regulated Chlorophyll Degradation in Spinach Leaves during Storage. *Journal of the American Society for Horticultural Science*, **116**(1), pp. 58-62.

Zhang, Q-W., Lin, L-G., and Ye, W-C., 2018. Techniques for extraction and isolation of natural products: a comprehensive review. *Chinese Medicine*, **13**:20.

Zhao, S., Baik, O., Choi., Y., and Kim, S., 2014. Pretreatments for the Efficient Extraction of Bioactive Compounds From Plant-Based Biomaterials. *Critical Reviews in Food Science and Nutrition*, **54**(10), pp. 1283-1297.

Appendix I: Calorimetric measurements

Calorimetry was used to investigate the differences between electrical and calorimetric US powers at both scales. At laboratory scale, 50 mL of deionized water was placed in the reaction vessel, which was equipped with temperature probe of the ultrasonicator as well as an additional temperature probe connected to an independent thermometer. The vessel was not thermostated. During ultrasonication, temperature increase of the sample was measured. Experiments were done for nominal US powers of 20, 40, 60, and 80 W. Calorimetric heat was calculated with Equation (A-1) (Tamminen & Koiranen, 2015), and calorimetric US power with Equation (A-2) (Tiwari, 2015).

$$Q_c = mC_p\Delta T \tag{A-1}$$

Where Q_c Heat in reaction vessel, J
m Sample mass, kg
C_p Specific heat capacity of material, J/(kg·K)
ΔT Temperature change of material, K

$$P_{cal} = mC_p\left(\frac{dT}{dt}\right) \tag{A-2}$$

Where P_{cal} Calorimetric ultrasonic power, W
T Temperature, K
t Time, s

In pilot scale, no separate calorimetric measurements were made. Instead, temperature rises in the reaction pipe as well as jacket were measured during the extraction tests, and their approximate calorimetric powers were calculated with Equation (A-3) (Cooke et al., 2011).

$$P_{cal} = \dot{m}C_p\Delta T \tag{A-3}$$

Where $\dot{m}$ Mass flow rate, kg/s

During the extraction experiments, mass flow rates of the reactor outflow was measured simultaneously to the flow rates by weighing the samples. For the jacket, mass flow rates were calculated from volumetric flow rates and fluid densities. Volumetric flow rates calculated for the jacket using a linear correlation between thermostat pump pressure and volumetric flow rate Equation A-4) given in the operating instructions of the thermostat (Lauda, 2006). Density was calculated for 78 wt% glycerol in the jacket with Equation (A-5) based on experimental measurements in temperatures of 20-40 °C performed by Takamura et al. (2012).

$$\frac{Q}{\mathrm{L/min}} = \frac{\frac{p_\mathrm{j}}{\mathrm{bar}} - 3.2704}{-0.0803} \tag{A-4}$$

Where Q Volumetric flow rate

p_j Pressure generated by thermostat pump

$$\frac{\rho_\mathrm{G}}{\mathrm{kg/m^3}} = -0.0006\,\frac{T}{\mathrm{°C}} - 1.216 \tag{A-5}$$

Where ρ_G Density of aqueous glycerol

T Temperature

During the laboratory scale experiments, it was observed that electrical power of the ultrasonic generator had a tendency to spike at the beginning, after which it decreased towards the set power. As a result, temperature increases at the start of each experiment were similar regardless of the power value set. This is evident in calculated heat values, which are shown in Figure A-1.

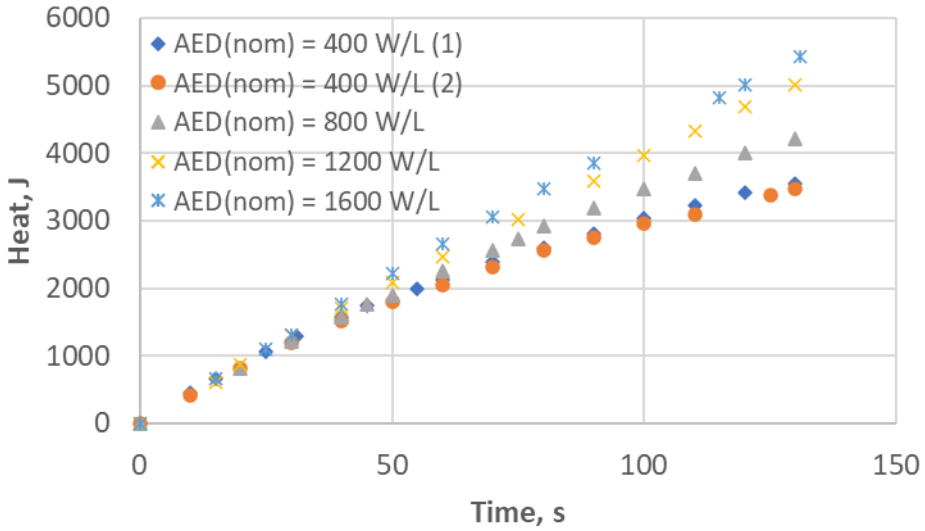

Figure A-1 Increase of heat in 50 mL of deionized water ultrasonicated with an ultrasonic horn at nominal acoustic energy densities of 400-1600 W/L.

For better representative calculations, it was decided to calculate calorimetric powers starting only after 50 s of ultrasonication, when electrical powers had begun to settle, for each experiment. Determined net electrical AEDs as well as calorimetric AEDs are compared to the nominal AED in Table A-1 and Figure A-2. In Table A-1, electrical efficiencies of ultrasonication ε_{US}, (AED_{cal}/AED_{el}) are also shown.

Table A-1 Nominal, net electrical, and calorimetric acoustic energy densities, as well as and electrical efficiencies of ultrasonication in laboratory scale calorimetric experiments.

AED_{nom}, W/L	**AED_{el}, W/L**	**AED_{cal}, W/L**	**ε_{US}**
400	590.4	419	0.71
400	590.4	418.6	0.69
800	914	574.8	0.63
1200	1237.4	771.6	0.59
1600	1560-8	794.8	0.51

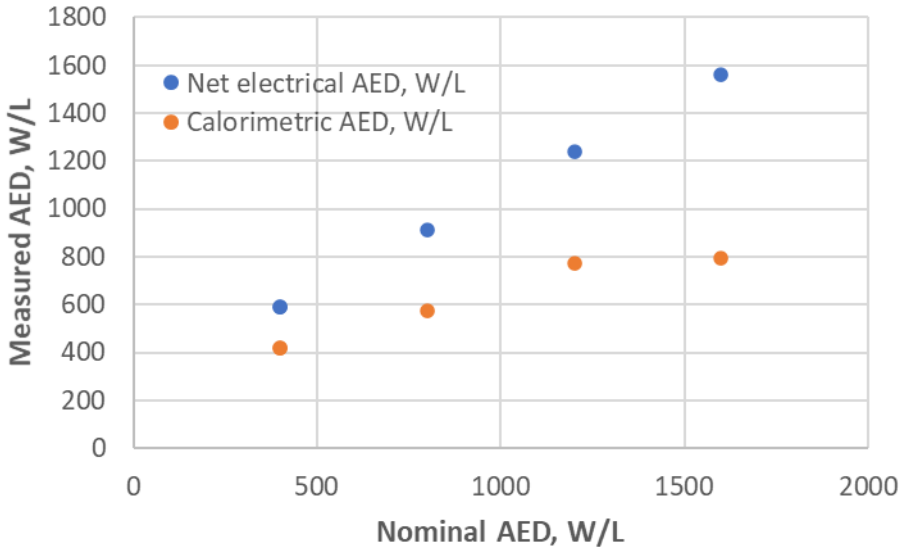

Figure A-2 Net electrical and calorimetric acoustic energy densities compared to the nominal acoustic energy densities of the laboratory scale horn.

Table A-1 and Figure A-2 show that electrical AEDs were well in line with nominal values when higher powers were used, while the opposite was true for calorimetric AEDs. As a result, an increase in power also resulted in a decrease in electrical efficiency.

During the pilot scale experiments, it was observed that temperature changes in the jacket and reaction tube were small, namely around 1 °C. This led to large deviation in the results. For module A, calculated average calorimetric AED for both the jacket and reaction tube was 697 W/L (stdev 45.6) and electrical efficiency was 0.44, while the corresponding numbers for module B were 791 W/L (stdev 94.9) and 0.40. Acoustic energy densities inside the reaction tubes were roughly 15 W/L.

Appendix references

Cooke, M., Rodgers, T., and Kowalski, A., 2011. Power consumption characteristics of an in-line silverson high shear mixer. *AIChE Journal*, **58**(6), pp. 1683-1692.

Lauda, 2006. *Operating Instructions LAUDA Water Circulation coolers*, pp. 39.

Takamura, K., Fischer, H., and Morrow, N., 2012. Physical properties of aqueous glycerol solutions. *Journal of Petroleum Science and Engineering*, **98-99**, pp. 50-60.

Tamminen, J. & Koiranen, T., 2015. Mixing performance comparison of milliscale continuous high-shear mixers. *The Canadian Journal of Chemical Engineering*, **93**(12), pp. 2245-2252.

Tiwari, B., 2015. Ultrasound: A clean, green extraction technology. *TrAC Trends in Analytical Chemistry*, **71**, pp. 100-109.